HOKKAIDO UNIVERSITY

Title	Boundary and Finite Element Analyses of Helically Symmetric Electromagnetic Fields
Author(s)	Igarashi, Hajime
Degree Grantor	北海道大学
Degree Name	博士(工学)
Dissertation Number	乙第4182号
Issue Date	1992-12-25
DOI	https://doi.org/10.11501/3065020
Doc URL	https://hdl.handle.net/2115/51172
Type	doctoral thesis
File Information	000000257058.pdf

Hokkaido University Collection of Scholarly and Academic Papers : HUSCAP

Boundary and Finite Element Analyses of Helically Symmetric Electromagnetic Fields

Hajime IGARASHI

Boundary and Finite Element Analyses of Helically Symmetric Electromagnetic Fields

Hajime IGARASHI

ACKNOWLEDGMENTS

The author wishes to express his sincere gratitude to Professor T. Honma for his support, guidance and encouragement; without these this work could not have been achieved.

The author also wishes to express this thanks to Professor J. Todoroki of National Institute for Fusion Science for helpful suggestions to the present work.

The author would like to thank Mr. Kawaguchi, Research Associate of Hokkaido University, for his helpful discussions and encouragement.

The author wishes to acknowledge the help of Mr. T. Omori and Mr. H. Kumada, students of Hokkaido University, for the computer implementation of this work.

The author is grateful to Mr. H. Yamanaka and Mr. S. Suzuki, Okuma Machinery Works Ltd., for the helical metal columns and helpful discussions.

The author wishes to express his sincere thanks to Professor I. Fukai, Professor T. Enoto and Professor M. Koshiba of Hokkaido University for their helpful suggestions.

Finally, the author wishes to thank his wife Kaoru for her assistance in many ways.

ACKNOWLEDGEMENTS

CONTENTS

1. INTRODUCTION
1.1 Helical systems in electrical engineering 1
1.2 Analytical and numerical approaches to helical systems 4
1.3 Motivation and purpose of this thesis 5
1.4 Subject of this thesis 7
1.5 Organization of this thesis 7
REFERENCES 9

2. CURVILINEAR COORDINATES SYSTEM
2.1 General curvilinear coordinates system 11
2.1.1 Definition 11
2.1 2 Unitary vectors 12
2.1.3 Metric tensors 14
2.1.4 Covariant and contravariant components 14
2.1.5 Scalar and vector products 15
2.1.6 Line, surface and volume elements 16
2.1.7 Differential operators 17
2.2 Helical coordinates system 21
2.2.1 Twisted coordinates system 21
2.2.2 Helical polar coordinates system 26
REFERENCES 29

3. FUNDAMENTAL SOLUTIONS
3.1 Derivation of fundamental solutions 30
3.2 Numerical evaluation of fundamental solutions 37
3.2.1 Convergence of infinite series 37
3.2.2 Computing times for infinite series and integral representations 40
3.3 Singularity of fundamental solutions 42
3.4 Summary 45
REFERENCES 46

4. POTENTIAL PROBLEMS
4.1 Formulation for scalar potential problems 47
4.1.1 BE formulation 48
4.1.2 FE formulation for closed region 53
4.1.3 FE formulation for open region 54
4.2 Analysis of scalar potential problems 57
4.2.1 Closed boundary problem 57
4.2.2 Open boundary problem 59
4.2.3 Coupling losses in superconducting composite 65
4.3. Formulation for vector potential problems (G-S equation) 69
4.3.1 Derivation of the G-S equation 69
4.3.2 BE and FE formulation for G-S equation 76
4.4 Analysis of Vector potential problems 78
4.4.1 Linear problem 79
4.4.2 Non-linear problem 82
4.4.3 Analysis of straight heliacs 88
4.5 Summary 94
REFERENCES 96

5. EIGENVALUE PROBLEMS
5.1 Formulation for scalar Helmholtz equation 98
5.1.1 Hertz vector and scalar Helmholtz equation 98
5.1.2 Lewin's perturbation analysis 101
5.1.3 BE formulation for scalar Helmholtz equation 104
5.1.4 FE formulation for scalar Helmholtz equation 107
5.2 Analysis of a scalar eigenvalue problem 110
5.3 Formulation for vectorial eigenvalue problems 114
5.4 Analysis of a vectorial eigenvalue problem 118
5.5 Summary 121
REFERENCES 122

6. SUMMARY AND CONCLUSIONS 123

APPENDICES 126

CHAPTER 1

INTRODUCTION

1.1 Helical systems in electrical engineering

Recently there has been considerable progress in the three dimensional computation of electromagnetic fields. However, two dimensional analyses of fields are still of importance because of their simplicity, wise economy and accuracy. Those two dimensional analyses are performed mainly for translational and axisymmetric systems and numerical schemes for such symmetric systems seem well established.

In addition to the translational and axial symmetries, helical symmetry can also be seen in various electrical engineering devices. These three types of symmetry are illustrated in Fig. 1.1. As will be shown in Sec. 1.3, the helical symmetry is the third, last class of symmetry in the three dimensional Euclidean space. The helical symmetry can be seen in the following diverse systems and devices in electrical engineering.

Twisted-Pair Line [1.1]

A twisted-pair line is composed of two insulated conductors twisted together and it can effectively remove inductive coupling because the current induced by external magnetic fields is canceled in one period. In addition, the twisted pair line scarcely produces electromagnetic noise because magnetic fields induced by the line may also cancel each other. For the above reasons, the twisted-pair line is often used for data transmission between electronic devices and telephone networks. However, the stray capacitance between twisted lines sometimes causes difficulty in high speed communication.

Twisted Waveguide [1.2]

A twisted waveguide has a progressive rotation of its cross section about a longitudinal axis. That is used for the connection of two straight waveguides of different polarization planes. In general, it is difficult to rigorously analyze the electromagnetic fields even in a twisted hollow waveguide. Numerical analyses of this waveguide will be described in detail in Chap. 5.

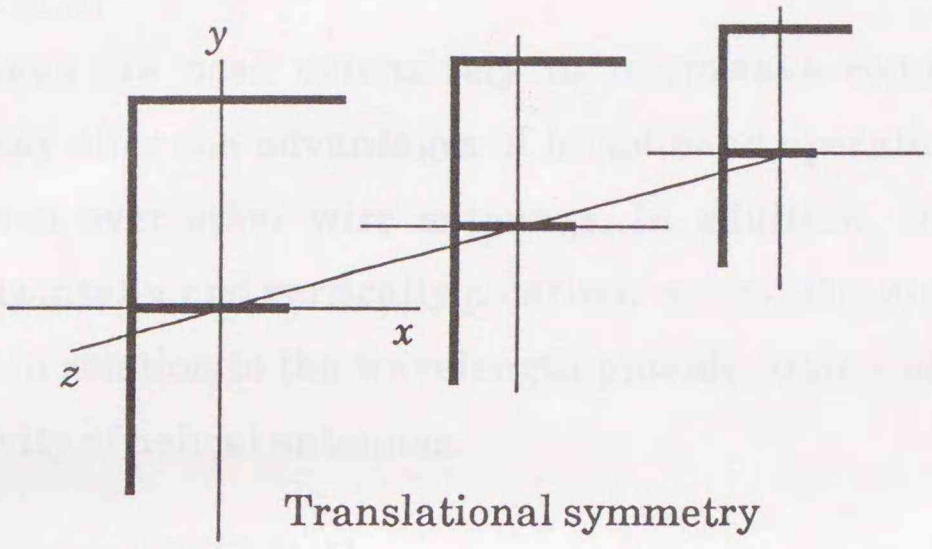

Translational symmetry

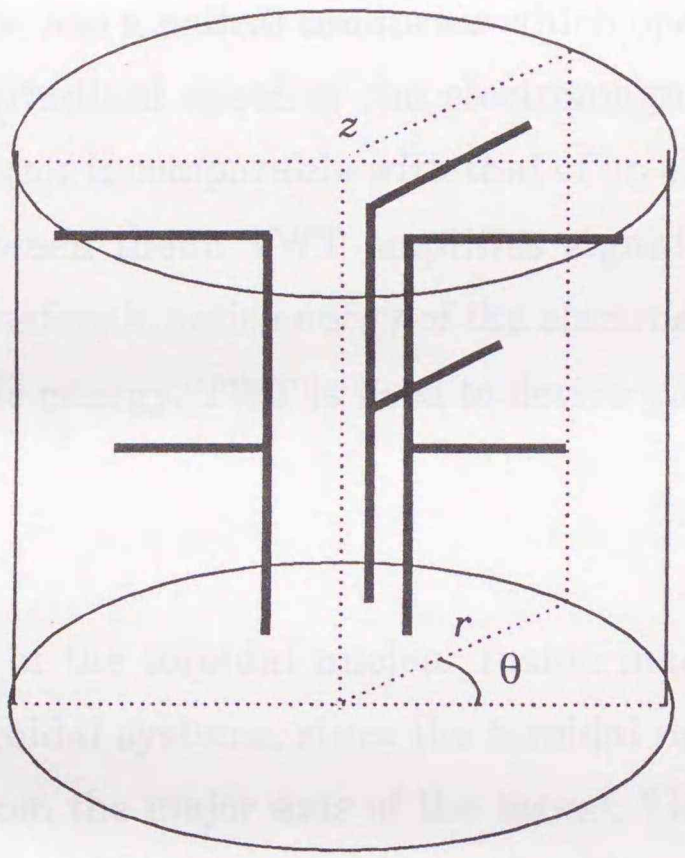

Axial symmetry

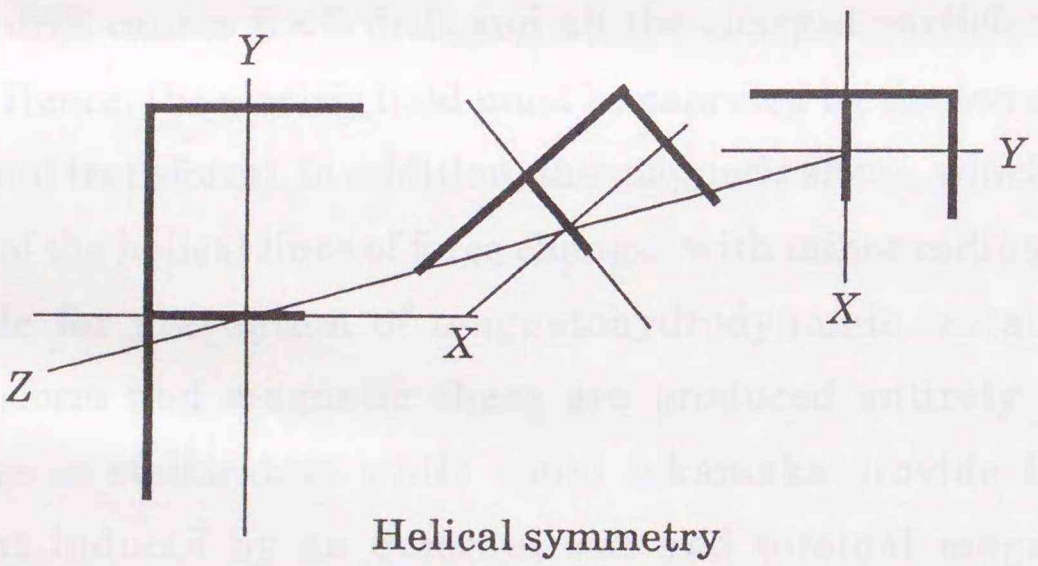

Helical symmetry

Fig. 1.1 Three classes of symmetry in the three dimensional Euclidean space

Helical Antenna [1.3]

Helical antennas are used extensively in microwave communications and broadcasting. They offer the advantages of broad-band operation and circularly polarized radiation over other wire antennas. In addition, the antennas can radiate both horizontally and vertically polarized waves. The diameter, pitch and number of turns in relation to the wavelength provide control of the polarization state and directivity of helical antennas.

Traveling Wave Tubes (TWT) [1.4]

A traveling wave tube has a helical conductor which operates as the slow wave circuit. When the longitudinal speed of the electromagnetic wave propagating along the helical conductor is comparable with that of an electron beam, there can be the interaction between them. TWT amplifies signals on the basis of this principle, *i.e.*, TWT transfers kinetic energy of the electrons running through the helix to electromagnetic energy. TWT is used to derive power gain, primarily at microwave frequencies.

Stellarator [1.5]

Stellarators are one of the toroidal nuclear fusion machines using magnetic confinement. In the toroidal systems, since the toroidal magnetic field varies as $1/r$ (r is the distance from the major axis of the torus), ∇B drift occurs, and as a result, ions and electrons drift in opposite direction. Moreover, the electric field induced by the drift causes $E \times B$ drift and all the charged particles tend to run away outward. Hence, the electric field must be canceled by the twist of the lines of force (rotational transform). In addition, the magnetic shear, which means that the pitch angle of the helical lines of force changes with minor radius of the torus, is indispensable for prevention of magnetohydrodynamic instabilities. The rotational transform and magnetic shear are produced entirely by external helical windings in stellarators while usual tokamaks provide them by the toroidal current induced by an external coil and toroidal magnetic fields. Stellarators have, therefore, advantage of operation in steady state over tokamaks.

There are other helical elements and devices such as super conducting transmission lines [1.6], helically wound optical fibers [1.7] and helical transformers proposed recently [1.8].

1.2 Analytical and numerical approaches to helical systems

Electromagnetic fields in the above mentioned helical systems have been analyzed by various methods. This section briefly surveys those methods.

In microwave engineering, the perturbation seems to be a common method for the analysis of helical systems. For example, the twisted waveguide has been analyzed by solving the scalar [1.9] and vector [1.10, 1.11] Helmholtz equations on the basis of perturbation in which the solutions are expanded in the series of the helical wavenumber. The perturbation analysis gives useful dispersion relations in closed form for the twisted waveguide. However, the dependence of accuracy of the perturbed solution on the wavenumber (or convergence of the perturbed solution) has not been discussed. (The above mentioned approaches will be described in some detail in Chap. 5) The perturbation analyses were also applied to the helically wound optical fiber [1.7] and helical antenna with dielectric load [1.12].

The property of electromagnetic wave propagation in TWT has been investigated using the sheath model in which an actual helix is replaced by a cylindrical tube, which is assumed to have infinite conductivity in the direction of the original winding and zero conductivity in a direction normal to the turns of the winding [1.13]. Though this simple model can describe an essential property of TWT, the approximation is valid only if the actual helix consists of many turns per wavelength. A more rigorous model called tape helix has also been proposed for explanation of the forbidden band in dispersion relation [1.14]. The dispersion relation obtained from this model is accurate, but highly involved.

In the analysis of helical systems in electrical engineering, the most advanced field seems to be nuclear fusion engineering. In fact, even if we restrict ourselves to the analysis of helically symmetric magnetohydrodynamic (MHD) equilibria, which approximate three dimensional equilibria in a helical torus, we can see the

following diverse approaches. That is, force free MHD equilibria with helical symmetry have been analyzed using a highly sophisticated method [1.15] in which the vectorial proper equation $\nabla \times B = \lambda B$ is transformed to the scalar Helmholtz equation which can be solved analytically. However, this method may not be suitable for numerical approaches because the boundary condition includes the second order differentiation of the magnetic stream function to be obtained. An analytical solution to helically symmetric linear MHD equilibrium equation has been obtained by the Fourier expansion technique providing that the cross section of the plasma is circular [1.16]. Moreover a semi-analytical method [1.17], in which the magnetic stream function is expanded in power series and the coefficients in the series are determined from shape parameters such as the curvature of the magnetic axis and half-axes ratio of the cross section near the magnetic axis and so on, has been successfully applied to equilibrium calculation which is one of the important part of stability analysis of MHD plasmas. Furthermore a free boundary problem for helically symmetric MHD plasmas has been solved by the combination of the boundary integral equation method with the finite difference method on a curvilinear grid [1.18]. In this method, the equilibrium configuration is obtained over the whole solution region essentially by the boundary integral equation method which can efficiently calculate the magnetic fields in the infinite vacuum region surrounding the plasma. The two dimensional surface integral appearing in the integral equation, which is expensive to numerically evaluate, is eliminated using the field vanishing on the plasma boundary. In order to obtain the field, a fixed boundary problem is solved by the finite difference method.

1.3 Motivation and purpose of this thesis

As seen in the previous section, helical devices and systems in electrical engineering have been so far independently analyzed by diverse methods, which do not have wide applicability in general and are sometimes very difficult to use. Although there are a number of studies on fundamentals and applications of standard numerical methods such as boundary element (BE) and finite element (FE) methods for the systems with translational and axial symmetries, we can

find few efforts to apply them to the analysis of various helical systems and investigate their property and feasibility. The first purpose of this thesis is, for helical systems, to establish the numerical methods which have wide use and are economic and easy to handle.

On the other hand, electromagnetic fields in helical systems have often been analyzed by the perturbation method. When analyzing the problems by the perturbation technique, we can understand the physical properties such as field profiles and dispersion relations etc. more systematically than numerical approaches because we can obtain those properties in closed forms by the former method. When helical systems are analyzed by the perturbation method, the solutions are expanded in a series of small parameters like the helical wavenumber. However, in general, the dependence of the accuracy of the perturbed solutions on the small parameters has not usually been investigated well, which is probably due to difficulty in mathematical evaluation of the convergence of perturbed solution. Therefore, it is hard to estimate the applicable bounds of the perturbation method. Moreover, we also find difficulty in applying the perturbation method to analyze helical systems with deformed or complicated cross sections. It may be effective for the solution of the above problems to develop numerical methods in which the accuracy of the solutions are independent from all physical parameters. Recently the BE and FE methods have provided considerably powerful numerical computations of electromagnetic fields. This thesis, therefore, modifies and generalizes the BE and FE formulations and adapts them to the two dimensional analysis of helical systems.

This study was also motivated by the fact that there are the only three classes of symmetry in the three dimensional Euclidean space : translational symmetry, axial symmetry and helical symmetry [1.19]. (Proof of this theorem is outlined in appendix A-1.) The term symmetry here means that a system has an ignorable coordinate. A system has symmetry in this sense if one can choose coordinates (u^1, u^2, u^3) so that the metric tensor is independent of one of the coordinate, say u^3, and physical quantities in the system are independent of u^3. (The system is said to have symmetry even if physical quantities have the dependence on the u^3 in the form $exp\ (-j\beta u^3)$) The symmetry considering here does not include the symmetries with respect to finite transformation such as bilateral symmetry (the symmetry

of right and left) and rotational symmetry (the symmetry in something keeping its shape same after finite rotational transforms).

From the view point of numerical computation, property and usefulness of helical symmetry still remain unclear in contrast with those of the other symmetries. If numerical methods which can make the best use of helical symmetry are developed, researches on two dimensional numerical analyses will be accomplished. In addition, study on helical symmetry may enable us to unify the two dimensional analyses and define the relation among them.

For the above reasons, the BE and FE methods for helically symmetric systems in electric engineering will be reported in detail in this thesis. Potential and eigenvalue problems are chosen as subjects of this thesis because they are typical and major in electrical engineering especially at low frequencies (or in static states) and high frequencies.

The goals of this thesis are summarized as follows :

(1) Development and characterization of BE and FE element methods for helically symmetric systems.

(2) To show applicability and feasibility of the present methods.

(3) Comparison of the present methods with conventional methods.

1.4 Subject of this thesis

This thesis deals with electromagnetic fields in 'straight' helical systems whose cross sections rotate about a straight axis, and does not deal with systems with three dimensional (non-planar) helical axes like stellarator-type fusion machines. (Those fusion machines, however, can be regarded as straight helical systems under a certain assumption as described later.) Hence, in this thesis, straight helical systems will be called just 'helical systems' for simplicity.

1.5 Organization of this thesis

The rest of this thesis is organized as follows. Chapter 2 describes mathematical foundations of the vector analysis in general curvilinear coordinates. Then, helical coordinates systems are introduced and some vectorial

formula in them are derived. Chapter 3 provides a unified derivation of fundamental solution to modified Helmholtz-type equations for helically symmetric systems. Chapter 4 gives BE and FE formulations for helically symmetric potential problems, which involve scalar potential problems with closed and open boundaries, and (fixed boundary) linear and nonlinear MHD equilibrium problems. Chapter 5 describes BE and FE formulations for scalar eigenvalue problems for wave propagation in helical systems. This chapter also gives a vectorial FE formulation for helical waveguides. Some concluding remarks are given in Chap. 6.

REFERENCES

1.1 H. W. Ott, *Noise Reduction Techniques in Electronic Systems*, John Wiley & Sons, New York, pp. 44-45, 1976.

1.2 R. G. Brown, R. A. Sharpe and W. L. Hughes, *Lines, Waves and Antennas*, The Ronald Press Company, New York, pp. 167-168, 1961.

1.3 A. Z. Fradin, *Microwave Antennas*, Pergamon Press, London, pp. 619-660, 1961.

1.4 R. E. Collin, *Field Theory of Guided Waves*, McGraw-Hill, New York, pp.401-405, 1960.

1.5 F. F. Chen, *Introduction to Plasma Physics*, Plenum Press, New York, pp.287-289, 1974.

1.6 Superconducting Application Group in Rutherford Laboratory, "Experimental and Theoretical Studies of Filamentary Superconducting Composites", *J. Phys.* D, **3**, pp. 1517-1585, 1970.

1.7 X-S Fang and Z-Q Lin, "Field in Single-Mode Helically-Wound Optical Fibers", *IEEE Trans. Microwave Theory and Tech.*, **33**, pp. 1150-1154, 1985.

1.8 Y. Saito, "A New Type High Frequency Transformer", IEE Jpn, MAG-91-86, 1991, (in Japanese).

1.9 L. Lewin, *Theory of Waveguides*, Newnes-Butherworths, London, pp.96-101, 1975.

1.10 H. Yabe and Y. Mushiake, "An Analysis of a Hybrid-Mode in a Twisted Rectangular Waveguide", *IEEE Trans. Microwave Theory Tech.*, **32**, pp.65-71, 1984.

1.11 H. Yabe, K. Nishio and Y. Mushiake, "Dispersion Characteristics of Twisted Rectangular Waveguides", *ibid*, **32**, pp.91-96, 1984.

1.12 M. T. Wlodarczyk and S. R. Seshadri, "Exitation and Scattering of Guided Modes on a Helically Corrugated Dielectric Cylinder", *ibid*, **34**, pp.8-18, 1986.

1.13 J. R. Pierce, *Travelling Wave Tubes*, D. Van Nostrand Company, Princeton, 1950.

1.14 S. Sensiper, "Electromagnetic Wave Propagation on Helical Structures", *Proc. IRE*, **43**, pp. 149-161, 1955.

1.15 P. Barberio-Corsetti, "Force-Free Helical Equilibria", *Plasma Phys.* **15**, pp.1131-1139, 1973.

1.16 D. Correa and D. Lortz, "A Class of Helically Symmetric MHD-Equilibria", *Nucl. Fusion*, **13**, pp.127-129, 1973.

1.17 P. Merkel, "HERA : Application to Helical Geometry", in *Finite Element Methods in Linear Ideal Magnetohydrodynamics* (Eds. R. Gruber and J. Rappaz), Springer-Verlag, Berlin, pp. 118-133, 1985.

1.18 H. J. Gardner, R. L. Dewar and W. N-C. Sy, "The Free-Boundary Equilibrium Problem for Helically Symmetric Plasmas", *J. Comp. Phys.*, 74, pp. 477-487, 1988.

1.19 J. W. Edenstrasser, "The Only Three Classes of Symmetric MHD Equilibria", *J. Plasma Phys.*, 24, pp. 515-518, 1980.

CHAPTER 2

CURVILINEAR COORDINATES SYSTEM

Helically symmetric systems can be regarded as being two dimensional when they are described in helical coordinates which will be introduced in Sec. 2.2. Since the helical coordinates system is not orthogonal, mathematical formulation in the system must be based on the vector analysis for general curvilinear coordinates. This chapter will first describe the vector analysis for general curvilinear coordinates in some detail. Then, the helical coordinates will be introduced.

2.1 General curvilinear coordinates system[2.1-2.2]

2.1.1 Definition

Let us consider three independent, continuous, single-valued functions of the Cartesian coordinates (x, y, z)

$$u^1 = f_1(x, y, z), \quad u^2 = f_2(x, y, z), \quad u^2 = f_2(x, y, z), \tag{2.1}$$

in the three dimensional Euclidean space. (See Fig. 2.1.) The inverse relation to (2.1) is written in the form

$$x = \Phi_1(u^1, u^2, u^3), \quad y = \Phi_2(u^1, u^2, u^3), \quad z = \Phi_3(u^1, u^2, u^3). \tag{2.2}$$

Since the above mapping is injection, the variables u^i $(i=1, 2, 3)$ determine a point uniquely in space and they form a general curvilinear coordinates system. On the coordinate surfaces u^i=const., one variable is constant and two are variable. Those surfaces pass a point P and the surfaces do not always meet at right angles at P. Two surfaces intersect in a curve, shown as u^i-curve in Fig. 2.1, along which two variables are constant and one is variable. The tangential vectors $\mathbf{e}_i$ of the curves at P depend on the position of P in general while they are independent of P in the Cartesian coordinates.

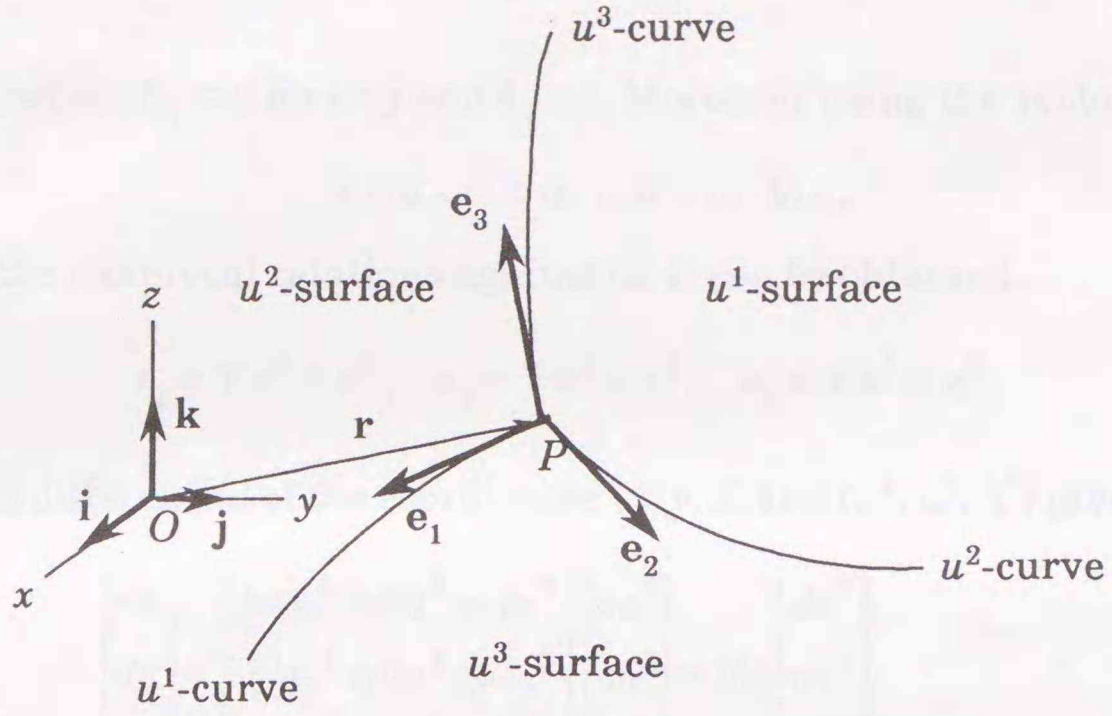

Fig. 2.1 Curvilinear coordinates system

2.1.2 Unitary vectors

The tangential vectors $\mathbf{e}_i$ mentioned in 2.1.1 are called the unitary vectors (or contravariant basis vectors) associated with the point P in the coordinates (u^1, u^2, u^3) and they are defined in terms of the position vector $\mathbf{r}$ as follows :

$$d\mathbf{r} = \mathbf{e}_i \, du^i, \quad \mathbf{e}_i = \frac{\partial \mathbf{r}}{\partial u^i}, \tag{2.3}$$

where the reputation of the index in a term once as a subscript and once as a superscript denotes a summation with respect to that index over its range. This rule will be kept in the rest of this thesis. (Here, note that vectors $\mathbf{e}_i$ are not always unit.) The unitary vectors $\mathbf{e}_i$ constitute a base system of reference for all other vectors associated with that particular point.

On the other hand, the reciprocal unitary vectors (covariant basis vectors) $\mathbf{e}^i$ are defined in terms of $\mathbf{e}_i$ as

$$\mathbf{e}^1 = \frac{\mathbf{e}_2 \times \mathbf{e}_3}{V}, \quad \mathbf{e}^2 = \frac{\mathbf{e}_3 \times \mathbf{e}_1}{V}, \quad \mathbf{e}^3 = \frac{\mathbf{e}_1 \times \mathbf{e}_2}{V}, \tag{2.4}$$

where V denotes the volume of the parallelepiped determined by the vectors $\mathbf{e}_i$ and are expressed by $\mathbf{e}_1 \cdot (\mathbf{e}_2 \times \mathbf{e}_3) = \mathbf{e}_3 \cdot (\mathbf{e}_1 \times \mathbf{e}_2) = \mathbf{e}_2 \cdot (\mathbf{e}_3 \times \mathbf{e}_1)$. The vectors $\mathbf{e}^i$ as well as $\mathbf{e}_i$ constitute a base system. From (2.3) and (2.4), an important relation

$$\mathbf{e}^i \cdot \mathbf{e}_j = \delta_{ij} \tag{2.5}$$

is derived, where $\delta_{ij} = 0$ for $i \neq j$ and $\delta_{ii} = 1$. Moreover using the vector identity

$$\mathbf{a} \times (\mathbf{b} \times \mathbf{c}) = (\mathbf{a} \cdot \mathbf{c})\,\mathbf{b} - (\mathbf{a} \cdot \mathbf{b})\,\mathbf{c}\,, \tag{2.6}$$

and (2.5), the reciprocal relations against (2.4) can be obtained.

$$\mathbf{e}_1 = V\,\mathbf{e}^2 \times \mathbf{e}^3\,, \quad \mathbf{e}_2 = V\,\mathbf{e}^3 \times \mathbf{e}^1\,, \quad \mathbf{e}_3 = V\,\mathbf{e}^1 \times \mathbf{e}^2\,. \tag{2.7}$$

The total differential of the coordinates (x, y, z) and (u^1, u^2, u^3) gives

$$\begin{bmatrix} dx \\ dy \\ dz \end{bmatrix} = \begin{bmatrix} \partial x/\partial u^1 & \partial x/\partial u^2 & \partial x/\partial u^3 \\ \partial y/\partial u^1 & \partial y/\partial u^2 & \partial y/\partial u^3 \\ \partial z/\partial u^1 & \partial z/\partial u^2 & \partial z/\partial u^3 \end{bmatrix} \begin{bmatrix} du^1 \\ du^2 \\ du^3 \end{bmatrix} = [A] \begin{bmatrix} du^1 \\ du^2 \\ du^3 \end{bmatrix} \tag{2.8}$$

$$\begin{bmatrix} du^1 \\ du^2 \\ du^3 \end{bmatrix} = \begin{bmatrix} \partial u^1/\partial x & \partial u^1/\partial y & \partial u^1/\partial z \\ \partial u^2/\partial x & \partial u^2/\partial y & \partial u^2/\partial z \\ \partial u^3/\partial x & \partial u^3/\partial y & \partial u^3/\partial z \end{bmatrix} \begin{bmatrix} dx \\ dy \\ dz \end{bmatrix} = [A]^{-1} \begin{bmatrix} dx \\ dy \\ dz \end{bmatrix} \tag{2.9}$$

where $det[A]$ is proved to be V. From these relations, we have

$$\frac{\partial u^1}{\partial x} = V\left(\frac{\partial y}{\partial u^2}\frac{\partial z}{\partial u^3} - \frac{\partial y}{\partial u^3}\frac{\partial z}{\partial u^2}\right), \quad \frac{\partial u^1}{\partial y} = V\left(\frac{\partial z}{\partial u^2}\frac{\partial x}{\partial u^3} - \frac{\partial x}{\partial u^3}\frac{\partial z}{\partial u^2}\right), \quad \frac{\partial u^1}{\partial z} = V\left(\frac{\partial x}{\partial u^2}\frac{\partial y}{\partial u^3} - \frac{\partial y}{\partial u^3}\frac{\partial x}{\partial u^2}\right)$$

$$\frac{\partial u^2}{\partial x} = V\left(\frac{\partial y}{\partial u^3}\frac{\partial z}{\partial u^1} - \frac{\partial y}{\partial u^1}\frac{\partial z}{\partial u^3}\right), \quad \frac{\partial u^2}{\partial y} = V\left(\frac{\partial z}{\partial u^3}\frac{\partial x}{\partial u^1} - \frac{\partial x}{\partial u^1}\frac{\partial z}{\partial u^3}\right), \quad \frac{\partial u^2}{\partial z} = V\left(\frac{\partial x}{\partial u^3}\frac{\partial y}{\partial u^1} - \frac{\partial y}{\partial u^1}\frac{\partial x}{\partial u^3}\right),$$

$$\frac{\partial u^3}{\partial x} = V\left(\frac{\partial y}{\partial u^1}\frac{\partial z}{\partial u^2} - \frac{\partial y}{\partial u^2}\frac{\partial z}{\partial u^1}\right), \quad \frac{\partial u^3}{\partial y} = V\left(\frac{\partial z}{\partial u^1}\frac{\partial x}{\partial u^2} - \frac{\partial x}{\partial u^2}\frac{\partial z}{\partial u^1}\right), \quad \frac{\partial u^3}{\partial z} = V\left(\frac{\partial x}{\partial u^1}\frac{\partial y}{\partial u^2} - \frac{\partial y}{\partial u^2}\frac{\partial x}{\partial u^1}\right). \tag{2.10}$$

On the other hand, comparing the coefficients of du^i in (2.3) and the relation

$$\begin{aligned} d\mathbf{r} &= \mathbf{i}\,dx + \mathbf{j}\,dy + \mathbf{k}\,dz \\ &= \mathbf{i}\,\frac{\partial x}{\partial u^i}du^i + \mathbf{j}\,\frac{\partial y}{\partial u^i}du^i + \mathbf{k}\,\frac{\partial z}{\partial u^i}du^i\,, \end{aligned} \tag{2.11}$$

where $\mathbf{i}, \mathbf{j}, \mathbf{k}$ are the unitary vectors of the Cartesian coordinates, we find

$$\mathbf{e}_i = \mathbf{i}\,\frac{\partial x}{\partial u^i} + \mathbf{j}\,\frac{\partial y}{\partial u^i} + \mathbf{k}\,\frac{\partial z}{\partial u^i}\,. \tag{2.12}$$

Consequently, the insertion of (2.10) and (2.12) in (2.4) yields

$$\mathbf{e}^i = \nabla u^i . \tag{2.13}$$

2.1.3 Metric tensors

The unitary vectors are related with reciprocal unitary vectors are related by

$$\begin{aligned} \mathbf{e}_i &= g_{ij}\mathbf{e}^j , \\ \mathbf{e}^i &= g^{ij}\mathbf{e}_j , \end{aligned} \tag{2.14}$$

where the matrices $[g_{ij}]$ and $[g^{ij}]$ are often referred to as the covariant and contravariant metric tensors. Naturally, they satisfy the relation $[g_{ij}] = [g^{ij}]^{-1}$. The components of these tensors are obtained from (2.5) and (2.14) as follows :

$$g_{ij} = \mathbf{e}_i \cdot \mathbf{e}_j , \tag{2.15}$$

$$g^{ij} = \mathbf{e}^i \cdot \mathbf{e}^j . \tag{2.16}$$

From these relations, we readily see that the metric tensors are symmetric. Moreover, since $[g_{ij}] = A^2$, the determinant g of $[g_{ij}]$ can be proved to be V^2 using the relation $det[PQ] = det[P]det[Q]$.

2.1.4 Covariant and contravariant components

Considering two unitary base systems $[\mathbf{e}_1, \mathbf{e}_2, \mathbf{e}_3]$ and $[\mathbf{e}'_1, \mathbf{e}'_2, \mathbf{e}'_3]$, they are assumed to be related by

$$\mathbf{e}'_i = a^h{}_i \, \mathbf{e}_h . \tag{2.17}$$

If those systems are independent, then the matrix $[a^h{}_i]$ is regular and hence the inverse matrix $[b^h{}_i] = [a^h{}_i]^{-1}$ exists. On the other hand, using (2.5), it can be proved that the transformation of the reciprocal unitary vectors can be written in terms of $[b^h{}_i]$ as

$$\mathbf{e}'^h = b^h{}_i \, \mathbf{e}^i . \tag{2.18}$$

In the unitary base system, an arbitrary vector $\mathbf{F}$ can be expressed in the form

$$\mathbf{F} = F^i \mathbf{e}_i , \quad F^i = \mathbf{F} \cdot \mathbf{e}^i . \tag{2.19}$$

Representation of the vector $\mathbf{F}$ in the two systems

$$\mathbf{F} = F^h \mathbf{e}_h = F'^k \mathbf{e}'_k , \tag{2.20}$$

and the use of (2.17) and (2.18) yield

$$F^h = a^h{}_k F'^k . \tag{2.21}$$

Hence we have

$$F'^h = b^h{}_i F^i . \tag{2.22}$$

By comparing (2.18) and (2.22), one see that the components F^h transform in the same form as the reciprocal unitary vectors. These variables F^h are called the contravariant components of the vector **F**. Note that du^i in (2.3) are contravariant components of $d\mathbf{r}$.

The vector **F** can also be written in terms of the reciprocal unitary vectors,

$$\mathbf{F} = F_i \mathbf{e}^i , \quad F_i = \mathbf{F} \cdot \mathbf{e}_i . \tag{2.23}$$

The components F_i transform in the form (2.17), and they are called the covariant components of the vector **F**.

The relations between F_i and F^i can be easily derived from (2.5), (2.19) and (2.23) as follows :

$$F_i = g_{ij} F^j , \tag{2.24}$$

$$F^i = g^{ij} F_j . \tag{2.25}$$

2.1.5 Scalar and vector products

The scalar products of vectors **F** and **G** are written in the forms

$$\begin{aligned} \mathbf{F} \cdot \mathbf{G} &= (F_i \mathbf{e}^i) \cdot (G^j \mathbf{e}_j) = F_i G^i = F^i G_i \\ &= (F_i \mathbf{e}^i) \cdot (G_j \mathbf{e}^j) = g^{ij} F_i G_j \\ &= (F^i \mathbf{e}_i) \cdot (G^j \mathbf{e}_j) = g_{ij} F^i G^j . \end{aligned} \tag{2.26}$$

The vector products take the form

$$\begin{aligned} \mathbf{F} \times \mathbf{G} &= (F_i \mathbf{e}^i) \times (G_j \mathbf{e}^j) \\ &= \frac{1}{\sqrt{g}} [(F_2 G_3 - F_3 G_2) \mathbf{e}_1 + (F_3 G_1 - F_1 G_3) \mathbf{e}_2 + (F_1 G_2 - F_2 G_1) \mathbf{e}_3] . \end{aligned} \tag{2.27}$$

Similarly they can be written as

$$\mathbf{F}\times\mathbf{G} = \sqrt{g}\,[\,(F^2G^3 - F^3G^2)\,\mathbf{e}^1 + (F^3G^1 - F^1G^3)\mathbf{e}^2 + (F^1G^2 - F^2G^1)\mathbf{e}^3\,]\,. \tag{2.28}$$

2.1.6 Line, surface and volume elements

Using (2.3) and (2.26), the magnitude of a line element $d\mathbf{r}$ is expressed in the form

$$\begin{aligned} ds^2 &= d\mathbf{r}\cdot d\mathbf{r} \\ &= g_{ij}\,du^i\,du^j\,. \end{aligned} \tag{2.29}$$

The magnitude of infinitesimal line elements $d\mathbf{s}_i$ along the u^i-curve is given by

$$\begin{aligned} ds_1 &= |\,\mathbf{e}_1\,du^1\,| = \sqrt{g_{11}}\,du^1\,, \\ ds_2 &= |\,\mathbf{e}_2\,du^2\,| = \sqrt{g_{22}}\,du^2\,, \\ ds_3 &= |\,\mathbf{e}_3\,du^3\,| = \sqrt{g_{33}}\,du^3\,. \end{aligned} \tag{2.30}$$

For a surface element dS_1, which lies on the surface of $u^1 =$ constant as shown in Fig. 2.2, using the vector identity

$$(\mathbf{a}\times\mathbf{b})\cdot(\mathbf{c}\times\mathbf{d}) = (\mathbf{a}\cdot\mathbf{c})\,(\mathbf{b}\cdot\mathbf{d}) - (\mathbf{a}\cdot\mathbf{d})\,(\mathbf{b}\cdot\mathbf{c}) \tag{2.31}$$

we have

$$\begin{aligned} dS_1 &= |\,d\mathbf{s}_2\times d\mathbf{s}_3\,| \\ &= \sqrt{(\mathbf{e}_2\times\mathbf{e}_3)\cdot(\mathbf{e}_2\times\mathbf{e}_3)}\;du^2du^3 \\ &= \sqrt{g_{22}g_{33} - g_{23}^{\,2}}\;du^2du^3\,. \end{aligned} \tag{2.32}$$

Similarly, for dS_2 and dS_3, we get

$$\begin{aligned} dS_2 &= \sqrt{g_{11}g_{33} - g_{13}^{\,2}}\,du^1du^3\,, \\ dS_3 &= \sqrt{g_{11}g_{22} - g_{12}^{\,2}}\,du^1du^2\,. \end{aligned} \tag{2.33}$$

On the other hand, a volume element dv can be derived as follows :

$$\begin{aligned} dv &= d\mathbf{s}_1\cdot(d\mathbf{s}_2\times d\mathbf{s}_3) \\ &= \mathbf{e}_1\cdot(\mathbf{e}_2\times\mathbf{e}_3)\,du^1du^2du^3 \\ &= \sqrt{g}\,du^1du^2du^3\,. \end{aligned} \tag{2.34}$$

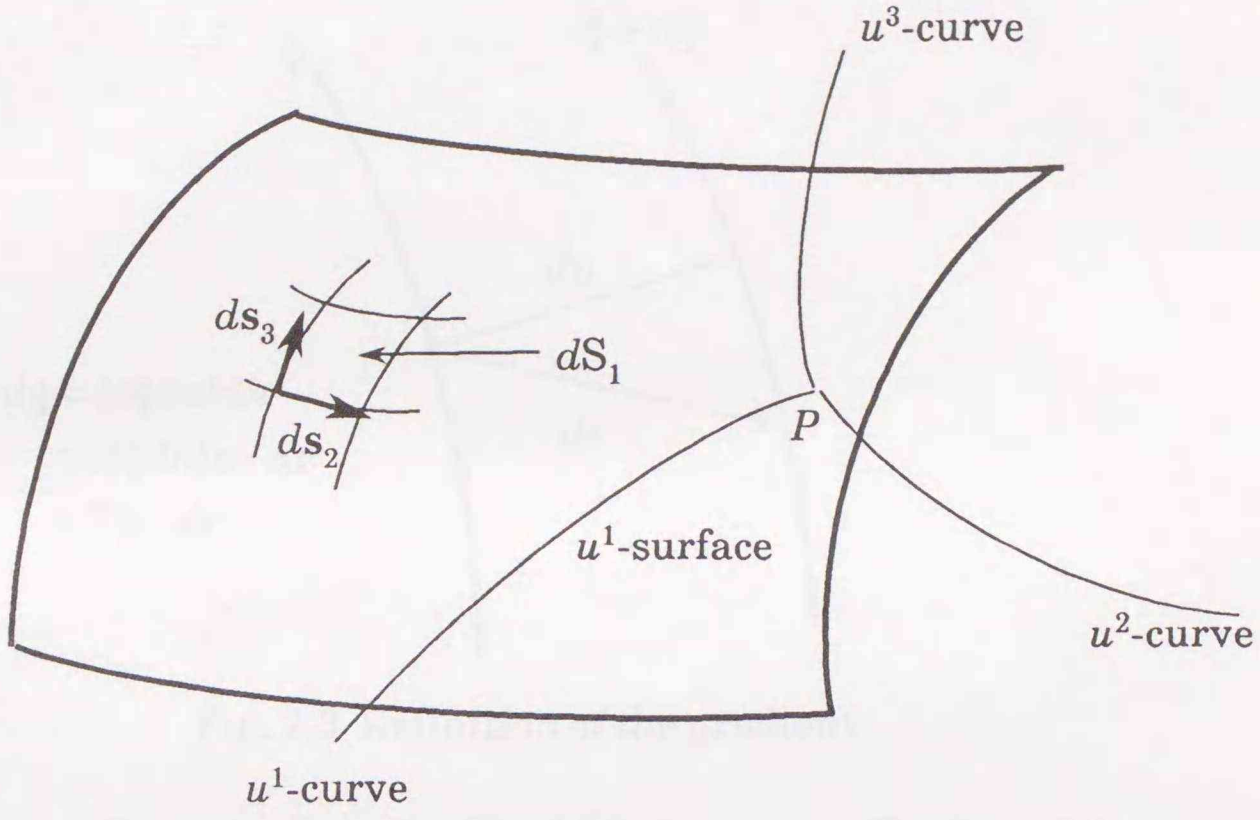

Fig. 2.2 A surface element dS_1 on u^1-surface

2.1.7 Differential operators

The gradient of scalar function ϕ is a vector whose magnitude is equal to the maximum rate of change of ϕ with respect to space variables and has the direction of that change. Hence, as shown in Fig. 2.3, the change in the function ϕ incurred during a displacement $d\mathbf{r}$ is given by

$$d\phi = \nabla\phi \cdot d\mathbf{r} = \frac{\partial\phi}{\partial u^i} du^i . \tag{2.35}$$

Here, the contravariant component du^i in (2.35) can be rewritten in the form $\mathbf{e}^i \cdot d\mathbf{r}$ since $d\mathbf{r} = \mathbf{e}_i du^i$. Then, (2.35) becomes

$$\left(\nabla\phi - \frac{\partial\phi}{\partial u^i}\,\mathbf{e}^i\right) \cdot d\mathbf{r} = 0 . \tag{2.36}$$

Since the displacement $d\mathbf{r}$ is arbitrary, we obtain

$$\nabla\phi = \frac{\partial\phi}{\partial u^i}\,\mathbf{e}^i . \tag{2.37}$$

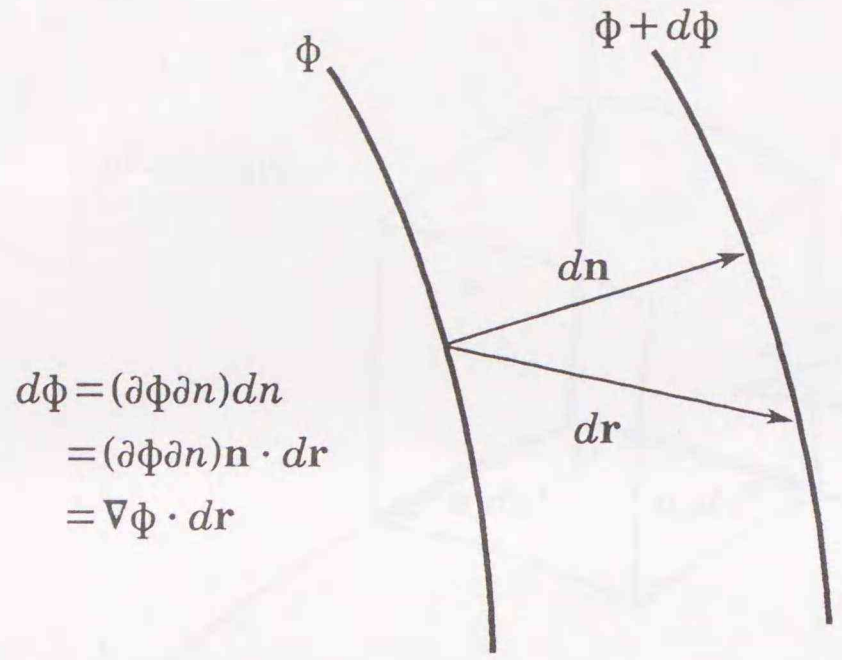

Fig. 2.3 Definition of the gradient

The divergence of a vector function **F**, which represents the flux of the vector **F** through a closed surface of an infinitesimal volume, is defined by

$$\nabla \cdot \mathbf{F} = \lim_{S \to 0} \frac{1}{V} \int_S \mathbf{F} \cdot d\mathbf{S} \,. \tag{2.38}$$

In order to derive the divergence in the coordinates (u^1, u^2, u^3), we consider the infinitesimal volume shown in Fig. 2.4. The net flux $d\Phi_2$ passing through the surfaces of $u^2 + du^2$ and u^2 is given by

$$d\Phi_2 = \left[\mathbf{F} \cdot (\mathbf{e}_3 \times \mathbf{e}_1)\, du^1 du^3 \right]_{u^2 + du^2} - \left[\mathbf{F} \cdot (\mathbf{e}_3 \times \mathbf{e}_1)\, du^1 du^3 \right]_{u^2}$$

$$= \frac{\partial}{\partial u^2} (\mathbf{F} \cdot \mathbf{e}_3 \times \mathbf{e}_1)\, du^1 du^2 du^3 \,. \tag{2.39}$$

Since the vector **F** can be written in the form $F^i \mathbf{e}_i$, we have $\mathbf{F} \cdot (\mathbf{e}_3 \times \mathbf{e}_1) = \sqrt{g}\, F^2$. Then (2.39) becomes

$$d\Phi_2 = \frac{1}{\sqrt{g}} \frac{\partial}{\partial u^2} (\sqrt{g}\, F^2)\, dv \,. \tag{2.40}$$

Calculating the other fluxes $d\Phi_1$ and $d\Phi_3$ in the same manner and inserting $d\Phi_i$ into (2.38), we obtain the divergence in (u^1, u^2, u^3) as follows :

$$\nabla \cdot \mathbf{F} = \frac{1}{\sqrt{g}} \frac{\partial}{\partial u^i} (\sqrt{g}\, F^i) \,. \tag{2.41}$$

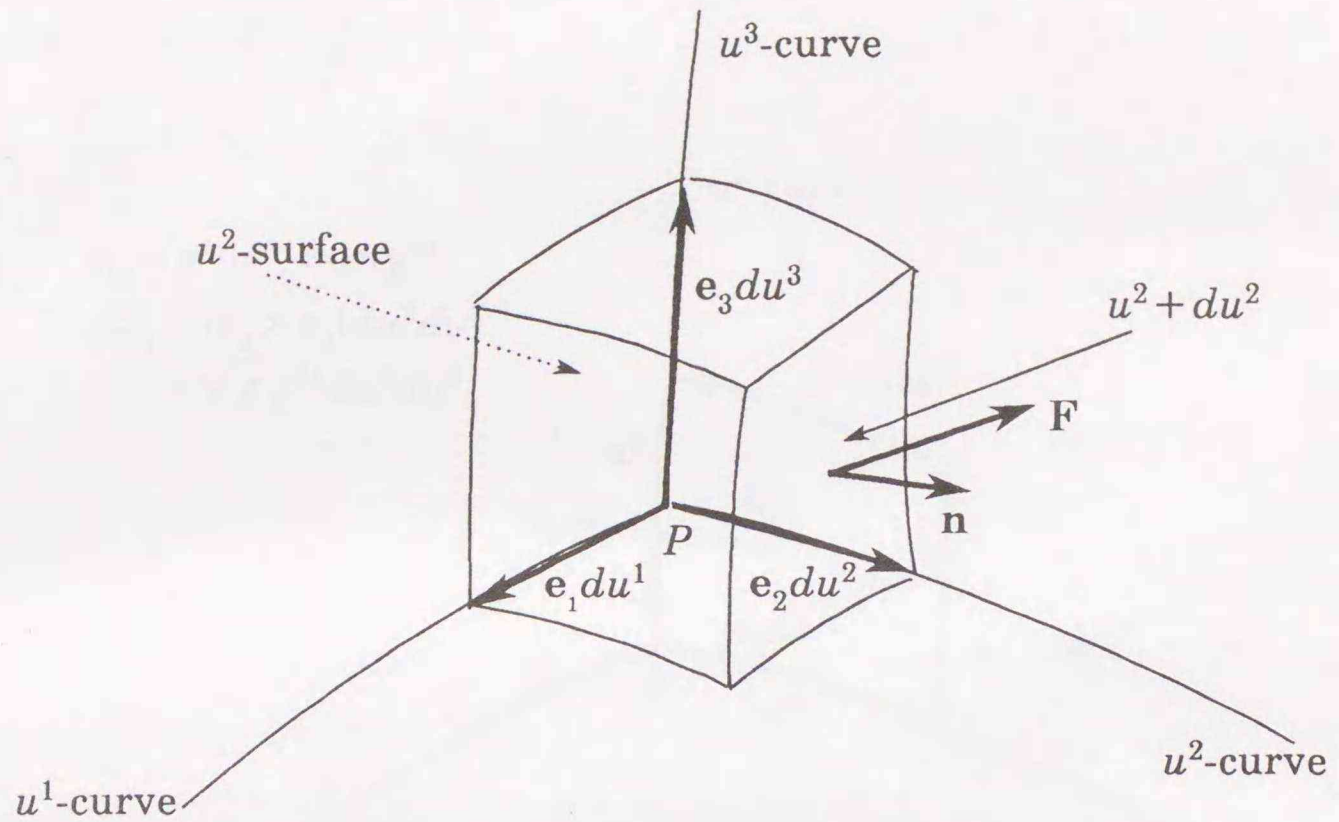

Fig. 2.3 Definition of the divergence

The rotation of a vector F is defined as a line integral around an infinitesimal closed pass shown in Fig. 2.4. The rotation of a vector F has the following component in a direction of a unit normal vector **n**,

$$\mathbf{n} \cdot (\nabla \times \mathbf{F}) = \lim_{C \to 0} \frac{1}{S} \int_C \mathbf{F} \cdot d\mathbf{s} . \tag{2.42}$$

When the normal vector $\mathbf{n}_1$ of the closed pass lying on the u^2-surface is chosen as the normal vector **n** in (2.42), the line integral dl_1 can be estimated as follows :

$$\begin{aligned} dl_1 &= \left[\mathbf{F} \cdot \mathbf{e}_3 du^3 \right]_{u^2 + du^2} - \left[\mathbf{F} \cdot \mathbf{e}_3 du^3 \right]_{u^2} - \left[\mathbf{F} \cdot \mathbf{e}_2 du^2 \right]_{u^3 + du^3} + \left[\mathbf{F} \cdot \mathbf{e}_2 du^2 \right]_{u^3} \\ &= \frac{\partial}{\partial u^2} (\mathbf{F} \cdot \mathbf{e}_3) du^2 du^3 - \frac{\partial}{\partial u^3} (\mathbf{F} \cdot \mathbf{e}_2) du^2 du^3 \\ &= \left(\frac{\partial F_3}{\partial u^2} - \frac{\partial F_2}{\partial u^3} \right) du^2 du^3 \end{aligned} \tag{2.43}$$

The other components dl_2 and dl_3 are easily obtained similarly. The substitution of them into (2.42) yields

$$\mathbf{n}_1 = \mathbf{e}^1/|\mathbf{e}^1| = \mathbf{e}^1/g^{11}$$
$$dS_1 = |\mathbf{e}_2 \times \mathbf{e}_3| du^2 du^3$$
$$= \sqrt{g}\, g^{11} du^2 du^3$$

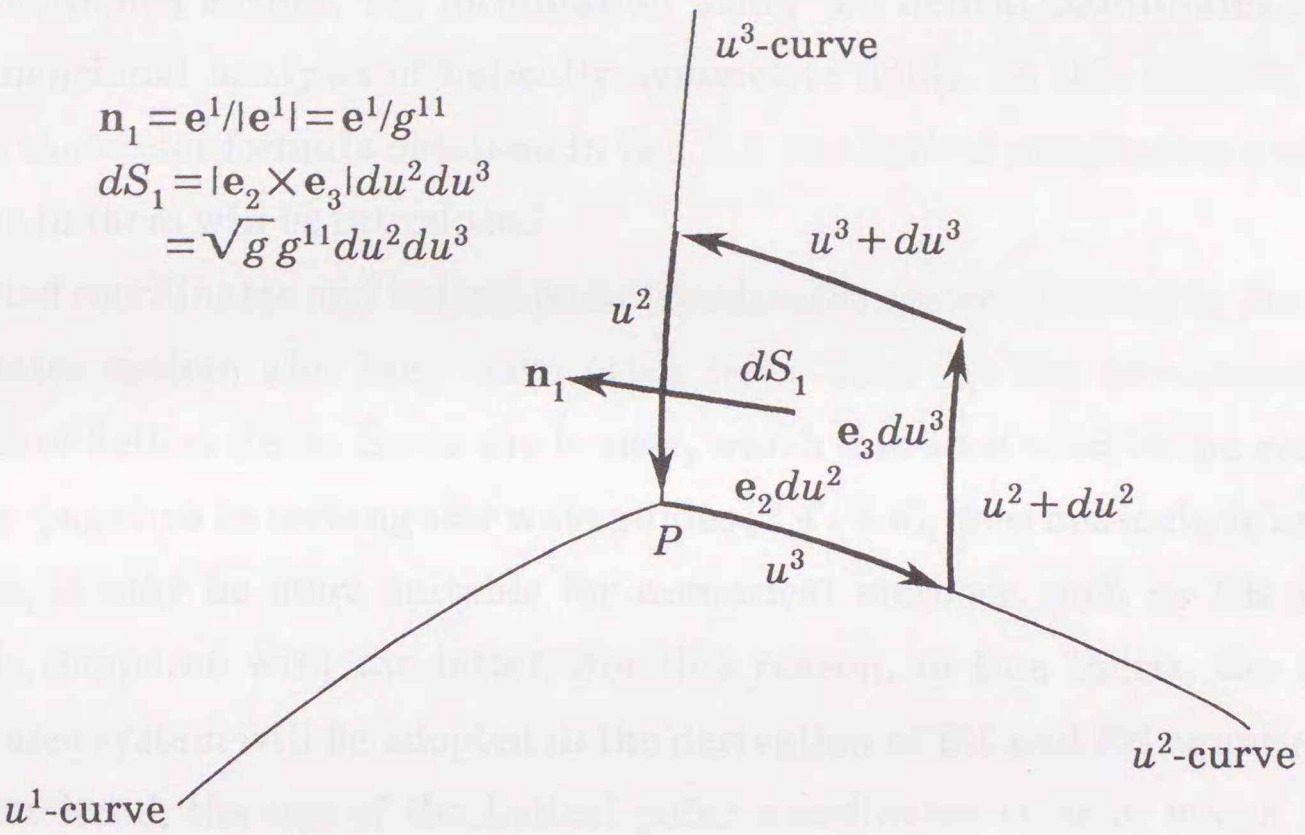

Fig. 2.4 Definition of the rotation

$$\mathbf{e}^1 \cdot (\nabla \times \mathbf{F}) = \frac{1}{\sqrt{g}} \left(\frac{\partial F_3}{\partial u^2} - \frac{\partial F_2}{\partial u^3} \right),$$
$$\mathbf{e}^2 \cdot (\nabla \times \mathbf{F}) = \frac{1}{\sqrt{g}} \left(\frac{\partial F_1}{\partial u^3} - \frac{\partial F_3}{\partial u^1} \right),$$
$$\mathbf{e}^3 \cdot (\nabla \times \mathbf{F}) = \frac{1}{\sqrt{g}} \left(\frac{\partial F_2}{\partial u^1} - \frac{\partial F_1}{\partial u^2} \right). \tag{2.44}$$

Consequently, the rotation $\nabla \times \mathbf{F}$ is expressed in the form

$$\nabla \times \mathbf{F} = \frac{1}{\sqrt{g}} \left[\left(\frac{\partial F_3}{\partial u^2} - \frac{\partial F_2}{\partial u^3} \right) \mathbf{e}_1 + \left(\frac{\partial F_1}{\partial u^3} - \frac{\partial F_3}{\partial u^1} \right) \mathbf{e}_2 + \left(\frac{\partial F_2}{\partial u^1} - \frac{\partial F_1}{\partial u^2} \right) \mathbf{e}_3 \right]. \tag{2.45}$$

The scalar Laplacian is defined by

$$\nabla^2 \phi = \nabla \cdot \nabla \phi . \tag{2.46}$$

Hence, rewriting (2.37) in terms of contravariant components and inserting it in (2.41), the function $\nabla^2 \phi$ is written in the explicit form

$$\nabla^2 \phi = \frac{1}{\sqrt{g}} \frac{\partial}{\partial u^i} \left(\sqrt{g}\, g^{ij} \frac{\partial \phi}{\partial u^j} \right). \tag{2.47}$$

2.2 Helical coordinates system

As mentioned earlier, the formulation using the helical coordinates leads to two-dimensional analysis of helically symmetric fields. In this section, on the basis of the vector formula obtained in Sec. 2.1, the helical coordinates and vector calculus in them will be introduced.

Twisted coordinates and helical polar coordinates systems belong to the helical coordinates system and they have often been used for the two-dimensional analysis of helical fields. Since the former, which has been used in the studies of wave propagation in rectangular waveguides [2.4 - 2.6], does not include an angle variable, it may be more suitable for numerical methods such as BE and FE methods compared with the latter. For this reason, in this thesis, the twisted coordinates system will be adopted in the derivation of BE and FE equations. On the other hand, the use of the helical polar coordinates system, which has an angle variable and, therefore, is suitable for the analysis of fields surrounding a circular or round boundary such as helically symmetric nuclear fusion plasmas, enables us to derive fundamental solutions (the Green functions in free space) of helically symmetric fields.

2.2.1 Twisted coordinates system [2.4, 2.5]

The twisted coordinates (X, Y, Z) are defined as

$$\begin{aligned} X &= x\cos(hz) + y\sin(hz), \\ Y &= y\cos(hz) - x\sin(hz), \\ Z &= z, \end{aligned} \tag{2.48}$$

where (x, y, z) are the Cartesian coordinates and h is the helical wave number ($h=2\pi/L$, where L is the distance in which the X, Y-axes make one complete rotation, and L is sometimes called pitch). The inverse relations are given by

$$\begin{aligned} x &= X\cos(hz) - Y\sin(hz), \\ y &= Y\cos(hz) + X\sin(hz), \\ z &= Z. \end{aligned} \tag{2.49}$$

Figure 2.5 illustrates the relation between the twisted and Cartesian coordinates on the surface of $Z=$constant. As shown in this figure, the orthogonal axes X and

Y are rotated with respect to fixed Cartesian axes x, y and the angle of rotation is proportional to the longitudinal axis z.

Figure 2.6 shows a three-dimensional view of the twisted coordinates system and a twisted column of pitch L with a rectangular cross-section.

In order to see an example of helical symmetry, let us consider here a scalar potential problem for ϕ in the column assuming that a boundary condition on the boundary ∂V is independent from Z. This boundary condition can be expressed by $\phi = \phi(X, Y)$ on ∂V. Since the variables X and Y depend on x, y and z, the field ϕ is three dimensional in the Cartesian coordinates system. Note here that $\partial/\partial z$ does not equal $\partial/\partial Z$ in general, *i.e.*,

$$\begin{aligned}\frac{\partial}{\partial z} &= \frac{\partial X}{\partial z}\frac{\partial}{\partial X} + \frac{\partial Y}{\partial z}\frac{\partial}{\partial Y} + \frac{\partial}{\partial Z} \\ &= hY\frac{\partial}{\partial X} - hX\frac{\partial}{\partial Y} + \frac{\partial}{\partial Z}\end{aligned} \tag{2.50}$$

The solutions to the problem can be described in terms of only the transverse space variables X and Y while they are the functions of x, y and z. That is, twisted coordinates system reduces the dimension of the problem by one. Since the solutions do not change along Z-axis, they are said to have a symmetry with respect to Z. This symmetry has been called helical symmetry.

In the twisted coordinates, the position vector $\mathbf{r}$ is written in the form

$$\mathbf{r} = [X\cos(hz) - Y\sin(hz)]\mathbf{i} + [X\sin(hz) + Y\cos(hz)]\mathbf{j} + Z\mathbf{k}\,. \tag{2.51}$$

From this equation and (2.3), the unitary vectors are derived as follows :

$$\begin{bmatrix}\mathbf{e}_X \\ \mathbf{e}_Y \\ \mathbf{e}_Z\end{bmatrix} = \begin{bmatrix}\cos(hz) & \sin(hz) & 0 \\ -\sin(hz) & \cos(hz) & 0 \\ -hy & hx & 1\end{bmatrix}\begin{bmatrix}\mathbf{i} \\ \mathbf{j} \\ \mathbf{k}\end{bmatrix} \tag{2.52}$$

On the other hand, the reciprocal unitary vectors are obtained from (2.13) and (2.48),

$$\begin{bmatrix}\mathbf{e}^X \\ \mathbf{e}^Y \\ \mathbf{e}^Z\end{bmatrix} = \begin{bmatrix}\cos(hz) & \sin(hz) & -hx\sin(hz) + hy\cos(hz) \\ -\sin(hz) & \cos(hz) & -hx\cos(hz) - hy\sin(hz) \\ 0 & 0 & 1\end{bmatrix}\begin{bmatrix}\mathbf{i} \\ \mathbf{j} \\ \mathbf{k}\end{bmatrix} \tag{2.53}$$

As seen in Sec. 2.1.4, the covariant components (F_X, F_Y, F_Z) and contravariant

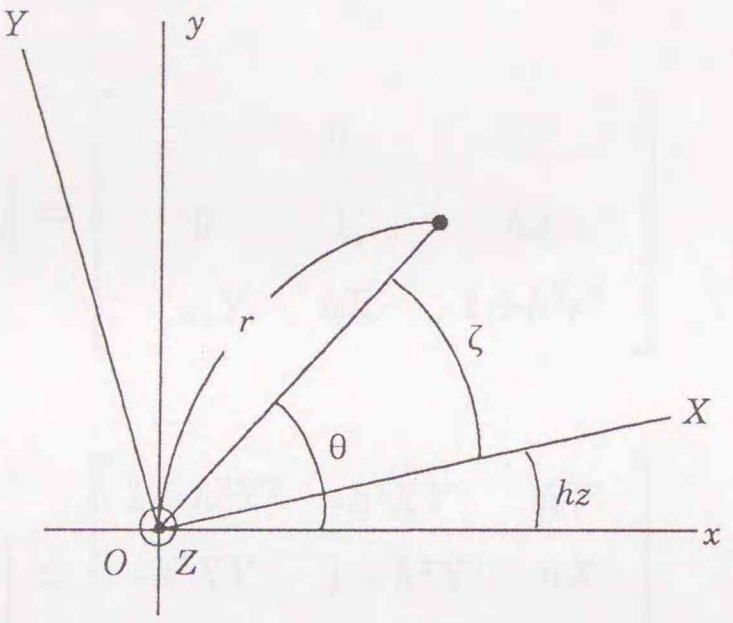

Fig. 2.5 Twisted Coordinates (X, Y, Z) and Cartesian coordinates (x, y, z)

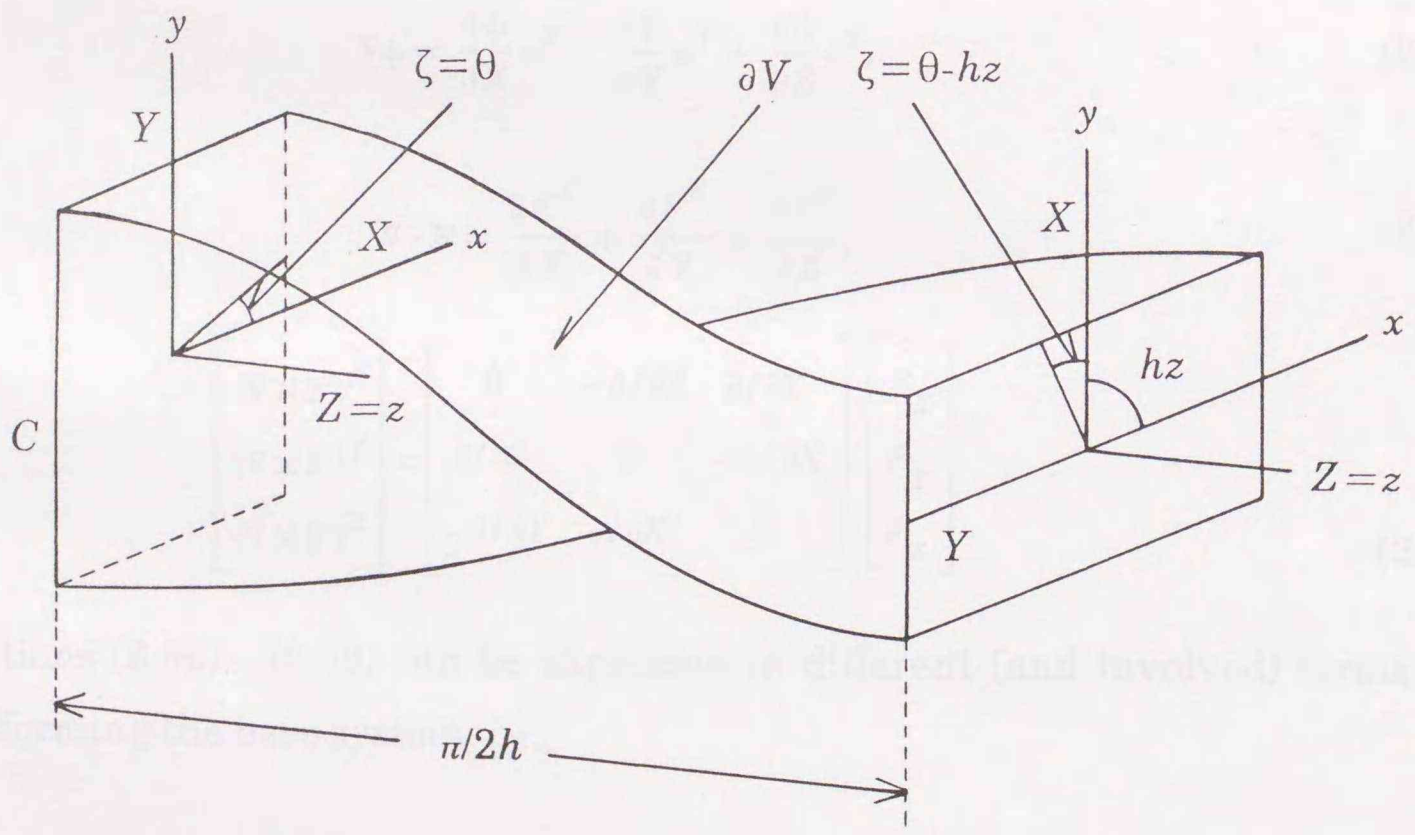

Fig. 2.6 A three-dimensional view of twisted Coordinates (X, Y, Z)

components (F^X, F^Y, F^Z) of a vector F are related to its Cartesian components (F_x, F_y, F_z) in the same forms as (2.52) and (2.53), respectively. Substituting (2.52) and (2.53) into (2.15) and (2.16), we have the covariant and contravariant metric tensors,

$$\left[g_{ij}\right] = \begin{bmatrix} 1 & 0 & -hY \\ 0 & 1 & hX \\ -hY & hX & 1+h^2r^2 \end{bmatrix}, \tag{2.54}$$

$$\left[g^{ij}\right] = \begin{bmatrix} 1+h^2Y^2 & -h^2XY & hY \\ -h^2XY & 1+h^2X^2 & -hX \\ hY & -hX & 1 \end{bmatrix}. \tag{2.55}$$

where $r^2 = X^2 + Y^2$. The Jacobian $\sqrt{g}$ is proved to be unit.

One can derive the gradient, divergence and rotation in the twisted coordinates from (2.37), (2.41) and (2.45) as follows :

$$\nabla\phi = \frac{\partial\phi}{\partial X}\mathbf{e}^X + \frac{\partial\phi}{\partial Y}\mathbf{e}^Y + \frac{\partial\phi}{\partial Z}\mathbf{e}^Z, \tag{2.56}$$

$$\nabla\cdot\mathbf{F} = \frac{\partial F^X}{\partial X} + \frac{\partial F^Y}{\partial Y} + \frac{\partial F^Z}{\partial Z}, \tag{2.57}$$

$$\begin{bmatrix} (\nabla\times\mathbf{F})^X \\ (\nabla\times\mathbf{F})^Y \\ (\nabla\times\mathbf{F})^Z \end{bmatrix} = \begin{bmatrix} 0 & -\partial/\partial Z & \partial/\partial Y \\ \partial/\partial Z & 0 & -\partial/\partial X \\ -\partial/\partial Y & \partial/\partial X & 0 \end{bmatrix} \begin{bmatrix} F_X \\ F_Y \\ F_Z \end{bmatrix} \tag{2.58}$$

Equations (2.56) - (2.58) can be expressed in different (and involved) forms by transforming the base system, *i.e.*,

$$\nabla\Phi = \frac{\partial\Phi}{\partial X}[(1+h^2Y^2)\mathbf{e}_X - h^2XY\mathbf{e}_Y + hY\mathbf{e}_Z] + \frac{\partial\Phi}{\partial Y}[-h^2XY\mathbf{e}_X + (1+h^2X^2)\mathbf{e}_Y - hX\mathbf{e}_Z]$$

$$+ \frac{\partial\Phi}{\partial Z}[hY\mathbf{e}_X - hX\mathbf{e}_Y + \mathbf{e}_Z]$$

$$= \left[(1+h^2Y^2)\frac{\partial\Phi}{\partial X} - h^2XY\frac{\partial\Phi}{\partial Y} + hY\frac{\partial\Phi}{\partial Z}\right]\mathbf{e}_X + \left[-h^2XY\frac{\partial\Phi}{\partial X} + (1+h^2X^2)\frac{\partial\Phi}{\partial Y} - hX\frac{\partial\Phi}{\partial Z}\right]\mathbf{e}_Y$$

$$+ \left[hY\frac{\partial\Phi}{\partial X} - hX\frac{\partial\Phi}{\partial Y} + \frac{\partial\Phi}{\partial Z}\right]\mathbf{e}_Z \tag{2.59}$$

$$\nabla\cdot\mathbf{F} = \frac{\partial}{\partial X}[(1+h^2Y^2)F_X - h^2XYF_Y + hYF_Z] + \frac{\partial}{\partial Y}[-h^2XYF_X + (1+h^2X^2)F_Y - hXF_Z]$$

$$+ \frac{\partial}{\partial Z}[hYF_X - hXF_Y + F_Z]$$

$$= \frac{\partial F_X}{\partial X} + \frac{\partial F_Y}{\partial Y} + \frac{\partial F_Z}{\partial Z} + h\left(Y\frac{\partial F_X}{\partial Z} - X\frac{\partial F_Y}{\partial Z} + Y\frac{\partial F_Z}{\partial X} - X\frac{\partial F_Z}{\partial Y}\right)$$

$$+ h^2\left(Y^2\frac{\partial F_X}{\partial X} - XY\frac{\partial F_X}{\partial Y} - XF_X + X^2\frac{\partial F_Y}{\partial Y} - XY\frac{\partial F_Y}{\partial X} - YF_Y\right) \tag{2.60}$$

$$\begin{bmatrix}(\nabla\times\mathbf{F})^X\\(\nabla\times\mathbf{F})^Y\\(\nabla\times\mathbf{F})^Z\end{bmatrix} = \begin{bmatrix}0 & -\partial/\partial Z & \partial/\partial Y\\ \partial/\partial Z & 0 & -\partial/\partial X\\ -\partial/\partial Y & \partial/\partial X & 0\end{bmatrix}\begin{bmatrix}1 & 0 & -hY\\ 0 & 1 & hX\\ -hY & hX & 1+h^2r^2\end{bmatrix}\begin{bmatrix}F_X\\F_Y\\F_Z\end{bmatrix} \tag{2.61}$$

$$\begin{bmatrix}(\nabla\times\mathbf{F})_X\\(\nabla\times\mathbf{F})_Y\\(\nabla\times\mathbf{F})_Z\end{bmatrix} = \begin{bmatrix}1 & 0 & -hY\\ 0 & 1 & hX\\ -hY & hX & 1+h^2r^2\end{bmatrix}\begin{bmatrix}0 & -\partial/\partial Z & \partial/\partial Y\\ \partial/\partial Z & 0 & -\partial/\partial X\\ -\partial/\partial Y & \partial/\partial X & 0\end{bmatrix}\begin{bmatrix}F^X\\F^Y\\F^Z\end{bmatrix} \tag{2.62}$$

$$\begin{bmatrix}(\nabla\times\mathbf{F})_X\\(\nabla\times\mathbf{F})_Y\\(\nabla\times\mathbf{F})_Z\end{bmatrix} = \begin{bmatrix}1 & 0 & -hY\\ 0 & 1 & hX\\ -hY & hX & 1+h^2r^2\end{bmatrix}\begin{bmatrix}0 & -\partial/\partial Z & \partial/\partial Y\\ \partial/\partial Z & 0 & -\partial/\partial X\\ -\partial/\partial Y & \partial/\partial X & 0\end{bmatrix}\begin{bmatrix}1+h^2Y^2 & -h^2XY & hY\\ -h^2XY & 1+h^2X^2 & -hX\\ hY & -hX & 1\end{bmatrix}\begin{bmatrix}F_X\\F_Y\\F_Z\end{bmatrix} \tag{2.63}$$

Finally, the (scalar) Laplacian in (X, Y, Z) is given by

$$\nabla^2\Phi = (1+h^2Y^2)\frac{\partial^2\Phi}{\partial X^2} - 2h^2XY\frac{\partial^2\Phi}{\partial X\partial Y} + (1+h^2X^2)\frac{\partial^2\Phi}{\partial Y^2} - h^2X\frac{\partial\Phi}{\partial X} - h^2Y\frac{\partial\Phi}{\partial Y}$$

$$+ \frac{\partial^2\Phi}{\partial Z^2} + 2hY\frac{\partial^2\Phi}{\partial X\partial Z} - 2hX\frac{\partial^2\Phi}{\partial Y\partial Z} \tag{2.64}$$

2.2.2 Helical polar coordinates [e. g. 2.7, 2.8]

The helical polar coordinates (r, ζ, Z), which can be regarded as the polar coordinates for the twisted coordinates as shown in Figs. 2.5 and 2.6, are defined by :

$$\begin{aligned} r &= \sqrt{x^2 + y^2} = \sqrt{X^2 + Y^2} \\ \zeta &= tan^{-1}\left(\frac{Y}{X}\right) \\ Z &= z \end{aligned} \tag{2.65}$$

The formula for the helical polar coordinates are obtained in the same manner as the previous section. Only the results are summarized below.

The unitary vectors :

$$\begin{bmatrix} \mathbf{e}_r \\ \mathbf{e}_\zeta \\ \mathbf{e}_Z \end{bmatrix} = \begin{bmatrix} 1 & 0 & 0 \\ 0 & r & 0 \\ 0 & hr & 1 \end{bmatrix} \begin{bmatrix} \boldsymbol{\rho} \\ \mathbf{t} \\ \mathbf{k} \end{bmatrix} \tag{2.66}$$

The reciprocal unitary vectors :

$$\begin{bmatrix} \mathbf{e}^r \\ \mathbf{e}^\zeta \\ \mathbf{e}^Z \end{bmatrix} = \begin{bmatrix} 1 & 0 & 0 \\ 0 & 1/r & -h \\ 0 & 0 & 1 \end{bmatrix} \begin{bmatrix} \boldsymbol{\rho} \\ \mathbf{t} \\ \mathbf{k} \end{bmatrix} \tag{2.67}$$

where $\boldsymbol{\rho}$, $\mathbf{t}$ and $\mathbf{k}$ are the basis vectors of cylindrical coordinates (r, θ, z). The covariant components (F_r, F_ζ, F_Z) and contravariant components (F^r, F^ζ, F^Z) of a vector $\mathbf{F}$ are related to its cylindrical components (F_r, F_θ, F_z) in the same forms as (2.66) and (2.67), respectively.

Covariant metric tensor :

$$\left[g_{ij}\right] = \begin{bmatrix} 1 & 0 & 0 \\ 0 & r^2 & hr^2 \\ 0 & hr^2 & 1+h^2r^2 \end{bmatrix} \tag{2.68}$$

Contravariant metric tensor :

$$\left[g^{ij}\right]=\begin{bmatrix} 1 & 0 & 0 \\ 0 & h^2+1/r^2 & -h \\ 0 & -h & 1 \end{bmatrix} \tag{2.69}$$

The Jacobian $\sqrt{g}$ is equal to r.

Covariant components of gradient of a scalar function ϕ :

$$\nabla\phi = \frac{\partial\Phi}{\partial r}\mathbf{e}^r + \frac{\partial\Phi}{\partial\zeta}\mathbf{e}^\zeta + \frac{\partial\Phi}{\partial Z}\mathbf{e}^Z \tag{2.70}$$

Contravariant components of gradient of a scalar function ϕ :

$$\begin{aligned}\nabla\phi &= \frac{\partial\Phi}{\partial r}\mathbf{e}_r + \frac{\partial\Phi}{\partial\zeta}\left[\left(h^2+\frac{1}{r^2}\right)\mathbf{e}_\zeta - h\mathbf{e}_Z\right] + \frac{\partial\Phi}{\partial Z}\left(-h\mathbf{e}_\zeta + \mathbf{e}_Z\right) \\ &= \frac{\partial\Phi}{\partial r}\mathbf{e}_r + \left[\left(h^2+\frac{1}{r^2}\right)\frac{\partial\Phi}{\partial\zeta} - h\frac{\partial\Phi}{\partial Z}\right]\mathbf{e}_\zeta + \left(-h\frac{\partial\Phi}{\partial\zeta} + \frac{\partial\Phi}{\partial Z}\right)\mathbf{e}_Z\end{aligned} \tag{2.71}$$

Divergence of a vector function **F** (represented in terms of contravariant components of **F**) :

$$\nabla\cdot\mathbf{F} = \frac{1}{r}\frac{\partial}{\partial r}(rF^r) + \frac{\partial F^\zeta}{\partial\zeta} + \frac{\partial F^Z}{\partial Z} \tag{2.72}$$

Divergence of a vector function **F** (represented in terms of covariant components of **F**) :

$$\begin{aligned}\nabla\cdot\mathbf{F} &= \frac{1}{r}\frac{\partial}{\partial r}(rF^r) + \frac{\partial}{\partial\zeta}\left[\left(h^2+\frac{1}{r^2}\right)F_\zeta - hF_Z\right] + \frac{\partial}{\partial Z}\left(-hF_\zeta + F_Z\right) \\ &= \frac{1}{r}\frac{\partial}{\partial r}(rF^r) + \frac{1}{r^2}\frac{\partial F_\zeta}{\partial\zeta} + \frac{\partial F_Z}{\partial Z} - h\left(\frac{\partial F_Z}{\partial\zeta} + \frac{\partial F_\zeta}{\partial Z}\right) + h^2\frac{\partial F_\zeta}{\partial\zeta}\end{aligned} \tag{2.73}$$

Contravariant components of rotation of a vector function **F** (represented in terms of covariant components of **F**) :

$$\begin{bmatrix}(\nabla\times\mathbf{F})^r \\ (\nabla\times\mathbf{F})^\zeta \\ (\nabla\times\mathbf{F})^Z\end{bmatrix} = \frac{1}{r}\begin{bmatrix} 0 & -\partial/\partial Z & \partial/\partial\zeta \\ \partial/\partial Z & 0 & -\partial/\partial r \\ -\partial/\partial\zeta & \partial/\partial r & 0 \end{bmatrix}\begin{bmatrix} F_r \\ F_\zeta \\ F_Z \end{bmatrix} \tag{2.74}$$

Contravariant components of rotation of a vector function **F** (represented in terms of covariant components of **F**) :

$$\begin{bmatrix} (\nabla\times\mathbf{F})^r \\ (\nabla\times\mathbf{F})^\zeta \\ (\nabla\times\mathbf{F})^Z \end{bmatrix} = \frac{1}{r}\begin{bmatrix} 0 & -\partial/\partial Z & \partial/\partial\zeta \\ \partial/\partial Z & 0 & -\partial/\partial r \\ -\partial/\partial\zeta & \partial/\partial r & 0 \end{bmatrix}\begin{bmatrix} 1 & 0 & 0 \\ 0 & r^2 & hr^2 \\ 0 & hr^2 & 1+h^2r^2 \end{bmatrix}\begin{bmatrix} F^r \\ F^\zeta \\ F^Z \end{bmatrix} \tag{2.75}$$

Covariant components of rotation of a vector function **F** (represented in terms of contravariant components of **F**) :

$$\begin{bmatrix} (\nabla\times\mathbf{F})_r \\ (\nabla\times\mathbf{F})_\zeta \\ (\nabla\times\mathbf{F})_Z \end{bmatrix} = \frac{1}{r}\begin{bmatrix} 1 & 0 & 0 \\ 0 & r^2 & hr^2 \\ 0 & hr^2 & 1+h^2r^2 \end{bmatrix}\begin{bmatrix} 0 & -\partial/\partial Z & \partial/\partial\zeta \\ \partial/\partial Z & 0 & -\partial/\partial r \\ -\partial/\partial\zeta & \partial/\partial r & 0 \end{bmatrix}\begin{bmatrix} F^r \\ F^\zeta \\ F^Z \end{bmatrix} \tag{2.76}$$

Covariant components of rotation of a vector function **F** (represented in terms of covariant components of **F**) :

$$\begin{bmatrix} (\nabla\times\mathbf{F})_r \\ (\nabla\times\mathbf{F})_\zeta \\ (\nabla\times\mathbf{F})_Z \end{bmatrix} = \frac{1}{r}\begin{bmatrix} 1 & 0 & 0 \\ 0 & r^2 & hr^2 \\ 0 & hr^2 & 1+h^2r^2 \end{bmatrix}\begin{bmatrix} 0 & -\partial/\partial Z & \partial/\partial\zeta \\ \partial/\partial Z & 0 & -\partial/\partial r \\ -\partial/\partial\zeta & \partial/\partial r & 0 \end{bmatrix}\begin{bmatrix} 1 & 0 & 0 \\ 0 & h^2+1/r^2 & -h \\ 0 & -h & 1 \end{bmatrix}\begin{bmatrix} F_r \\ F_\zeta \\ F_Z \end{bmatrix} \tag{2.77}$$

The (scalar) Laplacian :

$$\nabla^2\Phi = \frac{1}{r}\frac{\partial}{\partial r}\left(r\frac{\partial\Phi}{\partial r}\right) + \left(\frac{1}{r^2}+h^2\right)\frac{\partial^2\Phi}{\partial\zeta^2} + \frac{\partial^2\Phi}{\partial Z^2} - 2h\frac{\partial^2\Phi}{\partial\zeta\partial Z} \tag{2.78}$$

REFERENCES

2.1 J. A. Stratton, *Electromagnetic Theory*, McGraw-Hill, New York, pp.38-47, 1941.

2.2 I. Hirota and K. Chiyoda, "Vector Analysis in General Curvilinear Coordinates, - On the Magnetic Field in Plasma Confinement -", *Bul. Electrotech. Lab.*, 44, pp.641-678, 1980.

2.3 L. A. Pipes and L. R. Harvill, *Applied Mathematics for Engineers and Physicists*, McGraw-Hill, New York, pp. 937-952, 1971.

2.4 L. Lewin, *Theory of Waveguides*, Newnes-Butherworths, London, pp.96-101, 1975.

2.5 H. Yabe and Y. Mushiake, "An Analysis of a Hybrid-Mode in a Twisted Rectangular Waveguide", *IEEE Trans. Microwave Theory Tech.*, **32**, pp.65-71, 1984.

2.6 H. Yabe, K. Nishio and Y. Mushiake, "Dispersion Characteristics of Twisted Rectangular Waveguides", *ibid*, **32**, pp.91-96, 1984.

2.7 H. Grad, "Toroidal Confinement of a Plasma", *Phys. Fluids*, **10**, pp. 137-154, 1967.

2.8 J. P. Freidberg, "Stability of a Finite β, $l=2$ stellarator", *Phys. Fluids*, **16**, pp. 1349-1358, 1973.

CHAPTER 3

FUNDAMENTAL SOLUTIONS

This chapter derives the fundamental solutions to Helmholtz-type equations for helically symmetric systems, and moreover evaluates the computing times and singularity of them. The fundamental solutions discussed here will play an important role in the BE analysis described in the later chapters.

In Sec. 3.1, the fundamental solutions, which involve infinite series of the modified Bessel functions, will be derived by integrating the three dimensional fundamental solution along a source helix. Section 3.2 deals with a numerical evaluation of the fundamental solutions. In particular, the convergence of the infinite series in the fundamental solutions will be improved by a semi-analytical method. Moreover, the computing times of the fundamental solutions in the infinite-series form will be compared with those of the integral representations. In Sec. 3.3, the singularity of the fundamental solutions will be discussed.

3.1 Derivation of fundamental solutions [3.1]

Let us consider the fundamental solution **G** to the modified Helmholtz equation in the vectorial form for helically symmetric systems. The solution **G**, for a vectorial source with magnitude 4π in the direction **u** on a helix, satisfies

$$\nabla^2 \mathbf{G} - k^2 \mathbf{G} = -4\pi \mathbf{u} \frac{\delta(r-r_0)\delta(\zeta-\zeta_0)}{r}, \tag{3.1}$$

where we use the helical polar coordinates (r, ζ, Z) and the tangential vector **u** is defined by

$$\begin{aligned} \mathbf{u} &= \partial \mathbf{r}/\partial z_0 \\ &= h r_0 \mathbf{t}' + \mathbf{k} \\ &= \boldsymbol{\rho} h r_0 \sin(\theta-\theta_0) + \mathbf{t}\, h r_0 \cos(\theta-\theta_0) + \mathbf{k}, \end{aligned} \tag{3.2}$$

where $\boldsymbol{\rho}$, **t** and **k** are the unit basis vectors of the cylindrical coordinates (r, θ, z), and the prime denotes the vector at the source point.

A helical source (r_0, ζ_0) and field point (r, θ, z) are illustrated in Fig. 3.1. Notice that the fields produced by this source have helical symmetry.

In terms of the vectors $\boldsymbol{\rho}$, **t** and **k** at the field point, the solution **G** to (3.1) can be expressed in the following integral form

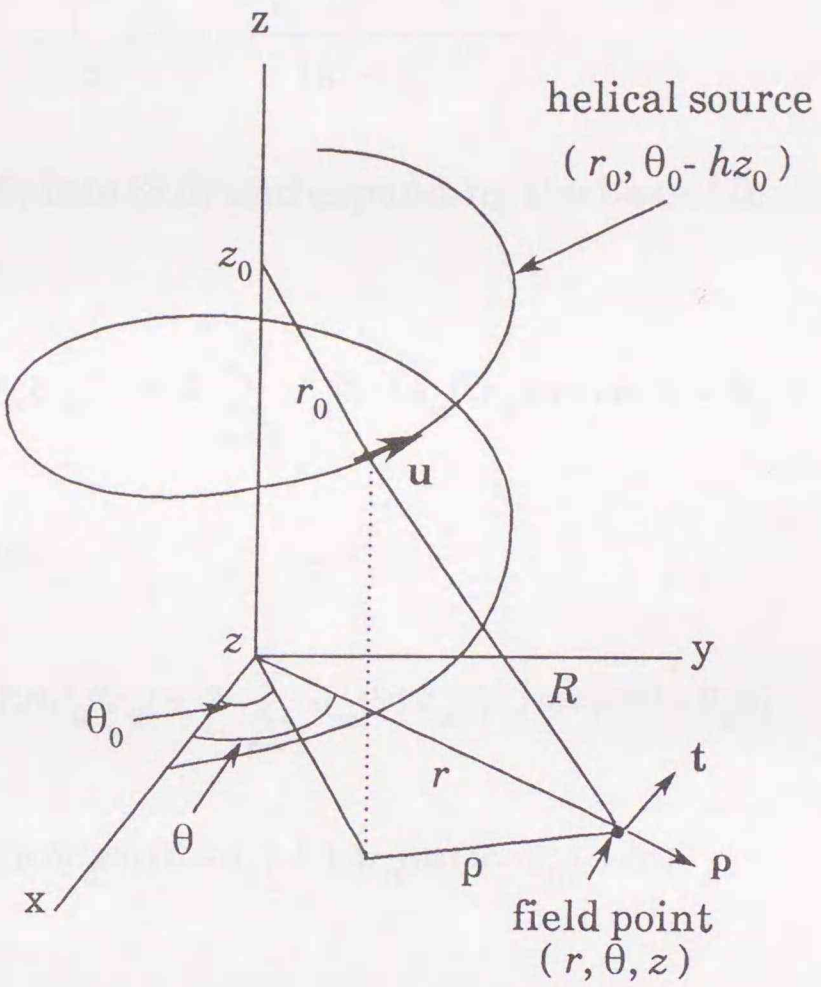

Fig.3.1 Helical source and field point

$$\mathbf{G} = \int_{-\infty}^{\infty} \frac{e^{-kR}}{R} \{ \boldsymbol{\rho}\, hr_0 \sin(\theta - \theta_0) + \mathbf{t}\, hr_0 \cos(\theta - \theta_0) + \mathbf{k} \}\, dz_0, \tag{3.3}$$

where $R = \{ r^2 + r_0^2 - 2rr_0 \cos(\theta - \theta_0) + (z - z_0)^2 \}^{1/2}$ and θ_0 is the function of z_0 because the integration is performed on a helix $r = r_0$, $\zeta = \zeta_0$ ($= \theta_0 - hz_0$). The vector function G denotes the superposition of the fields produced by infinitesimal vectorial sources on a helix. In order to evaluate the integral (3.3), we make use of the Fourier-Bessel theorem which states that

$$f(x) = \int_0^{\infty} \xi J_\nu(\xi x)\, d\xi \int_0^{\infty} \lambda f(\lambda) J_\nu(\xi\lambda)\, d\lambda, \tag{3.4}$$

where J_ν is the Bessel function of the first kind of ν-th order. Applying this theorem for $\nu = 0$ to the function e^{-kR} / R in (3.4), one can rewrite it as follows :

$$\frac{e^{-kR}}{R} = \int_0^{\infty} \xi J_0(\xi\rho)\, d\xi \int_0^{\infty} \frac{\lambda}{(\lambda^2 + Z^2)^{1/2}} e^{-k(\lambda^2 + Z^2)^{1/2}} J_0(\xi\lambda)\, d\lambda, \tag{3.5}$$

where $\rho = (R^2 - Z^2)^{1/2}$ and $Z = | z - z_0 |$. The integral with respect to λ can be performed as follows :

$$\frac{e^{-kR}}{R} = \int_0^\infty \xi J_0(\xi\rho) \frac{e^{-Z(k^2+\xi^2)^{1/2}}}{(k^2+\xi^2)^{1/2}} d\xi. \tag{3.6}$$

Moreover, substituting (3.6) into (3.3) and expanding the Bessel function by use of the addition theorem [3.2],

$$J_0(\xi\rho) = J_0(\xi r) J_0(\xi r_0) + 2 \sum_{m=1}^{\infty} J_m(\xi r) J_m(\xi r_0) \cos[m(\theta - \theta_0)] , \tag{3.7}$$

we obtain the representation

$$\mathbf{G} = \int_{-\infty}^{\infty} dz_0 \int_0^\infty d\xi \left[J_0(\xi r) J_0(\xi r_0) + 2 \sum_{m=1}^{\infty} J_m(\xi r) J_m(\xi r_0) \cos\{m(\theta-\theta_0)\} \right] \times \frac{\xi e^{-Z(\xi^2+k^2)^{1/2}}}{(\xi^2+k^2)^{1/2}} [\rho\, hr_0 \sin(\theta-\theta_0) + t\, hr_0 \cos(\theta-\theta_0) + k]. \tag{3.8}$$

Moreover, performing the integration in (3.8) with respect to z_0, we can obtain the θ- and z-components of G as follows (the derivation is given in A-2) :

$$G_\theta = 2hr_0 \int_0^\infty \left[P_0 Q_1 \cos(\zeta-\zeta_0) + \sum_{m=1}^{\infty} P_m Q_{m+1} \cos\{(m+1)(\zeta-\zeta_0)\} + \sum_{m=1}^{\infty} P_m Q_{m-1} \cos\{(m-1)(\zeta-\zeta_0)\} \right] d\xi, \tag{3.9}$$

$$G_z = 2 \int_0^\infty \left[P_0 Q_0 + 2 \sum_{m=1}^{\infty} P_m Q_m \cos\{m(\zeta-\zeta_0)\} \right] d\xi, \tag{3.10}$$

where

$$P_m = \xi J_m(\xi r)\, J_m(\xi r_0), \quad Q_m = (\xi^2 + m^2h^2 + k^2)^{-1}. \tag{3.11}$$

Equations (3.9) - (3.11) produce various kinds of the helically symmetric fundamental solutions. In the following, we derive three fundamental solutions considered useful in BE analysis of engineering problems.

We first consider the helically symmetric fundamental solution G to the scalar Laplace equation. It may correspond to the z-component of G given in (3.10) for $k = 0$ because the scalar source of G is not multiplied by trigonometric functions as

the z-component in (3.3) is. When evaluating (3.10), we have to pay attention to the fact that the first term of the integrand in (3.10) logarithmically diverges for $k=0$. Using the formula derived in Ref. 3.1,

$$\int_0^\infty J_0(\xi r) J_0(\xi r_0) e^{-z\xi}\, d\xi = \frac{1}{2\pi}\int_0^{2\pi} \frac{d\theta_0}{R}\,, \tag{3.12}$$

this divergence can be shown as follows :

$$\begin{aligned} 2\int_0^\infty P_0 Q_0\, d\xi &= \frac{1}{2\pi}\int_0^{2\pi} d\theta_0 \int_{-\infty}^{\infty} \frac{dz_0}{R} \\ &= \frac{1}{2\pi}\int_0^{2\pi} \left[\lim_{l\to\infty} \log \frac{l + \{l^2 + r^2 + r_0^2 - 2rr_0\cos(\theta-\theta_0)\}^{1/2}}{-l + \{l^2 + r^2 + r_0^2 - 2rr_0\cos(\theta-\theta_0)\}^{1/2}} \right] d\theta_0 \\ &= -2\log r_> + 2 \lim_{l\to\infty} \log(2l)\,, \end{aligned} \tag{3.13}$$

where $r_> \equiv max\,(r, r_0)$. This difficulty, which is due to infinity of the source, can be overcome if the divergence is canceled by an additional term in the definition of G as follows:

$$G = \int_{-\infty}^{\infty} \left[\frac{1}{R} - \frac{1}{\{a^2 + (z-z_0)^2\}^{1/2}} \right] dz_0\,, \tag{3.14}$$

where a is an arbitrary constant. Since this additional term diverges in the form,

$$\int_{-\infty}^{\infty} \frac{dz_0}{\{a^2 + (z-z_0)^2\}^{1/2}} = -2\log a + 2 \lim_{l\to\infty} \log(2l)\,, \tag{3.15}$$

the solution G defined by (3.14) comes to converge and can be expressed in the following form.

$$G = 2\log\left(\frac{a}{r_>}\right) + 4\sum_{m=1}^{\infty} \cos[m(\zeta-\zeta_0)] \int_0^\infty P_m Q_m\, d\xi\,. \tag{3.16}$$

Moreover, the integral in (3.16) can be evaluated by means of the identity [3.3],

$$\int_0^\infty P_m Q_n\, d\xi = I_m(q_n r_<) K_m(q_n r_>)\,, \qquad (n^2h^2 + k^2 > 0\,), \tag{3.17}$$

where $q_n = (n^2h^2 + k^2)^{1/2}$, $r_< \equiv min\,(r, r_0)$, I_m and K_m represent the m-th order modified Bessel functions of the first and second kind, respectively. Consequently, from (3.16) and (3.17), we obtain a representation of G as follows :

$$G = 2\log\left(\frac{a}{r_>}\right) + 4\sum_{m=1}^{\infty} I_m(mhr_<)K_m(mhr_>)\cos[m(\zeta-\zeta_0)]. \tag{3.18}$$

The representation (3.18) is equivalent to that introduced in Ref. 3.4 within a constant.

When $k \neq 0$ in (3.10), the z-component of **G** corresponds to the fundamental solution G_H to the scaler modified Helmholtz equation which governs, for example, the neutron diffusion and plasma sheath under some approximations [3.5]. In this case, since the divergence discussed above does not occur, we can easily obtain the representation of G_H from (3.10) and (3.17) as follows :

$$G_H = 2I_0(kr_<)K_0(kr_>) + 4\sum_{m=1}^{\infty} I_m(q_m r_<)K_m(q_m r_>)\cos[m(\zeta-\zeta_0)]. \tag{3.19}$$

Next, we deal with the helically symmetric MHD equilibrium equation which includes the vector Laplacian. When $k=0$ in (3.1), the third covariant component of **G** in the helical polar coordinates satisfies

$$\frac{1}{r}\left\{\frac{\partial}{\partial r}\left(\frac{r}{1+h^2r^2}\frac{\partial G_3}{\partial r}\right) + \frac{1}{r}\frac{\partial^2 G_3}{\partial \zeta^2}\right\} - \frac{4h}{(1+h^2r^2)^2} = -\frac{4\pi}{r}\delta(r-r_0)\delta(\zeta-\zeta_0), \tag{3.20}$$

where $G_3 = hrG_\theta + G_z$. On the other hand, the fundamental solution, G_S, to the MHD equilibrium equation satisfies [3.6]

$$\frac{h^2}{r}\left\{\frac{\partial}{\partial r}\left(\frac{r}{1+h^2r^2}\frac{\partial G_S}{\partial r}\right) + \frac{1}{r}\frac{\partial^2 G_S}{\partial \zeta^2}\right\} = -\frac{4\pi}{r}\delta(r-r_0)\delta(\zeta-\zeta_0). \tag{3.21}$$

Hence, the relation between G_S and G_3 is found to be

$$G_S = -(r^2 + r_0^2) + \frac{1}{h^2}G_3 \tag{3.22}$$

where the constant $-r_0$ is added to the right hand side for the symmetry of G_S in r and r_0. Since the function G_z defined by (3.10) logarithmically diverges as mentioned above, the definition of the fundamental solution G_S should also be modified again using the additional term helping convergence as follows :

$$G_S = -(r^2 + r_0^2) + \int_{-\infty}^{\infty} \frac{rr_0\cos(\theta-\theta_0)}{R}dz_0 + \frac{1}{h^2}\int_{-\infty}^{\infty}\left[\frac{1}{R} - \frac{1}{\{a^2+(z-z_0)^2\}^{1/2}}\right]dz_0. \tag{3.23}$$

Here, the second integral in the right hand side of (3.23) corresponds to G / h^2 obtained above. On the other hand, we can evaluate the first integral using (3.17) and the formula,

$$\int_0^\infty \frac{J_1(\xi r)\, J_1(\xi r_0)}{\xi}\, d\xi = \frac{r_<}{2r_>}, \tag{3.24}$$

as follows :

$$\begin{aligned}\int_{-\infty}^{\infty} \frac{r r_0 \cos(\theta-\theta_0)}{R}\, dz_0 = r_<^2 &+ 2rr_0 I_0(hr_<) K_0(hr_>) \cos(\zeta-\zeta_0) \\ &+ 2rr_0 \sum_{m=1}^{\infty} I_m((m+1)hr_<) K_m((m+1)hr_>) \cos[(m+1)(\zeta-\zeta_0)] \\ &+ 2rr_0 \sum_{m=2}^{\infty} I_m((m-1)hr_<) K_m((m-1)hr_>) \cos[(m-1)(\zeta-\zeta_0)].\end{aligned} \tag{3.25}$$

As a result, applying the identity (see A-3)

$$\begin{aligned}-4xy\, I_m'(mx) K_m'(my) = \\ 2xy\, I_{m-1}(mx) K_{m-1}(my) + 4\, I_m(mx) K_m(my) + 2xy\, I_{m+1}(mx) K_{m+1}(my),\end{aligned} \tag{3.26}$$

to (3.25), we can obtain the following representation

$$G_S = -r_>^2 + \frac{2}{h^2} \log\left(\frac{a}{r_>}\right) - 4rr_0 \sum_{m=1}^{\infty} I_m'(mhr_<) K_m'(mhr_>) \cos[m(\zeta-\zeta_0)]. \tag{3.27}$$

This representation is equivalent to that obtained in Ref. 3.6, which suggests that it is derived by a variable separation technique [3.7]. Appendix A-4 gives a derivation of the representation (3.27) on the basis of a variable separation.

By use of a procedure similar to the one mentioned above, the axisymmetric fundamental solutions to the Helmholtz-type equation can also be derived by considering a vector source on a ring [3.1, 3.5]. The Laplace equation and the corresponding fundamental solutions for translational, axial and helical symmetries are summarized in Table 3.1.

Table 3.1 The Laplace equation and fundamental solutions for the tree symmetric systems.

Symmetry	Laplace equation and fundamental solution	Coordinates
Translational $\partial/\partial z = 0$	$\frac{\partial^2\Phi}{\partial x^2} + \frac{\partial^2\Phi}{\partial y^2} = 0$ $G = -2\log r \ , r^2 = (x-x_0)^2 + (y-y_0)^2$	Cartesian coordinates (x, y, z)
Axial $\partial/\partial\theta = 0$	$\frac{1}{r}\frac{\partial}{\partial r}\left(r\frac{\partial\Phi}{\partial r}\right) + \frac{\partial^2\Phi}{\partial z^2} = 0$ $G = 2(r_0/r)^{1/2} k K(k)\,,\ k^2 = \frac{4r_0 r}{(r+r_o)^2+(z+z_o)^2}$ $K(k)$: The complete integral of the second kind	Cylindrical coordinates (r, θ, z)
Helical $\partial/\partial Z = 0$	$(1+h^2Y^2)\frac{\partial^2\Phi}{\partial X^2} - 2h^2XY\frac{\partial^2\Phi}{\partial X\partial Y} + (1+h^2X^2)\frac{\partial^2\Phi}{\partial Y^2} - h^2X\frac{\partial\Phi}{\partial X} - h^2Y\frac{\partial\Phi}{\partial Y} = 0$ (G : see below)	Twisted coordinates (X, Y, Z)
	$\frac{1}{r}\frac{\partial}{\partial r}\left(r\frac{\partial\Phi}{\partial r}\right) + \left(\frac{1}{r^2} + h^2\right)\frac{\partial^2\Phi}{\partial\zeta^2} = 0$ $G = \frac{2}{h}\log\left(\frac{a}{r_>}\right) + \frac{4}{h}\sum_{m=1}^{\infty} I_m(mhr_<) K_m(mhr_>)\cos[m(\zeta-\zeta_0)]$	Helical polar coordinates (r, ζ, Z)

3.2 Numerical evaluation of fundamental solutions

As described in the previous section, the fundamental solutions to helically symmetric problems can be written in two forms, that is, integral and infinite-series representations. This section deals with numerical evaluation of those solutions, especially from the view points of accuracy and computing times. First, the convergence of the infinite series in the vicinity of source points will be investigated. Next, the computing times for infinite-series representation will be compared with those for integral representation. Here, assuming that there is not significant difference in characteristics of the fundamental solutions derived in the previous section, the fundamental solution (3.14) to scalar Laplacian, which is equivalent to (3.18), is chosen as a typical example for the numerical evaluation.

3.2.1 Convergence of infinite series

Figure 3.2 shows convergence of the fundamental solution (3.18) in the vicinity of a source point located at $r_0=1.0$, $\zeta_0=0.0$. The ordinate and abscissa denote the value of the finite series G_N defined by

$$G_N = 4 \sum_{m=1}^{N} I_m(mhr_<) K_m(mhr_>) \cos[\, m(\zeta-\zeta_0)\,], \tag{3.28}$$

and the number of terms N. From Fig. 3.2, it can be seen that the convergence of the finite series becomes worse as the field point approaches the source point.

On the other hand, the modified Bessel functions in (3.28) can be expressed by the uniform asymptotic expansion [3.8]

$$I_m(mhr_<) \sim \frac{e^{m\sigma_<}}{\sqrt{2\pi m\tau_<}}[1 + O(1/m)], \tag{3.29}$$

$$K_m(mhr_>) \sim \frac{\sqrt{\pi}\, e^{-m\sigma_>}}{\sqrt{2m\tau_>}}[1 + O(1/m)], \tag{3.30}$$

where

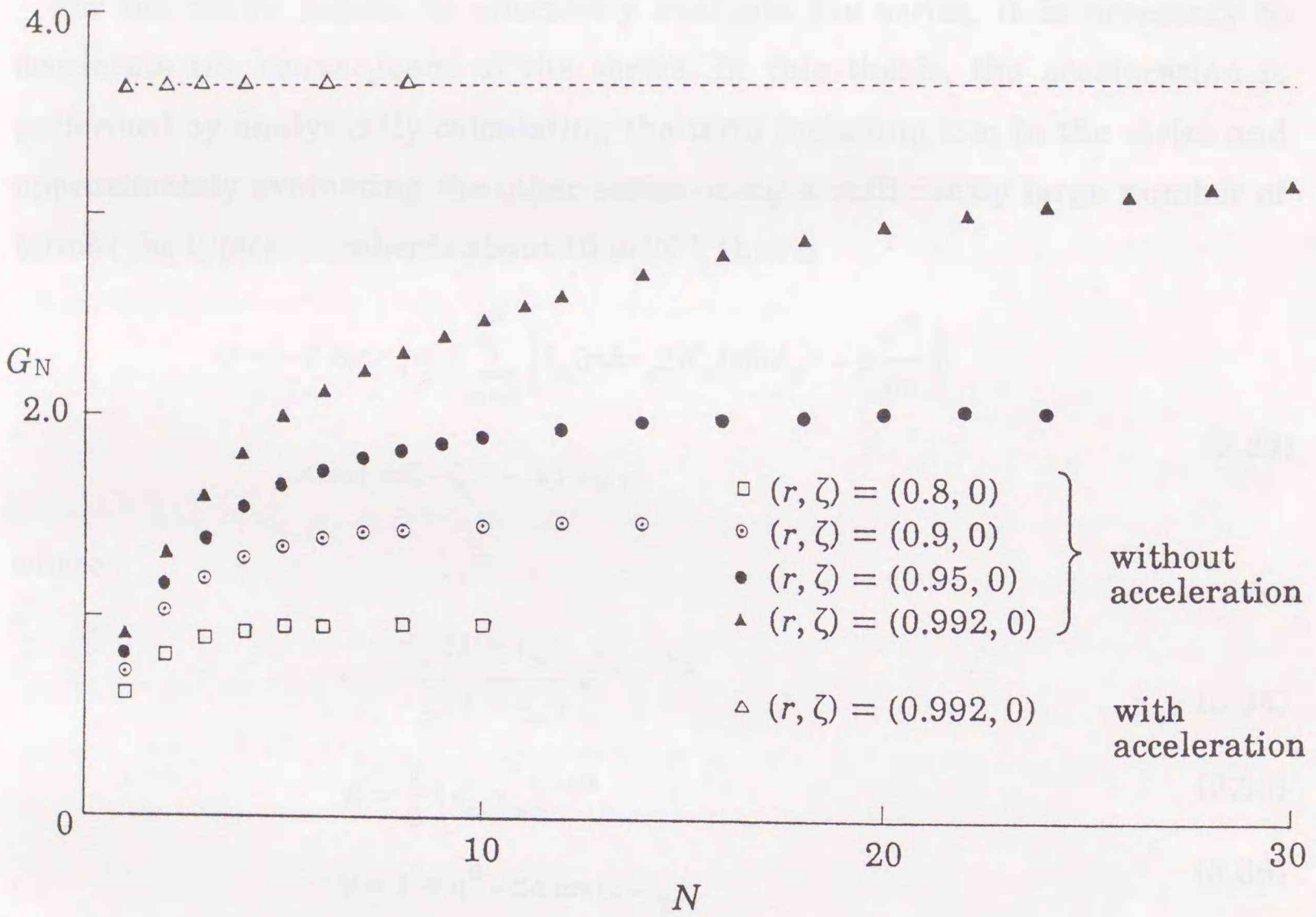

Fig. 3.2 Convergence of the infinite series in the fundamental solution G to the Laplace equation for $h = 2.0$. A source point is located at $r = 1.0$, $\zeta_0 = 0.0$.

$$\tau_< = \sqrt{1 + h^2 r_<^2}\,, \quad \tau_> = \sqrt{1 + h^2 r_>^2}\,, \tag{3.31}$$

$$\sigma_< = \tau_< + log\left(\frac{h r_<}{1 + \tau_<}\right), \quad \sigma_> = \tau_> + log\left(\frac{h r_>}{1 + \tau_>}\right). \tag{3.32}$$

From (3.28) - (3.32), it can be seen that the term $I_m(mhr_<)K_m(mhr_>)$ in the series exponentially decreases with an increase in m. Hence, the series (3.28) may fast converge when $r_> \gg r_<$. However, as the field point approaches the source, the convergence of the series in (3.28) becomes worse because $\sigma_< - \sigma_>$ approaches zero. This explains the tendency in Fig. 3.2

For the above reason, to effectively evaluate the series, it is necessary to accelerate the convergence of the series. In this thesis, the acceleration is performed by analytically calculating the term including $1/m$ in the series and approximately evaluating the other series using a sufficiently large number of terms (the typical number is about 10 to 20), that is

$$G \simeq -2\,log\,r_> + 4\sum_{m=1}^{M}\left[I_m(mhr_<)K_m(mhr_>) - \beta\frac{a^m}{m}\right] \times cos\,[\,m(\zeta - \zeta_0)\,] - 2\beta\,log\,\gamma\,, \tag{3.33}$$

where

$$a = \frac{r_<(1 + \tau_>)}{r_>(1 + \tau_<)}\,e^{\tau_< - \tau_>}, \tag{3.34}$$

$$\beta = \frac{1}{2}(\tau_<\,\tau_>)^{-1/2}, \tag{3.35}$$

$$\gamma = 1 + a^2 - 2a\,cos\,(\zeta - \zeta_0). \tag{3.36}$$

Similarly, the differentiations of G with respect to r and ζ are calculated as follows :

$$\frac{\partial G}{\partial r} \simeq -2\frac{\partial}{\partial r}\log r_> + 4\sum_{m=1}^{M}\left[\frac{\partial}{\partial r}\{I_m(mhr_<)K_m(mhr_>)\}\right.$$

$$\left.-a^{m-1}\left(\beta\frac{\partial a}{\partial r}+\frac{a}{m}\frac{\partial\beta}{\partial r}\right)\right]\cos[m(\zeta-\zeta_0)]-2\frac{\partial\beta}{\partial r}\log\gamma-4\beta\frac{\partial a}{\partial r}\frac{a-\cos(\zeta-\zeta_0)}{\gamma}, \quad (3.37)$$

$$\frac{\partial G}{\partial \zeta} \simeq -4\sum_{m=1}^{M} m\left[I_m(mhr_<)K_m(mhr_>)-\beta\frac{a^m}{m}\right]\sin[m(\zeta-\zeta_0)]$$

$$-\frac{4a\beta\sin(\zeta-\zeta_0)}{\gamma}. \quad (3.38)$$

The accelerated function G_N is plotted by triangles in Fig. 3.2, in which the convergence of the series is clearly improved. Consequently, the infinite series in (3.18) can be effectively evaluated by the acceleration presented here.

Figure 3.3 shows the contour-line plot of the fundamental solution G near a source point located at $r_0=1.0$, $\zeta_0=0.0$. As the pitch of the source ($2\pi/h$) decreases, the circular contour lines become bean-shaped ones.

3.2.2 Computing times for infinite-series and integral representations

As mentioned in Sec. 3.1, the fundamental solutions written in infinite-series form for helically symmetric systems can be derived by integrating the three dimensional fundamental solutions. Hence, we now have two representations for the solutions, *i.e.*, infinite-series and integral forms. For example, the fundamental solution to the helical Laplace equation can be written in the integral form (3.14) and infinite-series form (3.18). The computing times for the two representations will be numerically investigated below.

The integral in (3.14) is performed by means of the double exponential integral formula [3.9]. The integral region is divided into small portions so that the resultant integral value coincides the value by the infinite-series form in four digits. The convergence of infinite series in (3.18) is improved using the acceleration technique presented in the previous section. The number of terms N in the series is so chosen that the relative change $|G_{N+1}-G_N|$ is smaller than 1.0×10^{-6}. The computing times are evaluated around the source point r_0 located at $r_0=1.0$, $\zeta_0=0$.

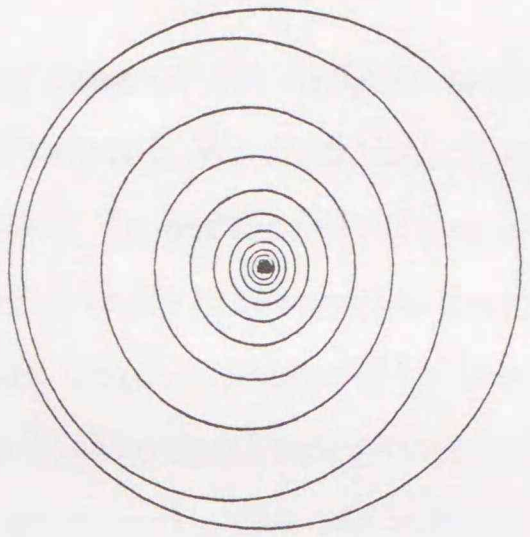

$h=0.5$

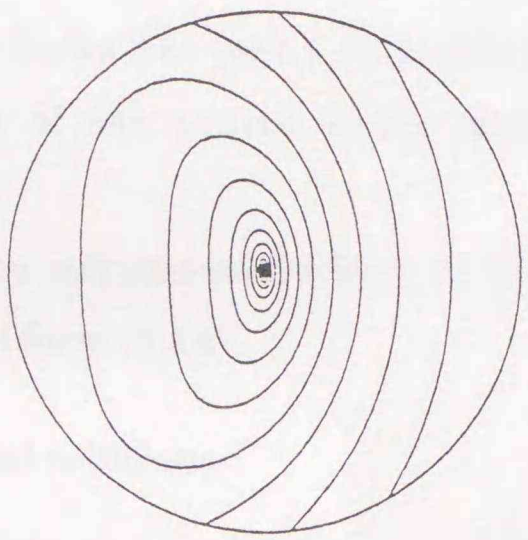

$h=2.0$

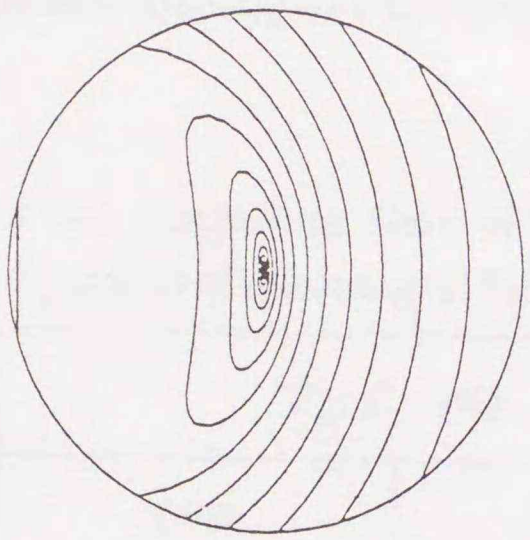

$h=4.0$

Fig. 3.3 The contour-line plot of the fundamental solution to the Laplace equation. A source point is located at $r=1.0$, $\zeta_0=0.0$.

The ratio of the computing time of the infinite-series form T_s to that of the integral form T_i is shown in Table 3.2. We find that T_s are clearly shorter than T_i at all points under consideration. In particular, there is a remarkable difference when the field point $\mathbf{r}$ is in the vicinity of the source point $\mathbf{r}_0$. The reason for this is that the numerical integration needs considerably fine subdivision because the integrand in (3.14) becomes a highly oscillatory function of z_0 when $\mathbf{r} \to \mathbf{r}_0$. This oscillation appears because, as $\mathbf{r} \to \mathbf{r}_0$, the periodicity in R with respect to z_0 becomes dominant compared with the decrease in R with increase of z_0. In other words, the helical effect of the source helix becomes strong when it is seen from near points while the source looks like just a straight line from far points. (The reduction of the pitch $2\pi/h$ of the source helix makes also the integrand oscillatory.)

It is concluded here that the infinite-series form (3.18) is more suitable for BE calculations than the integral form (3.14).

3.3 Singularity of fundamental solutions

The fundamental solution G given by (3.18) is singular at the source point $r=r_0$, $\zeta=\zeta_0$. Obviously, this singularity is attributed to the term $log(\gamma)$ given in (3.33) and (3.34)-(3.36). This section investigates the property of the term $log(\gamma)$ near the source point.

Table 3.2 The ratio of the computing time of the infinite-series form T_s to that of the integral form T_i ($h=2.0$)

r	T_s / T_i [%]	
	$\zeta=0$	$\zeta=\pi/4$
0.100	5.8	7.1
0.500	18.0	15.0
0.900	2.3	2.1
0.998	0.054	1.2
2.000	2.4	2.7

Let us consider a point (X, Y) distant l from the source point as shown in Fig. 3.4. The coordinates of the point are given by

$$X = X_0 + l\cos\phi\,,$$
$$Y = Y_0 - l\sin\phi\,. \tag{3.39}$$

Providing that l/r_0 is sufficiently small, the term $cos(\zeta - \zeta_0)$ in (3.36) can be written in the form

$$\begin{aligned}\cos(\zeta-\zeta_0) &= \cos\zeta\cos\zeta_0 + \sin\zeta\sin\zeta_0 \\ &= (XX_0+YY_0)/rr_0 \\ &= \frac{X_0(X_0+l\cos\phi)+Y_0(Y_0-l\sin\phi)}{r_0[(X_0+l\cos\phi)^2+(Y_0-l\sin\phi)^2]^{1/2}} \\ &\simeq (r_0^4 - l^2L^2)/r_0^4 \\ &= 1 + O(l^2)\,. \end{aligned} \tag{3.40}$$

where $L = X_0\cos\phi - Y_0\sin\phi$.

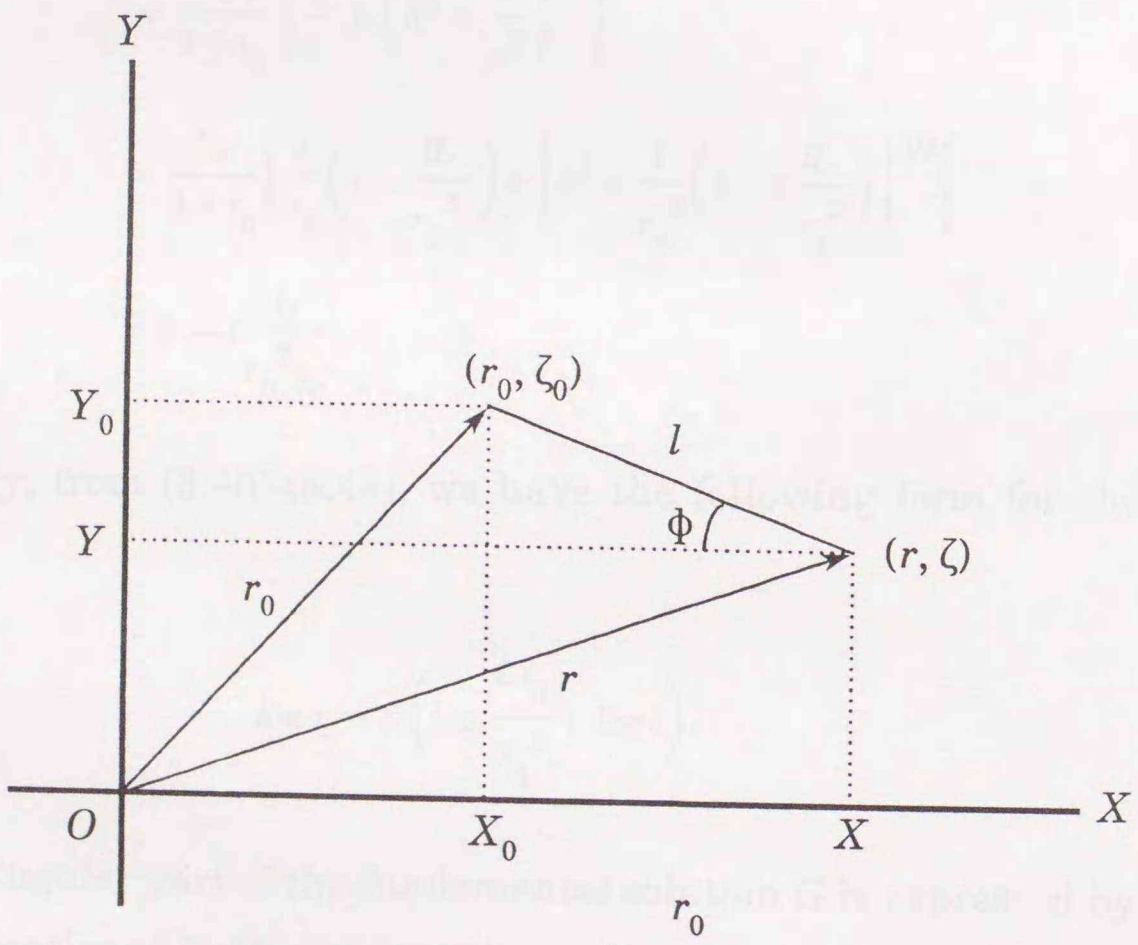

Fig. 3.4 The source point (r_0, ζ_0) and field point (r, ζ)

The exponential term $exp(\tau_< - \tau_>)$ in (3.34) can be evaluated as follows :

$$
\begin{aligned}
e^{\tau_< - \tau_>} &\simeq 1 + \tau_< - \tau_> \\
&\simeq 1 + \tau_0 - \tau_0 (1 + lL\,h^2/\tau_0^{\,2}) \\
&= 1 - lL\,h^2/\tau_0 ,
\end{aligned} \tag{3.41}
$$

where $\tau_0 = \sqrt{1 + h^2 r_0^{\,2}}$.

On the other hand, since $1/r$ and $1/r^2$ can be written in the form

$$
1/r = 1/[(X_0 + l\cos\phi)^2 + (Y_0 - l\sin\phi)^2]^{1/2}
$$

$$
\simeq (1 - lL/r_0^{\,2})/r_0 , \tag{3.42}
$$

$$
1/r^2 \simeq (1 - 2lL/r_0^{\,2})/r_0^{\,2}, \tag{3.43}
$$

the term $r_<(1+\tau_>)/r_>(1+\tau_<)$ in (3.34) is evaluated as

$$
\begin{aligned}
\frac{r_<(1+\tau_>)}{r_>(1+\tau_<)} &= \frac{r_0}{1+\tau_0}\frac{1+\tau}{r} \\
&= \frac{r_0}{1+\tau_0}\left[\frac{1}{r} + \left(h^2 + \frac{1}{r^2}\right)^{1/2}\right] \\
&\simeq \frac{r_0}{1+\tau_0}\left[\frac{1}{r_0}\left(1 - \frac{lL}{r_0^{\,2}}\right) + \left\{h^2 + \frac{1}{r_0^{\,2}}\left(1 - 2\frac{lL}{r_0^{\,2}}\right)\right\}^{1/2}\right] \\
&\simeq 1 - l\frac{L}{r_0^{\,2}\tau_0} .
\end{aligned} \tag{3.44}
$$

Consequently, from (3.40)-(3.44), we have the following form for the singular term $log\,\gamma$,

$$
log\,\gamma \simeq 2\left(log\,\frac{L\tau_0}{r_0^{\,2}} + log\,l\right). \tag{3.45}
$$

Hence, the singular part of the fundamental solution G is expressed by $-4\beta\ log\ l$. As will be mentioned in the next section, a line integration of G and its normal derivative over the singular element should be accurately evaluated in the BE

analysis. That integration will be performed on the basis of the result obtained here.

3.4 Summary

This chapter has been shown a unified derivation of the fundamental solutions to the Helmholtz-type equations with helical symmetry. The derivation has been performed by integrating the three dimensional fundamental solution along a source helix. These fundamental solutions have the infinite series whose convergence becomes very poor as a field point approaches the source point. The convergence has been improved by analytically evaluating the part of the slowest convergence in the solution. The infinite-series representation of the fundamental solution can be calculated in good accuracy much faster than the integral representation. The singularity in the fundamental solution is evaluated simply as $-4\beta \log l$.

REFERENCES

3.1 H. Igarashi and T. Honma, "On Axially and Helically Symmetric Fundamental Solutions to Modified Helmholtz-type Equations", *J. Appl. Math. Modelling*, **16**, pp. 314-319, 1992.

3.2 G. N. Watson, *Theory of Bessel Functions*, Cambridge University Press, London, pp. 358-372, 1922.

3.3 I. S. Gradshteyn and I. M. Ryzhik, *Table of Integrals, Series, and Products*, Academic Press, New York, 1965.

3.4 P. A. Merkel, Green Function Method for the Vacuum Contribution to the MHD Stability of Helically Symmetric Equilibria. *Z. Naturf.*, **37A**, pp. 859-866, 1982.

3.5 M. Tsuchimoto, T. Honma, H. Igarashi and K. Miya, Fundamental Solutions of the Axisymmetric Helmholtz-type Equations. *Appl. Math. Modelling*, 14, pp. 605-611, 1990.

3.6 H. J. Gardner, R. L. Dewar and W. N-C. Sy, "The Free-Boundary Equilibrium Problem for Helically Symmetric Plasmas", *J. Comp. Phys.*, 74, pp. 477-487, 1988.

3.7 J. D. Jackson, *Classical Electrodynamics*, John Wiley & Sons, New York, 1975.

3.8 F. W. J. Olver, *Handbook of Mathematical Functions* (Eds. M. Abramowitz and I. A. Segun), Dover, New York, p.378, 1964.

3.9 H. Takahashi and M. Mori, Double Exponential Formulas for Numerical Integration, *publ. R. I. M. S., Kyoto Univ.*, **9**, pp.721-741, 1974.

CHAPTER 4

POTENTIAL PROBLEMS

In this chapter, scalar and vector potential fields with helical symmetry will be analyzed using BE and FE methods, which are formulated in the twisted coordinates introduced in Sec. 2.2. The BE and FE formulations will be provided for helically symmetric scalar potential fields with closed and open boundaries. In the FE formulation for the open boundary problem, we will apply 'transfinite element method' [4.1] to helical system which gives a reasonable treatment of an integral over infinite region. The BE and FE solutions will be compared with exact and perturbed solutions. Moreover, the present FE method will be applied to analyze the coupling losses in a superconducting composite.

In the analysis of vector potential fields, we will consider the helical Grad-Shafranov (G-S) equation for a magnetic stream function that corresponds to one component of a vector potential. In particular, properties of iterative solution procedures for the non-linear G-S equation will be discussed.

4.1 Formulation for scalar potential problems

The helically symmetric Laplace equation is obtained by eliminating the term including $\partial\phi/\partial Z$ in (2.64) as

$$\nabla_T^2 \Phi = 0 \ , \tag{4.1}$$

$$\nabla_T^2 \Phi = (1+h^2Y^2)\frac{\partial^2\Phi}{\partial X^2} - 2h^2XY\ \frac{\partial^2\Phi}{\partial X\partial Y} + (1+h^2X^2)\frac{\partial^2\Phi}{\partial Y^2} - h^2X\frac{\partial\Phi}{\partial X} - h^2Y\frac{\partial\Phi}{\partial Y} \ . \tag{4.2}$$

This equation will be solved inside and outside a helical column of pitch $2\pi/h$ shown in Fig. 4.1. (Here, although a simply connected region is considered for simplicity, the formulation presented below can be easily extended to that for a multiply connected region.) We assume that the Dirichlet or Neumann boundary condition that is independent of Z is imposed on the surface of helical column ∂V_I enclosing the closed region V_C. The region V, which is composed of V_I and V_∞ and $2\pi/h$ long along Z-axis ($-\pi/h \leqq Z \leqq \pi/h$), is the solution region for an open boundary

boundary problem. The letter 'Ω' denotes the cut surface on Σ, where Σ is the plane of $Z=0$. For example, Ω_C and $\partial\Omega_I$ denote the two dimensional region $V_C \cap \Sigma$ and the curve $\partial V_I \cap \Sigma$, respectively. The BE and FE formulations for solving (4.1) will be given below.

4.1.1 BE formulation [4.2, 4.3]

As mentioned in Sec. 3.1, the fundamental solution G which satisfies

$$\nabla_T^2 G + 4\pi\,\delta(X-X_0)\,\delta(Y-Y_0) = 0\,, \tag{4.3}$$

can be expressed in the form

$$G = -2\log r_> + 4\sum_{m=1}^{\infty} I_m(mhr_<)\,K_m(mhr_>)\cos[\,m(\zeta-\zeta_0)\,]\,. \tag{4.4}$$

Here note that $\delta(X\text{-}X_0)\delta(Y\text{-}Y_0)=\delta(r\text{-}r_0)\delta(\zeta\text{-}\zeta_0)/r$.

We first consider a closed boundary problem in the following. Multiplying (4.1) by G and integrating it over the region V_C and assuming that the source point

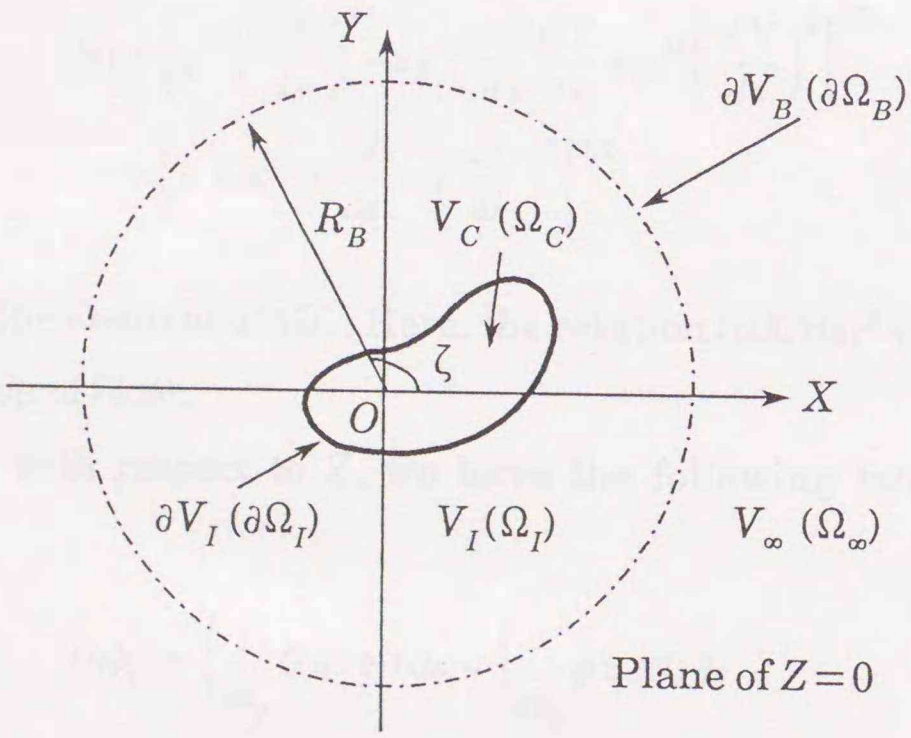

Fig. 4.1 . Cross section of a helical column and a three-dimensional solution region V_C and $V=V_I\cup V_\infty$. Ω is the corresponding two-dimensional region on the plane of $Z=0$.

exists in the region Ω_C, we obtain

$$4\pi\phi_0 \int_{-\frac{\pi}{h}}^{\frac{\pi}{h}} dZ = \int_{\partial V_I} G\, q\, dS - \int_{\partial V_I} \phi\, \frac{\partial G}{\partial n}\, dS\,, \tag{4.5}$$

where $\partial/\partial n = \mathbf{n}\cdot\nabla$, $\mathbf{n}$ is the outwardly directed unit normal vector on ∂V_I and $q = \partial\phi/\partial n$. In (4.5), the integrals over the surfaces $Z = \pm\pi/h$ cancel by periodicity. The surface element dS and operator $\partial/\partial n$ in (4.5) can be expressed in terms of a normal vector $\mathbf{N} /\!/ \mathbf{n}$ as follows :

$$dS = |\mathbf{N}|\, ds\, dZ\,, \tag{4.6}$$

$$\frac{\partial}{\partial n} = \mathbf{n}\cdot\nabla$$

$$= \frac{\mathbf{N}}{|\mathbf{N}|}\cdot\left(\mathbf{e}^X \frac{\partial}{\partial X} + \mathbf{e}^Y \frac{\partial}{\partial Y}\right), \tag{4.7}$$

where

$$\begin{aligned}\mathbf{N} &\equiv \frac{\partial \mathbf{r}}{\partial s} \times \frac{\partial \mathbf{r}}{\partial Z} \\ &= \left(\frac{dX}{ds}\mathbf{e}_X + \frac{dY}{ds}\mathbf{e}_Y\right) \times \mathbf{e}_Z \\ &= -\frac{dX}{ds}\mathbf{e}^Y + \frac{dY}{ds}\mathbf{e}^X \end{aligned} \tag{4.8}$$

$$\begin{aligned}|\mathbf{N}| &= \left[g^{22}\left(\frac{dX}{ds}\right)^2 - 2g^{12}\frac{dX}{ds}\frac{dY}{ds} + g^{11}\left(\frac{dY}{ds}\right)^2\right]^{1/2} \\ &= \left[1 + h^2\left(X\frac{dX}{ds} + Y\frac{dY}{ds}\right)^2\right]^{1/2} \end{aligned} \tag{4.9}$$

and ds denotes the line element of $\partial\Omega_I$. Here, the relation $(dX/ds)^2 + (dY/ds)^2 = 1$ is used in the derivation of (4.9).

Integrating (4.5) with respect to Z, we have the following two dimensional integral equation

$$4\pi\phi_0 = \int_{\partial\Omega_I} G\, q\, |\mathbf{N}|\, ds - \int_{\partial\Omega_I} \phi\, L(G)\, ds\,, \tag{4.10}$$

where

$$L = |\mathbf{N}| \frac{\partial}{\partial n}$$

$$= \mathbf{N} \cdot \left(\mathbf{e}^X \frac{\partial}{\partial X} + \mathbf{e}^Y \frac{\partial}{\partial Y} \right)$$

$$= \left(-g^{12} \frac{dX}{ds} + g^{11} \frac{dY}{ds} \right) \frac{\partial}{\partial X} + \left(-g^{22} \frac{dX}{ds} + g^{12} \frac{dY}{ds} \right) \frac{\partial}{\partial Y}$$

$$= \left\{ h^2 XY \frac{dX}{ds} + (1 + h^2 Y^2) \frac{dY}{ds} \right\} \frac{\partial}{\partial X} - \left\{ (1 + h^2 X^2) \frac{dX}{ds} + h^2 XY \frac{dY}{ds} \right\} \frac{\partial}{\partial Y}$$

$$= \frac{1}{r} \left(X \frac{dY}{ds} - Y \frac{dX}{ds} \right) \frac{\partial}{\partial r} - \frac{1}{r^2} \left(X \frac{dX}{ds} + Y \frac{dY}{ds} \right) (1 + h^2 r^2) \frac{\partial}{\partial \zeta} \quad . \tag{4.11}$$

Moreover, bringing the source point infinitely close to the boundary $\partial\Omega_I$, we have the (singular) boundary equation

$$C_0 \phi_0 = \int_{\partial\Omega_I} G\, q\, |\mathbf{N}|\, ds - \int_{\partial\Omega_I} \phi\, L(G)\, ds\,, \tag{4.12}$$

where C_0 is the geometric factor related to the Cauchy principal value of the boundary integral ($C_0 = 2\pi$ on a smooth boundary).

Subdividing $\partial\Omega_I$ into boundary elements Γ_j and using appropriate shape functions and values at nodes $[\phi]^T = (\phi_1, \phi_2 \ldots \phi_P)$ and $[q]^T = (q_1, q_2 \ldots q_P)$, we get the discretized form of (4.12)

$$[G_{ij}][q] = [H_{ij}][\phi]\,. \tag{4.13}$$

where the diagonal terms of the matrix $[H_{ij}]$ include the C_0 coefficients. Those diagonal terms can be easily calculated on the basis of the fact that the normal flux on $\partial\Omega_I$ must vanish when a uniform potential ϕ_{const} is applied over the whole boundary, *i.e.*,

$$[H_{ij}][\phi_{const}] = 0\,. \tag{4.14}$$

Then,

$$H_{ii} = -\sum_{\substack{j=1 \\ i \neq j}}^{P} H_{ij}\,. \tag{4.15}$$

On the other hand, the diagonal terms of the matrix $[G_{ij}]$ should be evaluated by separating the integrand of G_{ii} into regular and singular parts. For example,

when considering the constant element, we can rewrite G_{ii} in the form

$$G_{ii} = \int_{\Gamma_i} G\, ds$$

$$= \int_{-L_i/2}^{L_i/2} G\, dl$$

$$= \int_{-L_i/2}^{L_i/2} (G - G^{sing})\, dl + \int_{-L_i/2}^{L_i/2} G^{sing}\, dl \qquad (4.16)$$

where G^{sing} is the singular part of the fundamental solution G and L_i denotes the length of the boundary element including the source point at its center. As shown in Sec. 3.3, G^{sing} takes the form

$$G^{sing} = -4\beta_i \log |l| \qquad (4.17)$$

where $\beta_i = 1/(2\sqrt{1+h^2 r_i^2})$. Since the integrand of the first integral in (4.16) is regular, it is numerically integrated by the Gaussian integration. The second integral is analytically evaluated as

$$\int_{-L_i/2}^{L_i/2} G^{sing}\, dl = -4\beta_i L_i (\log L_i/2 - 1)\,. \qquad (4.18)$$

By solving (4.13) by numerical methods such as the Gaussian elimination or LU factorization, we can obtain the potential $[\phi]$ and flux $[q]$ at all nodes on $\partial\Omega_I$. Applying those values to (4.10), the value of the potential and flux can be calculated at any internal points.

Next we consider the open boundary problem. The boundary integral equation for the region Ω_I enclosed by the inner boundary $\partial\Omega_I$ and the outer circular boundary $\partial\Omega_B$ is given by

$$C_0\phi_0 = \int_{\partial\Omega_I} G\, q\, |\mathbf{N}|\, ds + \int_{\partial\Omega_B} G\, q\, |\mathbf{N}|\, ds - \int_{\partial\Omega_I} \phi\, L(G)\, ds - \int_{\partial\Omega_B} \phi\, L(G)\, ds\,. \qquad (4.19)$$

The integral path and normal vector are shown in Fig. 4.2. When the radius R_B of the outer boundary $\partial\Omega_B$ approaches infinity, the fundamental solution may become $-2\log r$ because the source helix looks like a straight line from a far field point. In fact, since $R^2 = r^2 + r_0^2 - 2rr_0\cos(\theta-\theta_0) + (z-z_0)^2 \simeq r^2 + (z-z_0)^2$ when $r \gg r_0$, the

fundamental solution G becomes

$$G \to \int_{-\infty}^{\infty} \left[\frac{1}{\{r^2 + (z - z_0)^2\}^{1/2}} - \frac{1}{\{1 + (z - z_0)^2\}^{1/2}} \right] dz_0$$
$$= -2 \log r . \tag{4.20}$$

where (3.14) in which the arbitrary constant α is set to unity is used.

On the other hand, on the circular boundary $\partial\Omega_B$, it can be proved that $|\mathbf{N}| = 1$ and $L = \partial/\partial r$. Hence, when $R_B \gg r_0$, the integrals on $\partial\Omega_B$ in (4.19) becomes

$$\int_{\partial\Omega_B} G\, q\, |\mathbf{N}|\, ds - \int_{\partial\Omega_B} \phi\, L(G)\, ds = -2R_B (\log R_B) \int_0^{2\pi} q\, d\zeta + 2 \int_0^{2\pi} \phi\, d\zeta . \tag{4.21}$$

When $\phi = O(1/r)$, the above integrals vanish. From these results, we obtain the boundary integral equation for the open boundary problem as follows :

$$C_0 \phi_0 = \int_{\partial\Omega_I} G\, q\, |\mathbf{N}|\, ds - \int_{\partial\Omega_I} \phi\, L(G)\, ds . \tag{4.22}$$

This equation is the same as (4.12) except the direction of the normal vector **n**. Consequently, all we have to do is to solve (4.22) on the boundary $\partial\Omega_I$. Discretization of (4.22) yields a simultaneous equation similar to (4.13). From the uniform potential condition over the whole boundaries, we have the diagonal

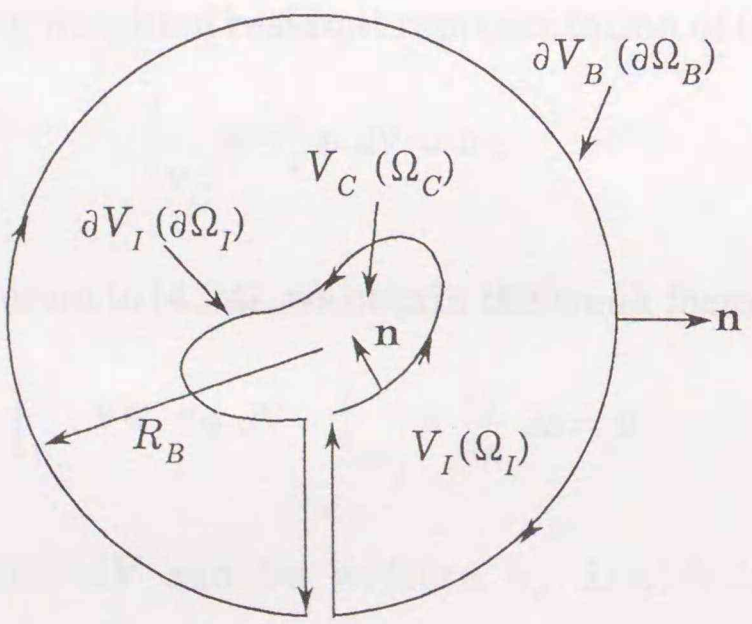

Fig. 4.2 The integral path and normal vector for the open boundary problem.

term of the H matrix as follows :

$$H_{ii} = -\sum_{\substack{j=1 \\ i \neq j}}^{P} H_{ij} - \lim_{R_B \to \infty} \int_{\partial \Omega_B} L(G)\, ds$$

$$= -\sum_{\substack{j=1 \\ i \neq j}}^{P} H_{ij} - \lim_{R_B \to \infty} \int_{0}^{2\pi} -\frac{2}{R_B} \cdot R_B\, d\zeta$$

$$= -\sum_{\substack{j=1 \\ i \neq j}}^{P} H_{ij} + 4\pi\,. \tag{4.23}$$

In conclusion, for both closed and open boundary potential problems, the simultaneous equations which can be numerically solved are derived from (4.12) and (4.22), respectively. The diagonal terms of the H matrix can be calculated from (4.15) and (4.23). Notice that there is no approximation in the boundary integral equations (4.12) and (4.22). Therefore, there may be no intrinsic difference in the accuracy of the BE methods for open boundary and closed boundary problems.

4.1.2 FE formulation for closed region [4.2]

In this section, for a closed region potential problem, an FE formulation for the Laplace equation (4.1) will be given on the basis of the method of weighted residuals.

Multiplying (4.1) by an weighted function W and integrating it over the region V_C ,we have the following weighted residual representation of (4.1)

$$\int_{V_C} W\, \nabla_T^2 \Phi\, dV = 0\,. \tag{4.24}$$

Applying the Gauss' theorem to (4.24), we obtain the weak form of (4.24)

$$\int_{V_C} \nabla W \cdot \nabla \phi\, dV - \int_{\partial V_I} W \frac{\partial \Phi}{\partial n}\, dS = 0\,. \tag{4.25}$$

In (4.25), $(\partial\phi/\partial n)dS$ and dV can be written by $L(\phi)dsdZ$ and $dXdYdZ$, respectively. Then , after integrating (4.25) with respect to Z, we find

$$\int_{\Omega_C} \nabla W \cdot \nabla \phi \, dXdY - \int_{\partial\Omega_I} W L(\phi) \, ds = 0 \, . \tag{4.26}$$

Here, the explicit form of (4.26) is given by

$$\int_{\Omega_C} \left[(1+h^2Y^2)\frac{\partial W}{\partial X}\frac{\partial \phi}{\partial X} - h^2XY\left(\frac{\partial W}{\partial X}\frac{\partial \phi}{\partial Y} + \frac{\partial W}{\partial Y}\frac{\partial \phi}{\partial X} \right) + (1+h^2X^2)\frac{\partial W}{\partial Y}\frac{\partial \phi}{\partial Y} \right] dX\, dY$$

$$- \int_{\partial\Omega_I} W \left[\left\{ h^2XY\frac{dX}{ds} + (1+h^2Y^2)\frac{dY}{ds} \right\}\frac{\partial \phi}{\partial X} - \left\{ (1+h^2X^2)\frac{dX}{ds} + h^2XY\frac{dY}{ds} \right\}\frac{\partial \phi}{\partial Y} \right] ds = 0. \tag{4.27}$$

Subdividing the solution region Ω_C into finite elements and using the Galerkin method, we can easily derive the simultaneous equation from (4.27) as follows :

$$[K_{ij}][\phi] = 0 \, . \tag{4.28}$$

4.1.3 FE formulation for open region [4.3]

In this section, we consider the Dirichlet problem for the open field V. The solution to (4.1) can be found by minimizing the functional

$$F(\phi) = \int_V (\nabla \phi)^2 \, dV \, , \tag{4.29}$$

where

$$(\nabla \phi)^2 = (1+h^2Y^2)\left(\frac{\partial \phi}{\partial X} \right)^2 - 2h^2XY\frac{\partial \phi}{\partial X}\frac{\partial \phi}{\partial Y} + (1+h^2X^2)\left(\frac{\partial \phi}{\partial Y} \right)^2 . \tag{4.30}$$

This variational approach gives the same solution obtained by the method of weighted residuals. Subdividing the region V in (4.29) into V_I and V_∞ and applying Green's theorem to the integration over the region V_∞, we have

$$F(\phi) = \int_{V_I} (\nabla \phi)^2 \, dV - \int_{V_\infty} \phi \nabla^2 \phi \, dV + \int_{\partial V_B} \phi \frac{\partial \phi}{\partial n} dS \, . \tag{4.31}$$

Integrating (4.31) with respect to Z in a manner similar to the one used in section 2.1, we have

$$F(\phi)=\int_{\Omega_I}(\nabla\phi)^2\,dXdY-\int_{\Omega_\infty}\phi\nabla^2\phi\,dXdY+\int_0^{2\pi}\phi\frac{\partial\phi}{\partial r}R_B\,d\zeta. \tag{4.32}$$

In the external region Ω_∞, the potential ϕ is expanded in terms of harmonic solutions to (4.1) as follows:

$$\phi=\sum_{m=1}^{M}K_m(mhr)[a_m cos(m\zeta)+b_m sin(m\zeta)]. \tag{4.33}$$

Since the series (4.33) is composed of solutions to the Laplace equation, the second integral of (4.32) vanishes. Hence, the contribution from the integral over the unbounded region Ω_∞ is reduced to the boundary integral on $\partial\Omega_B$ (a circle of radius R_B). The above mentioned approach was presented in [4.1] and called 'transfinite element method'. (see also [4.4])

In the region Ω_I, ϕ is interpolated using the appropriate shape functions ξ_i as follows :

$$\phi=\sum_{i=1}^{N}\xi_i^I\phi_i^I+\sum_{i=1}^{2M}\xi_i^B\phi_i^B, \tag{4.34}$$

where letters 'I' and 'B' denote values related to the inner region Ω_I which does not include $\partial\Omega_B$, and the boundary $\partial\Omega_B$, respectively. The boundary values $[\phi^B]^T=(\phi_1{}^B, \phi_2{}^B \ldots \phi_{2M}{}^B)$ are related with the coefficients $[c]^T=(a_1, b_1, \ldots a_M, b_M)$ in the form

$$[\phi^B]=[S_{ij}][c], \tag{4.35}$$

where

$$\left[S_{ij}\right]=\begin{bmatrix} K_1(hR)sin(\zeta_1) & \ldots. & K_M(MhR)cos(M\zeta_1) \\ \vdots & & \vdots \\ K_1(hR)sin(\zeta_{2M}) & \ldots. & K_M(MhR)cos(M\zeta_{2M}) \end{bmatrix}. \tag{4.36}$$

Consequently, (4.32) can written in a quadratic form

$$F(\phi)=[\psi]^T[C_{ij}]^T[K_{ij}][C_{ij}][\psi]+[c]^T[A_{ij}][c], \tag{4.37}$$

where $[\psi]^T=(\Phi_1, \Phi_2 \ldots \Phi_N, a_1, b_1, \ldots a_M, b_M)$ are connected to the nodal values $[\phi]^T=(\Phi_1, \Phi_2 \ldots \Phi_N, \Phi_1{}^B, \Phi_2{}^B \ldots \Phi_{2M}{}^B)$ by the matrix $[C_{ij}]$ as follows :

$$[\phi]=[C_{ij}][\psi]\,, \tag{4.38}$$

$$[C_{ij}]=\begin{bmatrix} [I] & [0] \\ [0] & [S_{ij}] \end{bmatrix}. \tag{4.39}$$

The matrices $[K_{ij}]$ and $[A_{ij}]$ in (4.37) are defined by

$$[K_{ij}]=\int_{\Omega_I}[\nabla\xi_i][\nabla\xi_j]^T\,dX\,dY\,, \tag{4.40}$$

$$\left[A_{ij}\right]=\pi hR\begin{bmatrix} K_1(hR)\,K_1'(hR) & & & \\ & K_1(hR)\,K_1'(hR) & & 0 \\ & & \ddots & \\ & & & MK_M(MhR)\,K_M'(MhR) \\ 0 & & & MK_M(MhR)\,K_M'(MhR) \end{bmatrix}. \tag{4.41}$$

Minimizing the functional (4.37) with respect to the variables $[\psi]^T$, we obtain the matrix equation to be numerically solved as follows :

$$\left[\begin{array}{c|c} [K_{ij}{}^{II}] & [K_{ij}{}^{IB}][S_{ij}] \\ \hline [S_{ij}]^T[K_{ij}{}^{BI}] & [S_{ij}]^T[K_{ij}{}^{BB}][S_{ij}]+[A_{ij}] \end{array}\right][\psi]=[0] \tag{4.42}$$

4.2 Analysis of scalar potential problems

In this section, the BE and FE formulations given in Sec. 4.1 will be applied to a few simple potential problems. As a closed boundary problem, a potential field in a helical column with a rectangular cross-section will be analyzed. The BE and FE solutions to this problem are compared with the perturbed solution. For the open boundary potential problem, the static magnetic field around a helical coil will be computed and the accuracy of the numerical solution will be tested by comparing it with the exact solution. Moreover, the static electric field around a twisted pair-line will be calculated by means of the BE and FE methods. Finally, the coupling losses in a twisted superconducting composite will be analyzed by the present FE method.

4.2.1 Closed boundary problem [4.2]

Consider the potential field in the helical column with a square cross-section shown in Fig 4.3. When the helical pitch is chosen as infinity, this problem corresponds to the well-known potential problem [4.5]. In the BE analysis, we subdivide the contour in Fig. 4.3 into 80 linear portions and use linear and

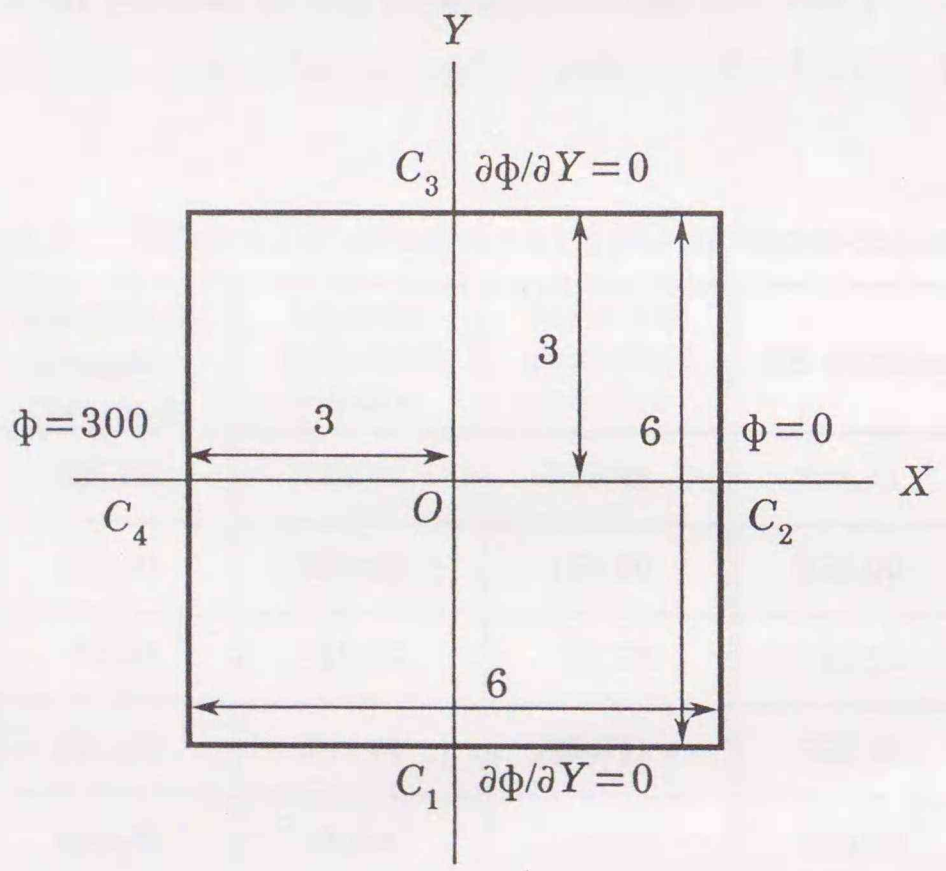

Fig. 4.3 A helical column with a square cross-section

constant interpolations for the potential Φ and flux q, respectively, in those portions. We use 800 triangle elements with linear interpolation for the finite element solution to (4.1).

On the other hand, after laborious, but straightforward calculations, we can obtain the following 2nd-order perturbed solution to (4.1) assuming that the helical pitch $2\pi/h$ is sufficiently large :

$$\phi \simeq \phi_0 + h^2\phi_1 + h^4\phi_2, \tag{4.43}$$

$$\phi_0 = -50(X-3), \tag{4.44}$$

$$\phi_1 = -\frac{25}{3}X(X+3)(X-3), \tag{4.45}$$

$$\phi_2 = -\frac{25}{12}X(X+3)(X-3)(X^2-4Y^2-9) - \frac{100\times 6^5}{\pi^4}\sum_{m=1}^{\infty}\frac{(-1)^m+1}{m^4}\sin\left\{\frac{m\pi}{6}(X+3)\right\} \times\cosh\left(\frac{Y}{6}m\pi\right)\frac{\cosh\left(\frac{1}{2}m\pi\right)}{\sinh(m\pi)}. \tag{4.46}$$

The above perturbed solution is derived in A-5.

The solutions by the above three methods for $h=0.3$, 0.5 are summarized in Table 4.1. From these results, it can be seen that the BE and FE solutions are in good agreement with the 2nd-order perturbed solution for $h=0.3$. However, there

Table 4.1 BE and FE solutions and perturbed solutions ($Y=0$)

Helical pitch h	X	Solution for Straight Column Φ_0	1st-order perturbed solution	2nd-order perturbed solution	FE solution	BE solution
0.3	-1.5	225.00	217.41	218.21	218.11	218.39
0.3	0.0	150.00	150.00	150.00	150.00	150.00
0.3	1.5	75.00	82.59	81.79	81.89	81.61
0.5	-1.5	225.00	203.91	210.11	208.40	208.63
0.5	0.0	150.00	150.00	150.00	150.00	150.00
0.5	1.5	75.00	96.09	89.89	91.60	91.37

are some discrepancies between the two numerical solutions and the 2nd-order perturbed solution for $h=0.5$. The reason for this may be that the perturbed solution does not converge in good accuracy for $h=0.5$. This can be understood from the differences between 1st- and 2nd-order solutions shown in table 4.1. From Fig. 4.4, in which the dependence of the values of ϕ at $X=-1.5$, $Y=0$ on h is shown, we can clearly understand this point. Namely, the 2nd-order perturbed solution has a physically meaningless characteristic for large values of the pitch whereas the BE and FE solutions monotonously decrease with the helical wavenumber h. Figure 4.5 shows the profile of the potential ϕ calculated by the BE method.

4.2.2 Open boundary problem [4.3]

The magnetic field produced by a helical solenoid shown in Fig. 4.6 is calculated by the BE and FE methods. When the current i_c flowing along the solenoid is assumed to be confined to planes of $Z=$constant, the magnetic field

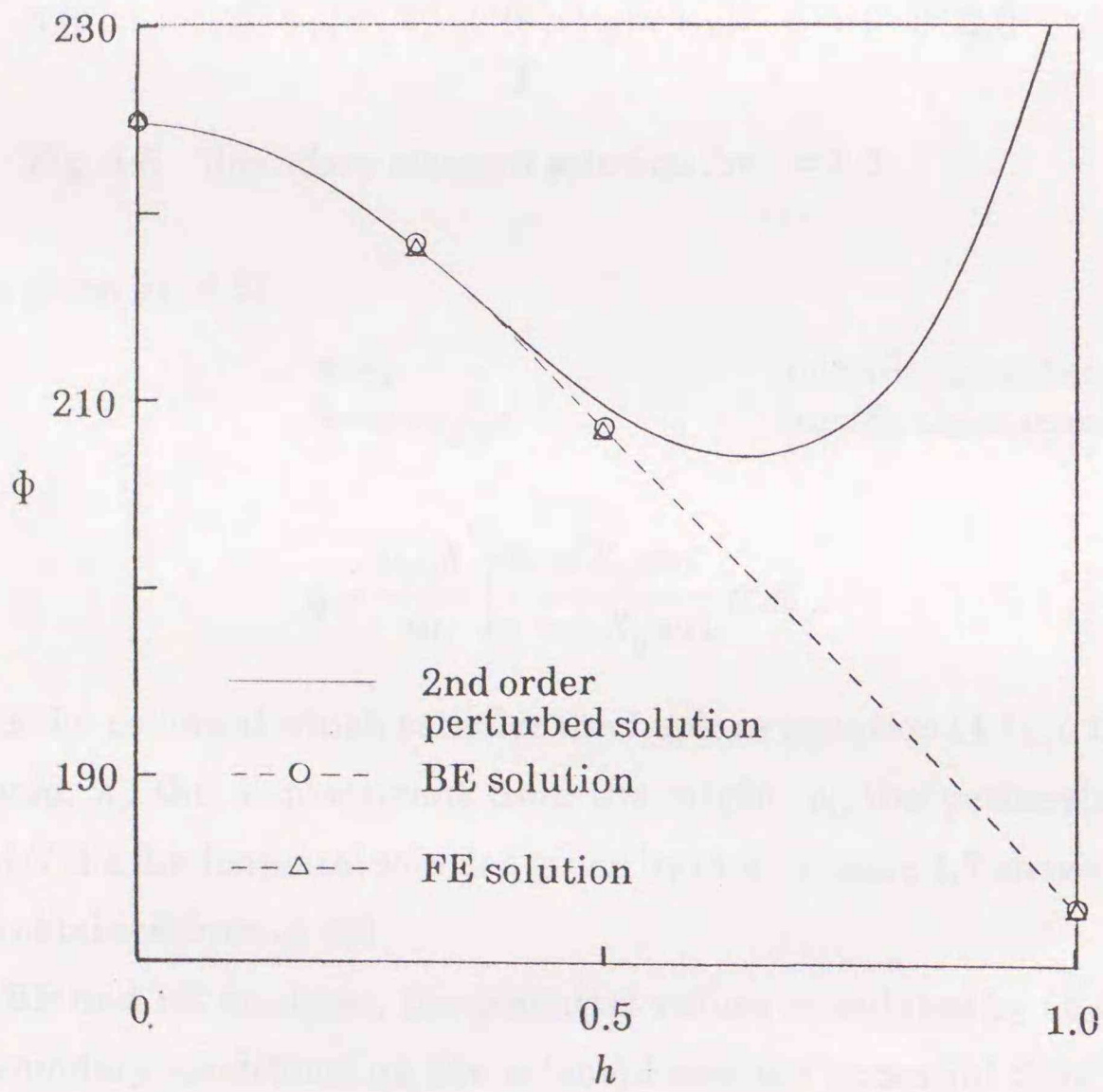

Fig. 4.4 Dependence of the value of ϕ at $X=-1.5$, $Y=0$ on h

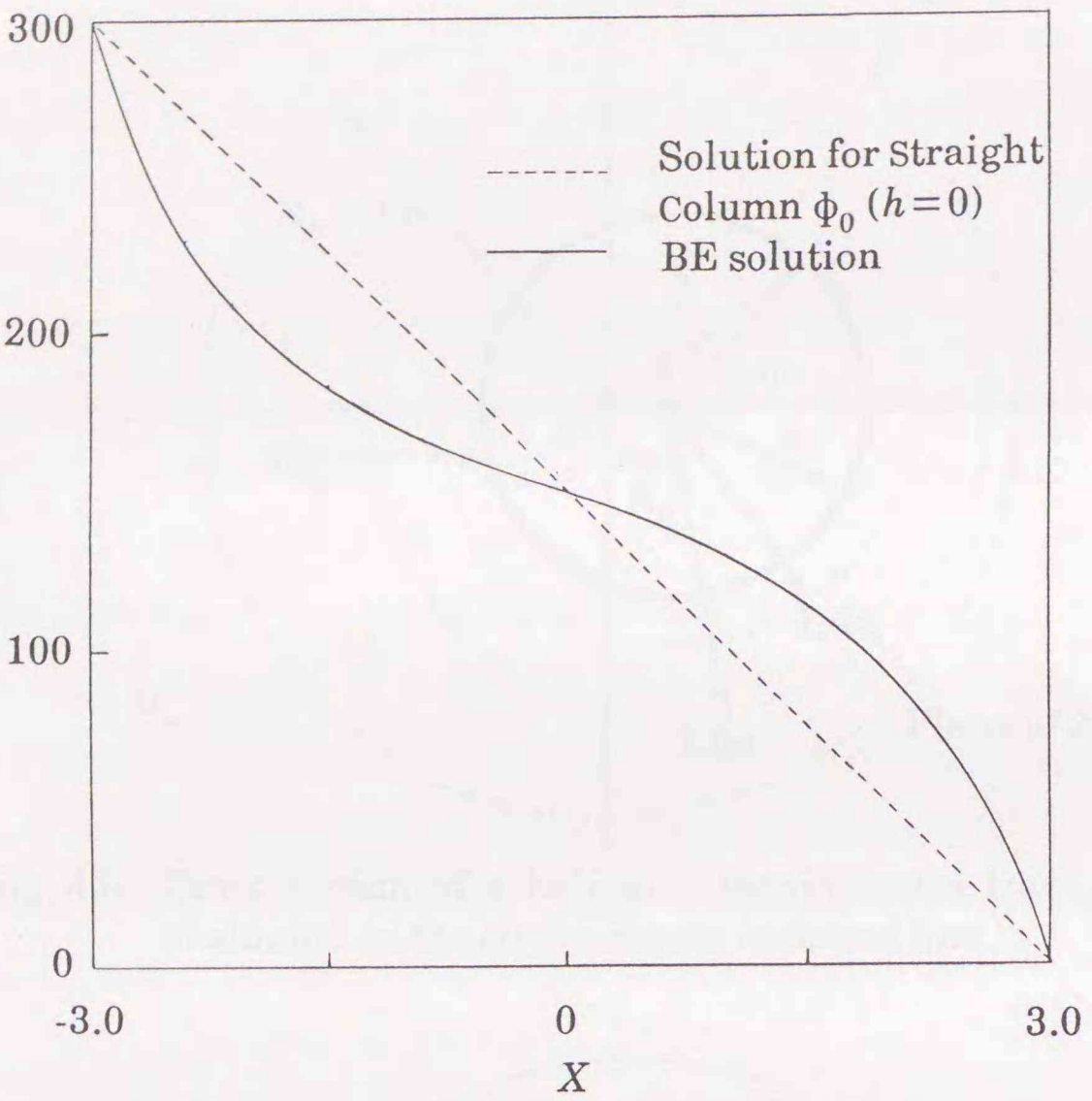

Fig. 4.5 Boundary element solution for $h=1.0$

$B=\nabla\Phi$ is given by [4.6]

$$\Phi=\phi \qquad \text{(outside the solenoid),} \qquad (4.47)$$

$$\Phi=\phi+\mu_0 i_c z \qquad \text{(inside the solenoid),} \qquad (4.48)$$

$$\phi=\frac{\mu_0 i_c h}{4\pi}\int_0^{2\pi}\frac{a^2 X_0 \sin\zeta}{a-X_0\cos\zeta}G\,d\zeta\,, \qquad (4.49)$$

where ϕ is the potential which satisfies the Laplace equation (4.1), a the radius of the solenoid, X_0 the displacement from the origin, μ_0 the permeability of free space and G the fundamental solution given by (4.4). Figure 4.7 shows the contour lines of ϕ obtained from (4.49).

In the BE and FE analyses, the potential values calculated by (4.49) are used for the boundary conditions on the solenoid and the potential field outside the solenoid is solved. The region between the solenoid and $\partial\Omega_B$ (a circle of radius $2.6a$) is discretized with 864 linear elements (468 nodes) for the FE calculation.

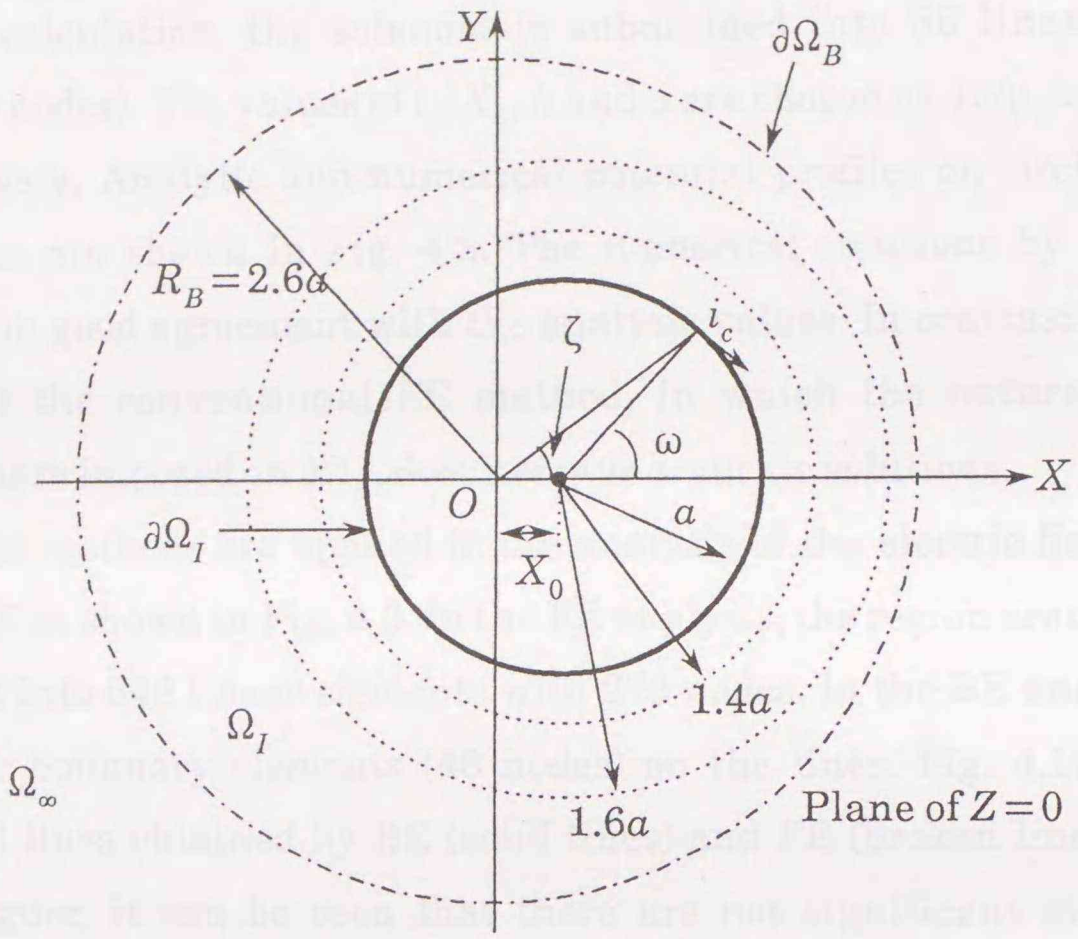

Fig. 4.6 Cross section of a helical solenoid (solid line). Accuracy is evaluated on the circles drawn in dotted line.

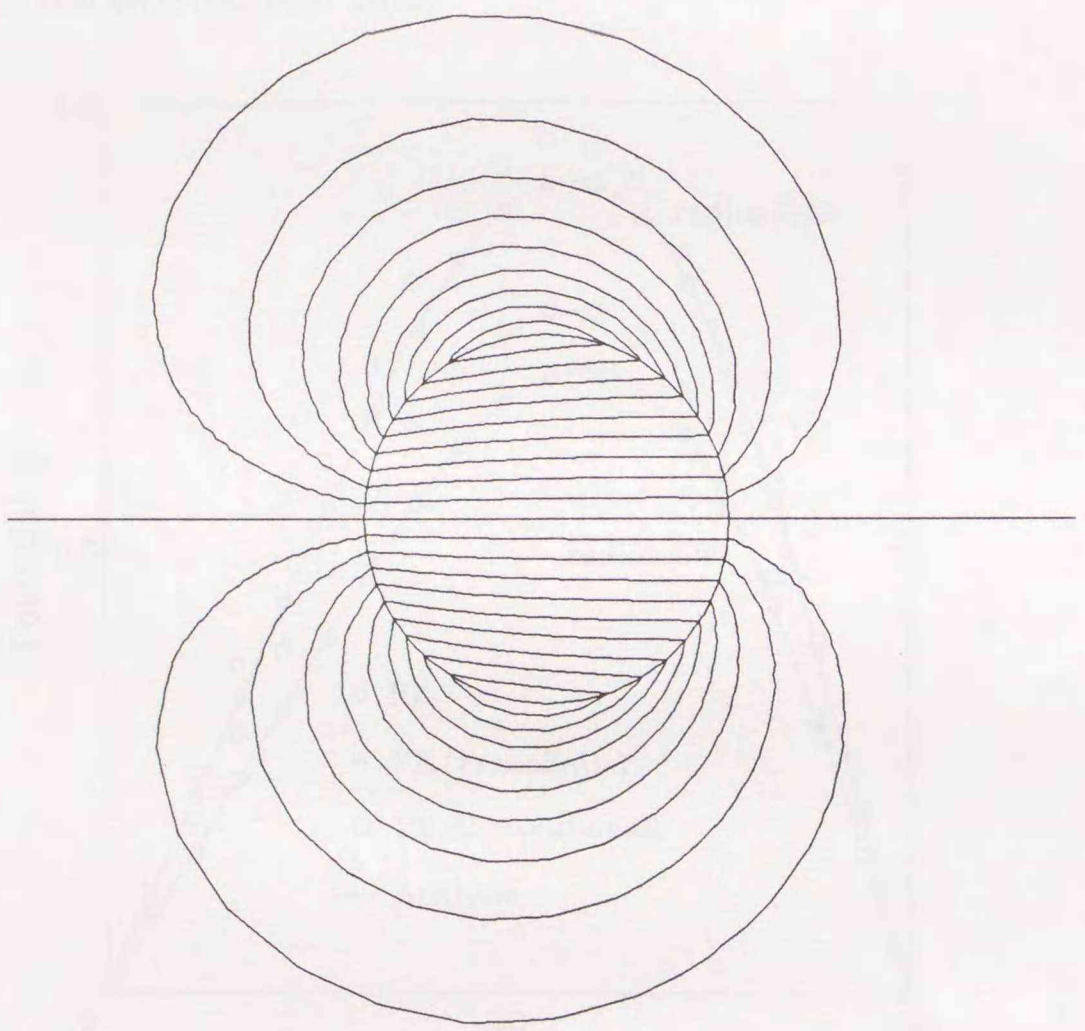

Fig. 4.7 An equipotential plot for the helical solenoid

For the BE calculation, the solenoid is subdivided into 36 linear boundary elements (36 nodes). The values of i_c, X_0, h and a are chosen as $4\pi/\mu_0 h$, 0.4, 1.0 and 1.0, respectively. Analytic and numerical potential profiles on circles of radius $1.4a$ and $1.6a$ are shown in Fig. 4.8. The numerical solutions by the present methods are in good agreement with the analytic values. In contrast with this, it is clear that the conventional FE method, in which the natural boundary condition is here imposed on $\partial\Omega_B$, does not give accurate solutions.

The present methods are applied to the analysis of the electric field around a twisted-pair line shown in Fig. 4.9. In the FE analysis, the region around the lines is subdivided into 648 linear elements with 273 nodes. In the BE analysis, there are 48 linear boundary elements (48 nodes) on the lines. Fig. 4.10 shows the equipotential lines obtained by BE (solid lines) and FE (broken lines) methods. From this figure, it can be seen that there are not significant discrepancies between the FE and BE solutions. Moreover, the electric fields come to shrink as the helical wavenumber h is increased. This indicates a nose reduction effect due to the helicity of the twisted-pair line.

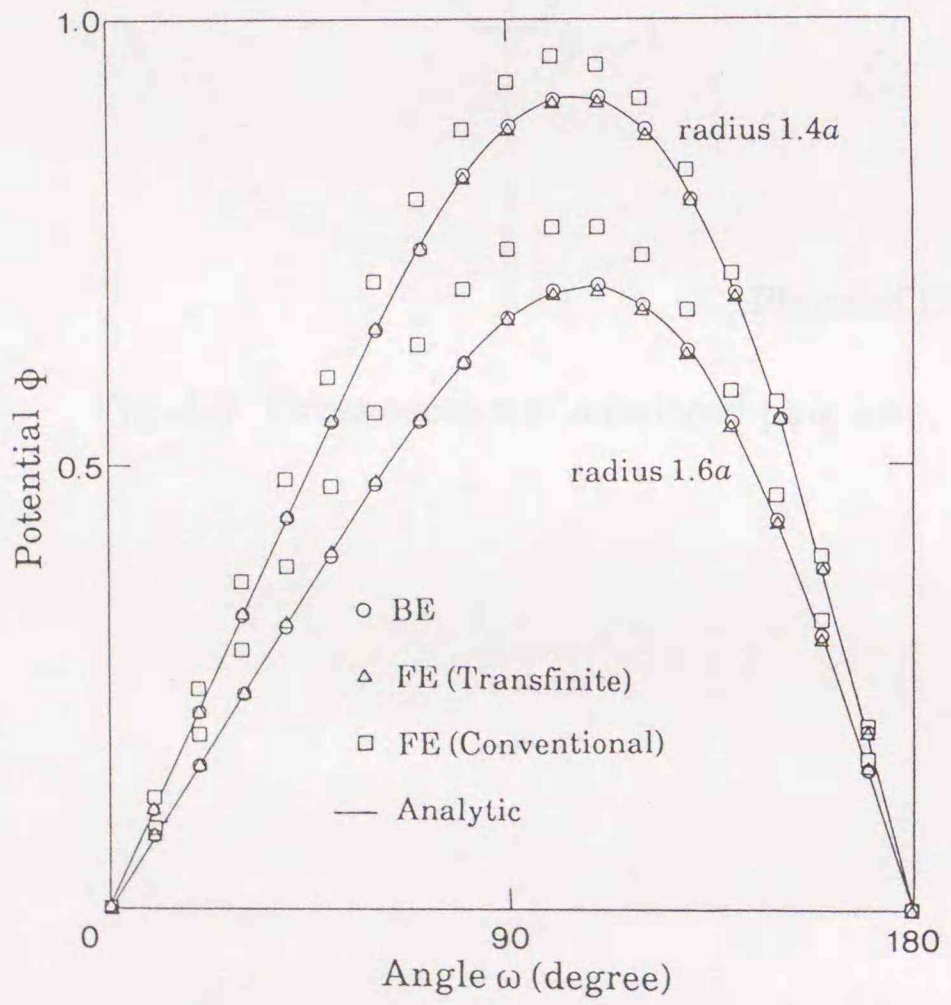

Fig. 4.8 Analytic and numerical potential profiles on the circles of radius $1.4a$ and $1.6a$ ($0 \leqq \omega \leqq 180°$).

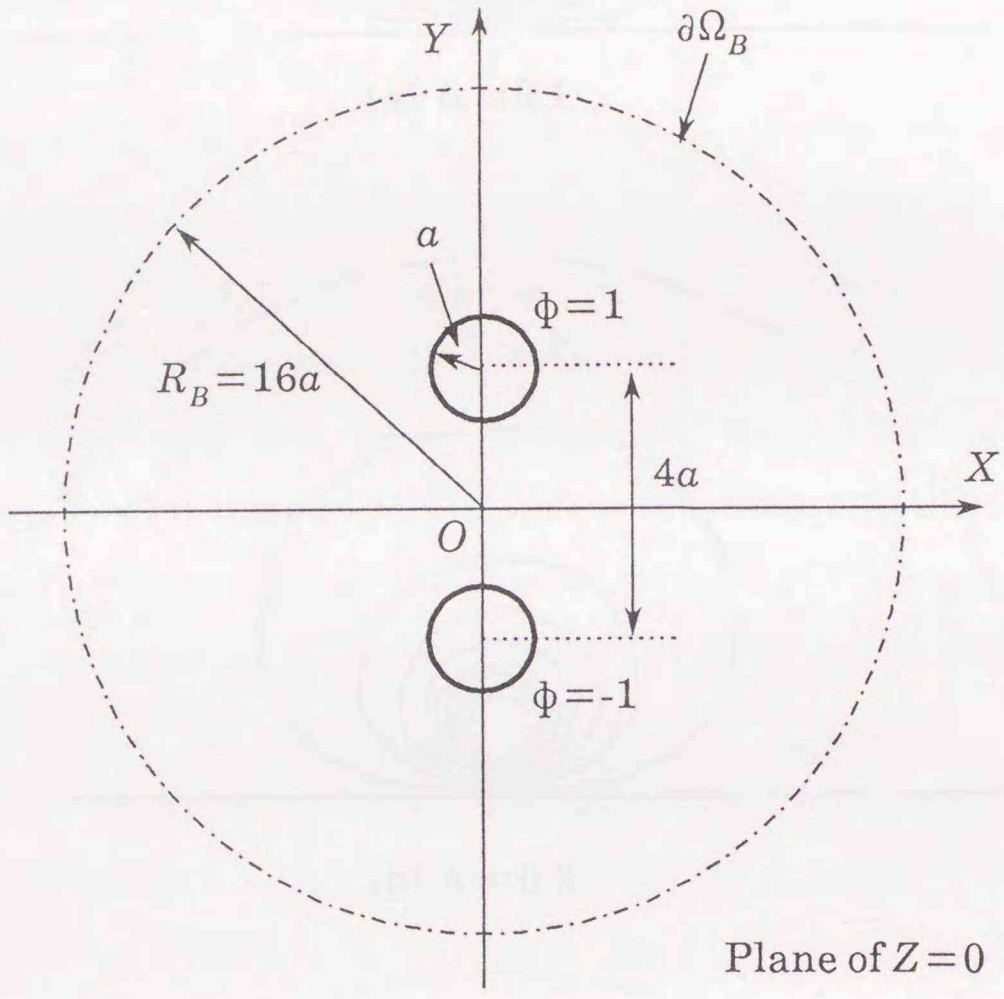

Fig. 4.9 Cross section of a twisted-pair line.

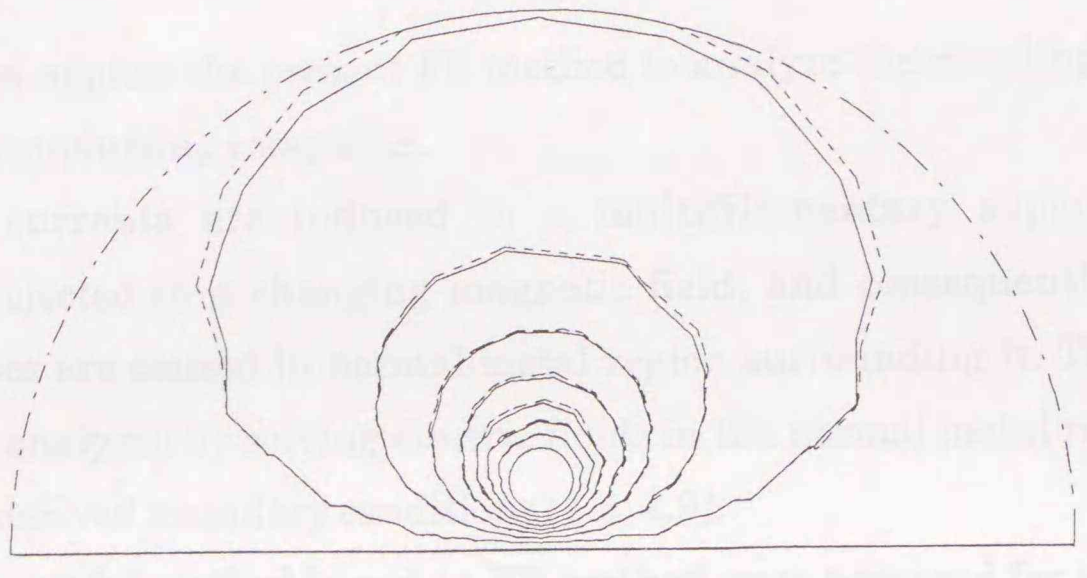

(a) $h = 0.1$

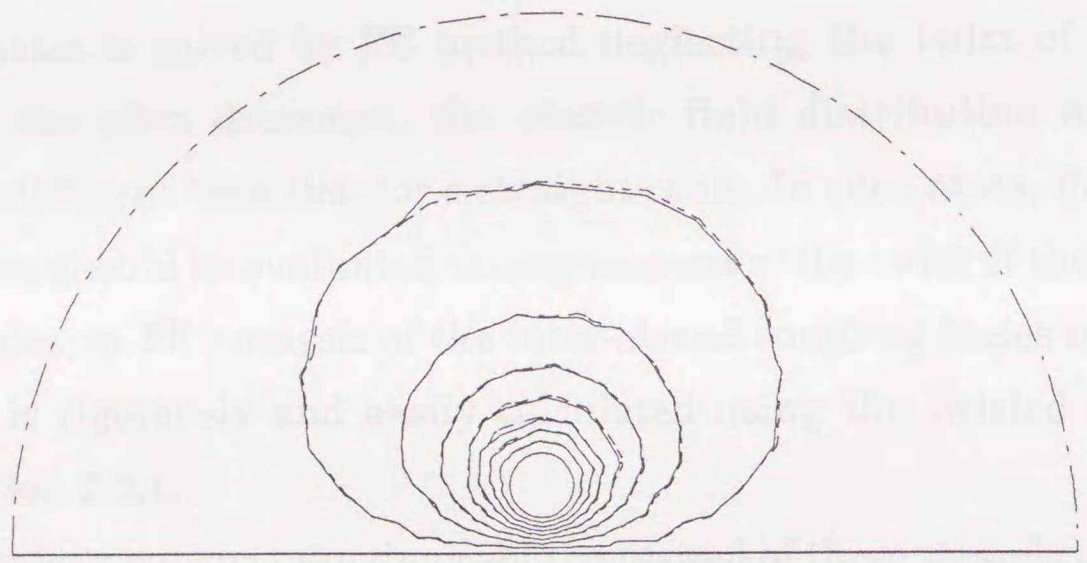

(b) $h = 0.2$

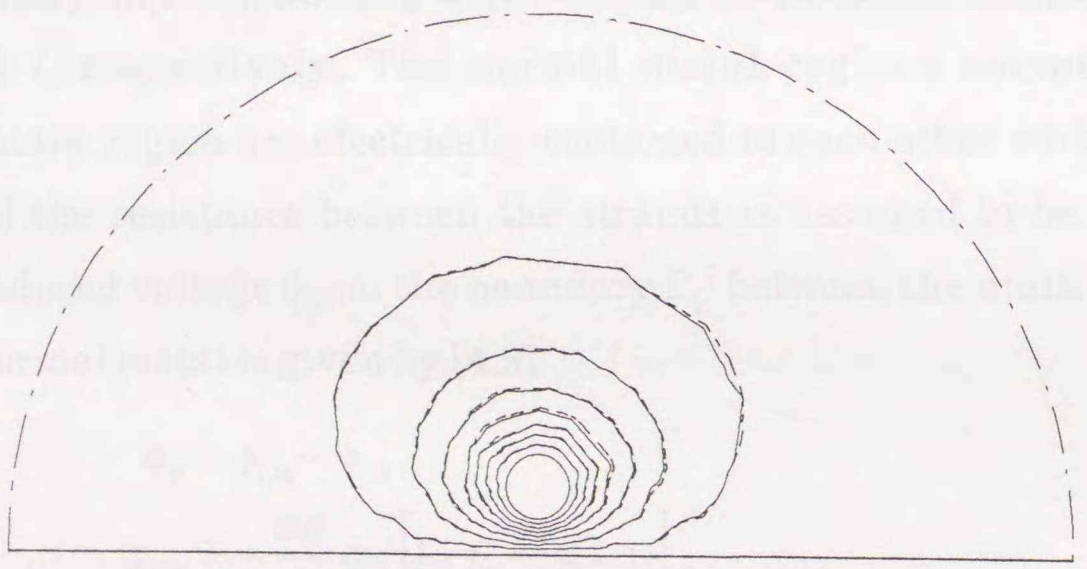

(c) $h = 0.3$

Fig. 4.10 Contour lines of electric potentials around twisted-pair line for $a = 1.0$. Solid and broken lines represent BE and FE solutions, respectively.

4.2.3 Coupling losses in a superconducting composite [4.7]

This section applies the present FE method to analyze the coupling losses in a twisted superconducting composite.

Coupling currents are induced in a multifilamentary superconducting composite subjected in a changing magnetic field, and consequently, so-called coupling losses are caused in normal metal region surrounding it. The coupling losses can be analyzed by solving electric fields in the normal metal region under analytically derived boundary conditions [4.8, 4.9].

Recently, a useful method based on FE method were proposed for the analysis of the inter-strand coupling losses in cables with complicated cross-sections [4.10]. In the method, the two-dimensional Laplace equation described in the fixed coordinates is solved by FE method neglecting the twist of the cables. However, as the pitch decreases, the electric field distribution may become considerably different from that for a straight cable. In such cases, therefore, the coupling losses should be evaluated taking account of the twist of the cable. This section provides an FE analysis of the inter-strand coupling losses in which the helical field is rigorously and easily calculated using the twisted coordinates described in Sec. 2.2.1.

Let us consider a superconducting cable composed of three strands immersed in a time harmonic magnetic field B in x-direction shown in Fig. 4.11 The multifilamentary superconducting wires and the three cables are twisted at the pitch L and l, respectively. The normal metal regions surrounding the multifilamentary region are electrically contacted to each other with an contact angle θ_c, and the resistance between the strands is assumed to be sufficiently small. The induced voltage ϕ_k on the boundary Γ_k^i between the multifilamentary region and normal metal is given by [4.9]

$$\begin{aligned}
\Phi_k &= \Phi_{Ok} + \Phi_{sk}, \\
\Phi_{Ok} &= -\frac{BR}{h}\cos\left[hz + \frac{2\pi}{3}(k-1)\right], \\
\Phi_{sk} &= -\frac{Br}{H}\cos\left[hz + \frac{2\pi}{3}(k-1) + \theta_k\right],
\end{aligned} \tag{4.50}$$

where $H=2\pi/L$, $h=2\pi/l$, r and R denote the radius of multifilamentary region

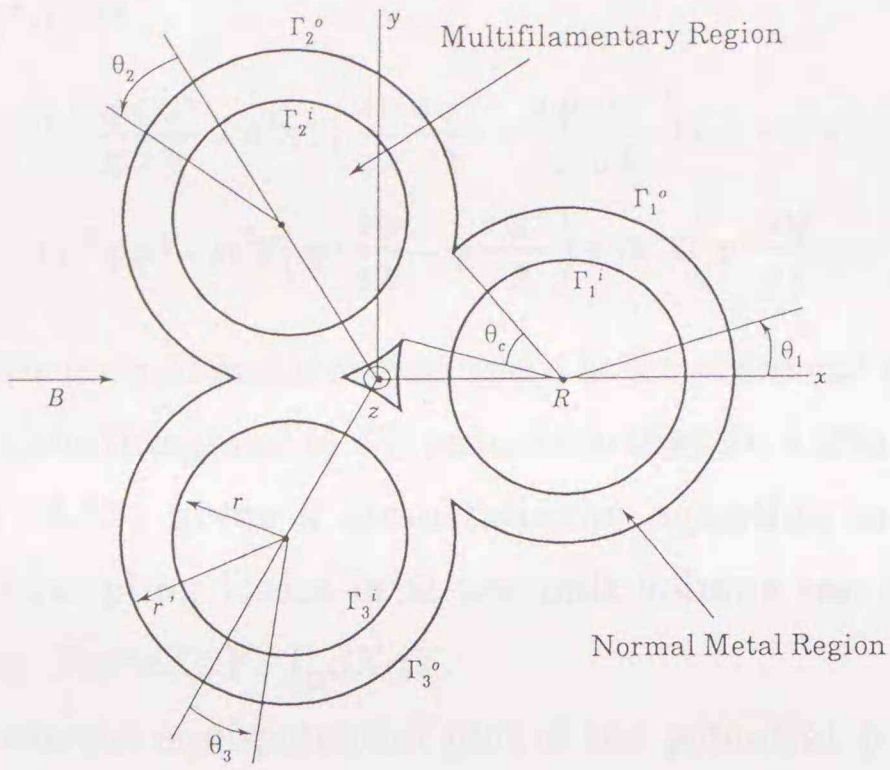

Fig. 4.11 Superconducting cable composed of three strands

and the distance between the center of the cable and the axis of rotation, respectively.

In order to calculate the losses in the normal metal region, the Laplace equation is solved under the boundary condition (4.50) and $\mathbf{n} \cdot \nabla\phi = 0$ on Γ_k^o, where $\mathbf{n}$ is the unit normal vector of the outer surface of the cable and Γ_k^o is the intersection of the surface and the plane of z=constant and ϕ is the potential function. When the electric field is described in the fixed Cartesian coordinates (x, y, z), the potential is the involved, three-dimensional function of the coordinates because the cables are twisted around the z-axis. However, the introduction of the twisted coordinates (2.48) in which the transverse axes X and Y rotate with the rotation of the cross-section of the cable, may allow us to express the potential in the simple form as

$$\Phi = \psi(X, Y)\, e^{jhZ}. \tag{4.51}$$

Moreover, the boundary condition (4.50) is rewritten in the complex form as

$$\Psi_k = -\frac{BR}{\sqrt{2}h} e^{j\frac{2\pi}{3}(k-1)} - \frac{Br}{\sqrt{2}H} e^{j\left[\frac{2\pi}{3}(k-1)+\theta_k\right]}. \tag{4.52}$$

The solution to the helical Laplace equation (4.1) can be found by minimizing the functional

$$F = \int_{\Omega} \sigma \nabla\psi \cdot \nabla\psi^* \, dXdY \ , \tag{4.53}$$

$$\nabla\psi \cdot \nabla\psi^* = (1+h^2Y^2)\frac{\partial\psi}{\partial X}\frac{\partial\psi^*}{\partial X} - h^2XY\left(\frac{\partial\psi}{\partial X}\frac{\partial\psi^*}{\partial Y} + \frac{\partial\psi}{\partial Y}\frac{\partial\psi^*}{\partial X}\right) + (1+h^2X^2)\frac{\partial\psi}{\partial Y}\frac{\partial\psi^*}{\partial Y}$$
$$+ h^2\psi\psi^* - jh^2Y\left(\psi^*\frac{\partial\psi}{\partial X} - \psi\frac{\partial\psi^*}{\partial X}\right) + jh^2X\left(\psi^*\frac{\partial\psi}{\partial Y} - \psi\frac{\partial\psi^*}{\partial Y}\right), \tag{4.54}$$

where Ω denotes the normal metal region and σ is the conductivity of Ω. Note that when $h \rightarrow 0$ ($l \rightarrow \infty$), the integrand (4.54) reduces to that for a straight cable. An FE discretization of (4.53) gives a simultaneous equation similar to (4.28). Consequently, the coupling losses in Ω per unit volume can be obtained from $P=[1-(r/r')^2]\int_{\Omega}\sigma\nabla\psi \cdot \nabla\psi^* dXdY / \int_{\Omega} dXdY$.

Figure 4.12 shows the equi-potential plot of the potential ϕ for $l/r=3.33$ and 20.0. The solutions obtained by neglecting the twist are shown in (a) and (c) and the corresponding solutions by the present method are (b) and (d). As shown in (a) and (b), for small pitch, there appear the clear differences in the potential distributions. In particular, (b) shows that the twist increases the electric field strength. In addition, as one can see in figures (b) and (d), the contour lines are not perpendicular to Γ_k^o because of the twist effect of the cable.

Figure 4.13 shows the dependence of the loss $\overline{P}$, which is normalized by P obtained by the present method for $l/L=0.1$, on the ratio l/L when the twist is taken into account (solid line) and not (broken line). As expected, when l/L increases, the curves asymptotically approach each other. (Practical values of l/L are usually greater than unity.) On the other hand, while both curves are parabolic, there are differences in the positions and values of their minima. Moreover, when $l/L \rightarrow 0$, the loss for the former case diverges while that for the latter case converges to a finite value. It is obvious that as $l/L \rightarrow 0$, the equi-potential lines infinitely approach each other, and consequently, the strength of the electric field becomes infinite. Therefore, we conclude that the result by the present method is more reasonable. The present method can be easily applied to the analysis of cables with more complicated cross-sections.

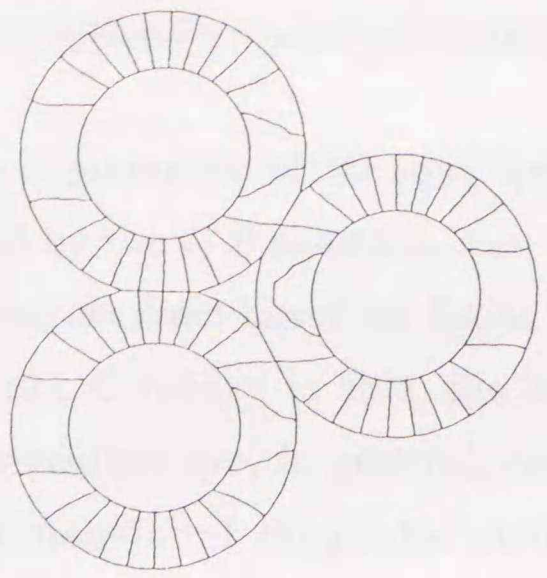

(a) $l/r=3.33$ (without twist effect)

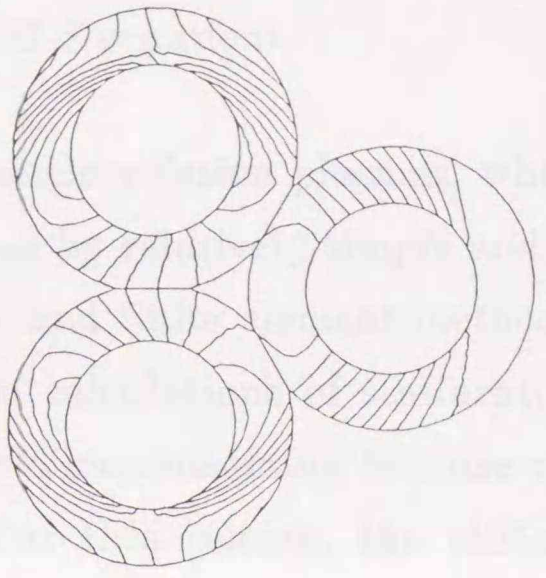

(b) $l/r=3.33$ (with twist effect)

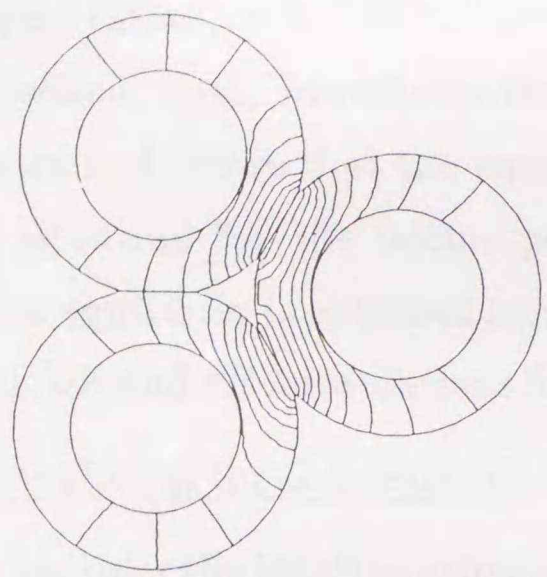

(c) $l/r=20.0$ (without twist effect)

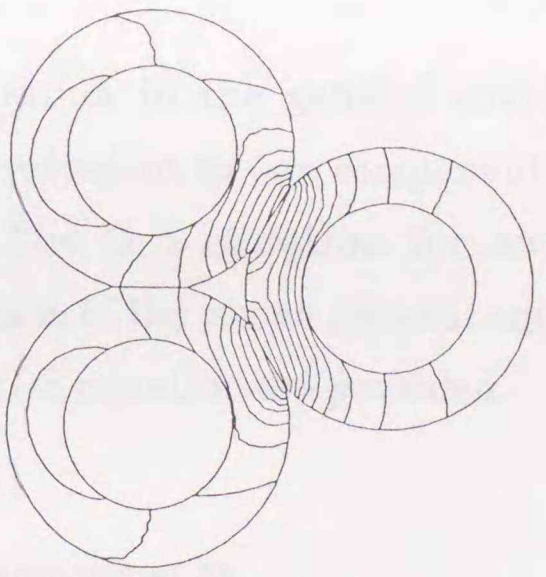

(d) $l/r=20.0$ (with twist effect)

Fig. 4.12 Equi-potential plot for $L/r=6.67$, $r'/r=1.67$, $\theta_c=30°$, $\sigma=$const.

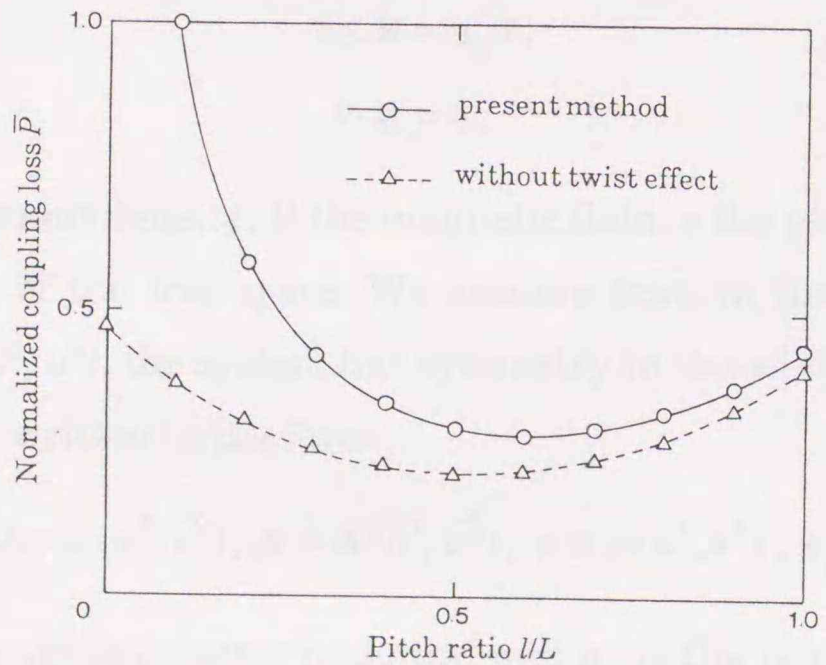

Fig. 4.13 Normalized coupling losse P plotted against pitch ratio l/L for $L/r=6.67\times10$, $r'/r=1.67$, $\theta_c=30°$, $\sigma=$const.

4.3 Formulation for vector potential problems (G-S equation)

The axisymmetric MHD equilibria of the nuclear fusion plasmas, which are governed by the G-S equation, can be obtained by relatively simple and small-scale computations based on finite difference and finite element methods [e.g. 4.11, 4.12]. Contrary to this, the equilibrium calculations of stellarator-type fusion machines are, in general, considerably time-consuming because of their three dimensional magnetic structures. For this reason, the stellarator configuration is often approximated as being helically symmetric in the limit of large aspect ratio.

This section, first, introduces the G-S equation in the general curvilinear coordinates and shows that the equation is equivalent to one component of the Poisson equation for the vector potential. The G-S equation for helically symmetric equilibria is obtained as a special case of the above general equation. Moreover, BE and FE formulations for helical G-S equation are provided.

4.3.1 Derivation of the G-S equation [4.13, 4.14]

Let us consider the MHD equilibrium equations given by

$$\mathbf{J} \times \mathbf{B} = \nabla p \,, \tag{4.55}$$

$$\nabla \times \mathbf{B} = \mu_0 \mathbf{J} \,, \tag{4.56}$$

$$\nabla \cdot \mathbf{B} = 0 \,, \tag{4.57}$$

where $\mathbf{J}$ is the current density, $\mathbf{B}$ the magnetic field, p the plasma pressure and μ_0 the permeability of the free space. We assume that, in the general curvilinear coordinates (u^1, u^2, u^3), the system has symmetry in the u^3-direction and physical quantities can be written in the form

$$\mathbf{B} = \mathbf{B}(u^1, u^2),\ \mathbf{J} = \mathbf{J}(u^1, u^2),\ \mathbf{A} = \mathbf{A}(u^1, u^2),\ p = p(u^1, u^2)\,,\ g_{ij} = g_{ij}(u^1, u^2), \tag{4.58}$$

where $\mathbf{A}$ is the magnetic vector potential and g_{ij} is the covariant metric tensor. From the relation $\mathbf{B} = \nabla \times \mathbf{A}$, the magnetic field $\mathbf{B}$ is expressed in terms of the vector potential $\mathbf{A}$ as

$$\mathbf{B} = B^1\mathbf{e}_1 + B^2\mathbf{e}_2 + B^3\mathbf{e}_3$$

$$= \frac{1}{\sqrt{g}}\frac{\partial A_3}{\partial u^2}\mathbf{e}_1 - \frac{1}{\sqrt{g}}\frac{\partial A_3}{\partial u^1}\mathbf{e}_2 + B^3\mathbf{e}_3$$

$$= \nabla A_3 \times \mathbf{e}^3 + B^3\mathbf{e}_3. \tag{4.59}$$

The magnetic lines lie on the surfaces of A_3 = constant because the magnetic field B satisfies the relation $\mathbf{B} \cdot \nabla A_3 = 0$ as shown in (4.59) (note that $\nabla A_3 \cdot \mathbf{e}_3 = 0$) and those surfaces are called the magnetic surfaces. In addition, the physical quantity which is constant on the magnetic surface is referred to as the surface quantity. The limiting magnetic surface which approaches a single magnetic line is called the magnetic axis. (see Fig. 4.14)

Similarly, from (4.56), we have

$$\mathbf{J} = J^1\mathbf{e}_1 + J^2\mathbf{e}_2 + J^3\mathbf{e}_3$$

$$= \frac{1}{\sqrt{g}}\frac{\partial B_3}{\partial u^2}\mathbf{e}_1 - \frac{1}{\sqrt{g}}\frac{\partial B_3}{\partial u^1}\mathbf{e}_2 + \mu_0 J^3\mathbf{e}_3$$

$$= \nabla B_3 \times \mathbf{e}^3 + \mu_0 J^3\mathbf{e}_3. \tag{4.60}$$

The substitution of (4.59) and (4.60) into (4.55) yields

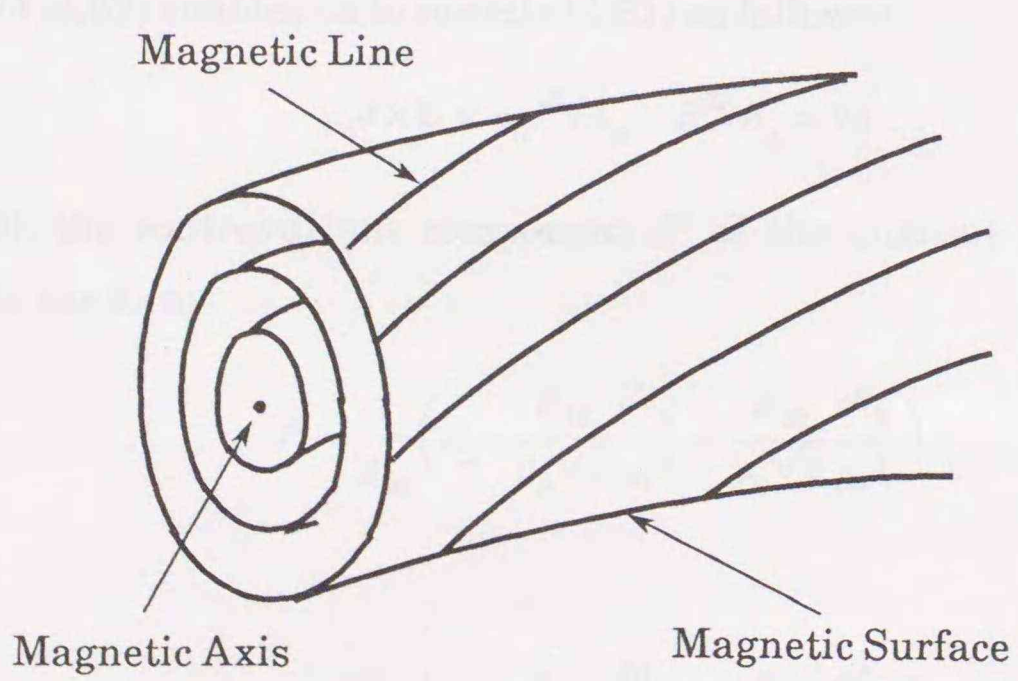

Fig. 4.14 Magnetic surfaces

$$\mu_0 \mathbf{J}\times\mathbf{B} = \mu_0 J^3 \nabla A_3 - B^3 \nabla B_3 + \frac{1}{\sqrt{g}}\left(\frac{\partial A_3}{\partial u^2}\frac{\partial B_3}{\partial u^1} - \frac{\partial A_3}{\partial u^1}\frac{\partial B_3}{\partial u^2}\right)\mathbf{e}^3$$

$$= \nabla p \ . \tag{4.61}$$

By considering $\partial p/\partial u^3 = 0$ in (4.61), we find

$$\frac{\partial A_3}{\partial u^2}\frac{\partial B_3}{\partial u^1} - \frac{\partial A_3}{\partial u^1}\frac{\partial B_3}{\partial u^2} = 0 \ . \tag{4.62}$$

Then,

$$B_3 = B_3(A_3) \ . \tag{4.63}$$

Hence, the third covariant component B_3 of the magnetic field is the surface quantity. In addition, since $\nabla p \cdot \mathbf{B} = 0$, we can similarly derive the relation

$$p = p(A_3) \ . \tag{4.64}$$

This implies that the plasma pressure is also the surface quantity. From (4.63) and (4.64), we obtain

$$\nabla B_3 = \frac{dB_3}{dA_3}\nabla A_3 \ , \tag{4.65}$$

$$\nabla p = \frac{dp}{dA_3}\nabla A_3 \ . \tag{4.66}$$

The use of (4.62) enables us to rewrite (4.61) as follows :

$$\mu_0 \mathbf{J}\times\mathbf{B} = \mu_0 J^3 \nabla A_3 - B^3 \nabla B_3 = \nabla p \ . \tag{4.67}$$

From (4.60), the contravariant component J^3 of the current in (4.67) can be expressed in the form

$$J^3 = \frac{1}{g_{33}}\left(J_3 - \frac{g_{13}}{\mu_0\sqrt{g}}\frac{\partial B_3}{\partial u^2} + \frac{g_{23}}{\mu_0\sqrt{g}}\frac{\partial B_3}{\partial u^1}\right). \tag{4.68}$$

Similarly,

$$B^3 = \frac{1}{g_{33}}\left(B_3 - \frac{g_{13}}{\mu_0\sqrt{g}}\frac{\partial A_3}{\partial u^2} + \frac{g_{23}}{\mu_0\sqrt{g}}\frac{\partial A_3}{\partial u^1}\right). \tag{4.69}$$

The insertion of (4.68) and (4.69) in (4.67) yields

$$\mu_0 \mathbf{J} \times \mathbf{B} = \frac{1}{g_{33}} (\mu_0 J_3 \nabla A_3 - B_3 \nabla B_3) = \nabla p \ . \tag{4.70}$$

Moreover, from (4.65), (4.66) and (4.70), we have

$$\mu_0 J_3 = \mu_0 g_{33} \frac{dp}{dA_3} + B_3 \frac{dB_3}{dA_3} \ . \tag{4.71}$$

On the other hand, the current component J_3 can be written in terms of the vector potential using (4.56) as follows :

$$\mu_0 J_3 = -[\nabla^2 \mathbf{A}]_3 \ . \tag{4.72}$$

(Here note that $[\nabla(\nabla \cdot \mathbf{A})]_3 = \partial/\partial u^3 (\nabla \cdot \mathbf{A}) = 0$) Consequently, from (4.71) and (4.72), we obtain the G-S equation in the general curvilinear coordinates,

$$\mu_0 J_3 = -[\nabla^2 \mathbf{A}]_3 = \mu_0 g_{33} \frac{dp}{dA_3} + B_3 \frac{dB_3}{dA_3} \ . \tag{4.73}$$

The explicit representation of the vector Laplacian in (4.73) is given by [4.14]

$$[\nabla^2 \mathbf{A}]_3 = g_{33} \nabla \cdot \left(\frac{\nabla A_3}{g_{33}} \right) - \frac{g_{33}}{\sqrt{g}} \left[\frac{\partial}{\partial u^1} \left(\frac{g_{23}}{g_{33}} \right) - \frac{\partial}{\partial u^2} \left(\frac{g_{13}}{g_{33}} \right) \right] B_3 \ . \tag{4.74}$$

As we can see in (4.73), the G-S equation can be regarded as the third covariant component of the vector Poisson equation. This equation has the inhomogeneous term consisting of the surface quantities in its right hand side, and the dependence of them on A_3 is determined from models of the plasma. Since the inhomogeneous term in (4.73) is the nonlinear function of A_3 except particular cases, the G-S equation must in general be solved iteratively.

In the following, we consider the physical meaning of the function A_3 [4.13]. We define the transverse flux Ψ as the flux through the ribbonlike surface S shown in Fig. 4.15. The contour ∂S of the surface S is composed of s_1, s_2, s_3 and s_4, and edges s_1 and s_3 lie on the surfaces of $u^3 =$ constant, and other edges s_2 and s_4 are parallel to u^3-axis (or $\mathbf{e}_3$). Moreover, the surface element $d\mathbf{S}$ on S is perpendicular to $\mathbf{e}_3$.

In this case, the transverse flux Ψ is given by

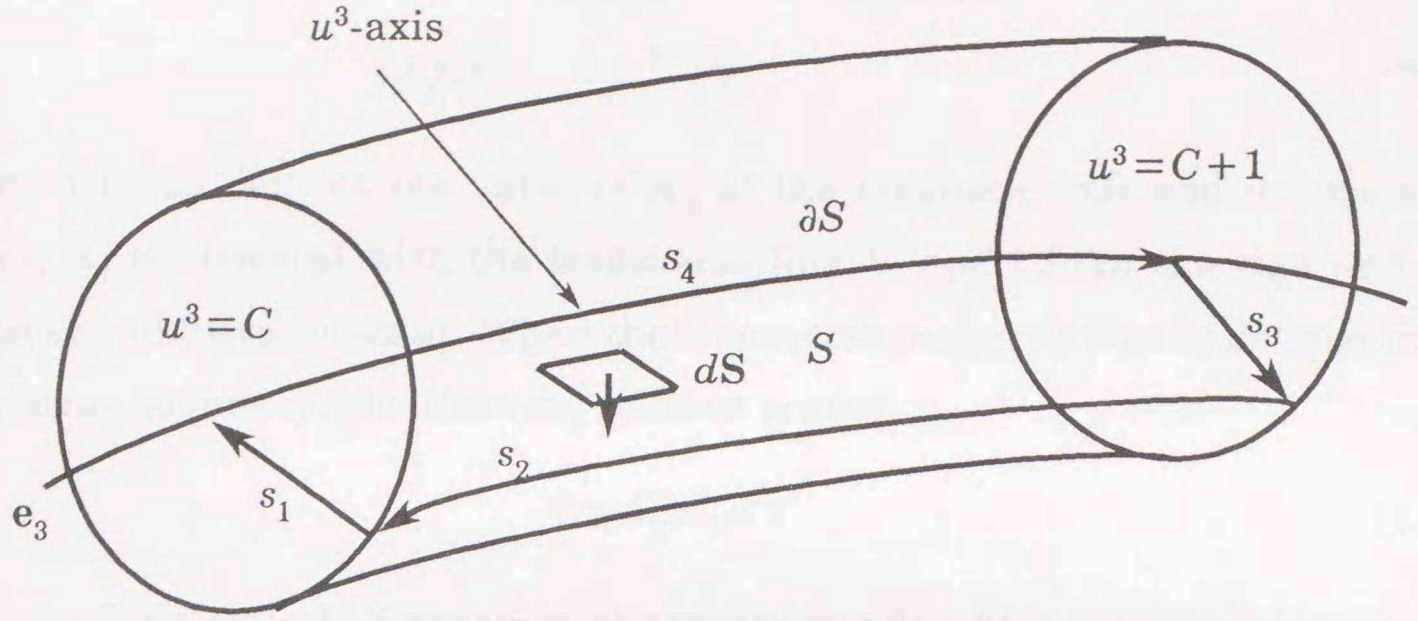

Fig. 4.15 Definition of the transverse flux (stream function) Ψ

$$\Psi = \int_S \mathbf{B} \cdot d\mathbf{S} \ . \tag{4.75}$$

The insertion of (4.59) in (4.75) yields,

$$\Psi = \int_S (\nabla A_3 \times \mathbf{e}^3) \cdot d\mathbf{S} \ . \tag{4.76}$$

Rewriting the integrand in (4.76) as,

$$\begin{aligned} \nabla A_3 \times \mathbf{e}^3 &= \nabla \times (A_3 \mathbf{e}^3) \\ &= \nabla \times [\, \nabla (u^3 A_3) - u^3 \nabla A_3 \,] \\ &= -\nabla \times (u^3 \nabla A_3) \quad , \end{aligned} \tag{4.77}$$

and applying the Stokes' theorem to (4.76), we have

$$\Psi = -\int_{\partial S} u^3 \nabla A_3 \cdot d\mathbf{s} \ . \tag{4.78}$$

Since s_2 and s_4 do not contribute to the above integral, the following relation can be obtained,

$$\Psi = -(C+1)\int_{A_3(\text{axis})}^{A_3(u^1,u^2)} dA_3 - C\int_{A_3(u^1,u^2)}^{A_3(\text{axis})} dA_3$$

$$= A_3(\text{axis}) - A_3(u^1, u^2), \tag{4.79}$$

where A_3(axis) denotes the value of A_3 at the magnetic axis and is constant. Hence, A_3 is identical with the transverse flux Ψ apart from the sign and an irrelevant additive constant. When the transverse magnetic flux is defined from the plasma boundary, the following relation is used

$$\Psi = A_3(u^1, u^2) \ . \tag{4.80}$$

In the analysis of the G-S equation, the transverse flux Ψ is usually chosen as an unknown function rather then A_3 and the function Ψ is often called the magnetic stream function.

There are a few typical and important cases for the inhomogeneous term in (4.73). In the remainder of this section, we discuss the relation among the magnetic field **B**, current **J** and pressure p.

Using (4.59), (4.60) and (4.65), the contravariant component J^1 of the current can be expressed in the form

$$J^1 = \frac{1}{\mu_0\sqrt{g}}\frac{\partial B_3}{\partial u^2}$$

$$= \frac{1}{\mu_0\sqrt{g}}\frac{dB_3}{dA_3}\frac{\partial A_3}{\partial u^2}$$

$$= \frac{1}{\mu_0}B^1\frac{dB_3}{dA_3} \ . \tag{4.81}$$

Similarly,

$$J^2 = \frac{1}{\mu_0}B^2\frac{dB_3}{dA_3} \ . \tag{4.82}$$

On the other hand, from (4.59), (4.65), (4.68) and (4.73), J^3 is written in terms of p and the components of **B** as follows :

$$J^3 = \frac{1}{g_{33}}\left(J_3 - \frac{g_{13}}{\mu_0\sqrt{g}}\frac{dB_3}{dA_3}\frac{\partial A_3}{\partial u^2} + \frac{g_{23}}{\mu_0\sqrt{g}}\frac{dB_3}{dA_3}\frac{\partial A_3}{\partial u^1}\right)$$

$$= \frac{1}{g_{33}}\left(J_3 - \frac{g_{13}}{\mu_0}B^1\frac{dB_3}{dA_3} - \frac{g_{23}}{\mu_0}B^2\frac{dB_3}{dA_3}\right)$$

$$= \frac{1}{g_{33}}\left(g_{33}\frac{dp}{dA_3} + \frac{B_3}{\mu_0}\frac{dB_3}{dA_3} - \frac{g_{13}}{\mu_0}B^1\frac{dB_3}{dA_3} - \frac{g_{23}}{\mu_0}B^2\frac{dB_3}{dA_3}\right)$$

$$= \frac{dp}{dA_3} + \frac{B^3}{\mu_0}\frac{dB_3}{dA_3} \quad . \tag{4.83}$$

Consequently, we obtain the following relation from (4.81)-(4.83),

$$\mu_0 \mathbf{J} = \frac{dB_3}{dA_3}\mathbf{B} + \mu_0\frac{dp}{dA_3}\mathbf{e}_3 \quad . \tag{4.84}$$

From (4.84), we see that when $dp/dA_3 = 0$, the MHD equilibrium represents the force-free state because the current **J** is parallel to **B**. In this case, the G-S equation becomes equivalent to the proper equation $\nabla \times \mathbf{B} = \lambda \mathbf{B}$, where $\lambda = dB_3/dA_3$.

On the other hand, when $dB_3/dA_3 = dp/dA_3 = 0$, the solutions to the G-S equation represent vacuum fields because the plasma current **J** vanishes.

4.3.2 BE and FE formulation for G-S equation [4.15, 4.16]

The G-S equation for helically symmetric MHD equilibria is readily derived by inserting the metric tensor (2.54) of the twisted coordinates into (4.73) as follows :

$$\nabla \cdot (\kappa \nabla \Psi) = f(r, \Psi), \tag{4.85}$$

where

$$\kappa = \frac{h^2}{1+h^2 r^2}, \tag{4.86}$$

$$f(r, \Psi) = \frac{2}{h}\kappa^2 g - \kappa g g' - \mu_0 h^2 p', \tag{4.87}$$

$\Psi = A_3$ and $g = B_3$. The function $f(\Psi, r)$ defined by (4.85) takes the same form when the G-S equation is described in the helical polar coordinates. The divergence and gradient in (4.85) are given in Sec. 2.2.1 for the twisted coordinates and Sec. 2.2.2 for the helical polar coordinates. The components of magnetic field and plasma current are expressed in terms of the stream function Ψ satisfying (4.85) as follows :

in the twisted coordinates (X, Y, Z)

$$B^X = \frac{\partial \Psi}{\partial Y}, \quad B^Y = -\frac{\partial \Psi}{\partial X}, \quad B^Z = \frac{1}{1+h^2 r^2}\left[g + h\left(X\frac{\partial \Psi}{\partial X} + Y\frac{\partial \Psi}{\partial Y}\right)\right], \tag{4.88}$$

$$J^X = \frac{1}{\mu_0}\frac{\partial g}{\partial Y}, \quad J^Y = -\frac{1}{\mu_0}\frac{\partial g}{\partial X}, \quad J^Z = p' + \frac{g'}{\mu_0(1+h^2 r^2)}\left[g + h\left(X\frac{\partial \Psi}{\partial X} + Y\frac{\partial \Psi}{\partial Y}\right)\right]. \tag{4.89}$$

in the helical polar coordinates (r, ζ, Z)

$$B^r = \frac{1}{r}\frac{\partial \Psi}{\partial \zeta}, \quad B^\zeta = -\frac{1}{r}\frac{\partial \Psi}{\partial r}, \quad B^Z = \frac{1}{1+h^2 r^2}\left(g + hr\frac{\partial \Psi}{\partial r}\right), \tag{4.90}$$

$$J^r = \frac{1}{\mu_0 r}\frac{\partial g}{\partial \zeta}, \quad J^\zeta = -\frac{1}{\mu_0 r}\frac{\partial g}{\partial r}, \quad J^Z = p' + \frac{g'}{\mu_0(1+h^2 r^2)}\left(g + hr\frac{\partial \Psi}{\partial r}\right). \tag{4.91}$$

In addition, using the relations (2.66) and (2.67), the functions Ψ and g can be written in terms of the components of B in the cylindrical coordinates (r, θ, z) as

$$B_r = \frac{1}{r}\frac{\partial \Psi}{\partial \zeta}, \quad B_\theta - hrB_z = -\frac{\partial \Psi}{\partial r}, \quad hrB_\theta + B_z = g. \tag{4.92}$$

We below deal with the BE and FE formulations for an MHD equilibrium problem in the fixed, closed plasma region V_C shown in Fig. 4.1. The boundary condition for the stream function Ψ, which is arbitrary to the extent that a constant can be added to itself, is given on the plasma boundary $\partial\Omega_I$ as

$$\Psi = 0 . \tag{4.93}$$

The integral equation for (4.85) can be derived after some mathematical procedures similar to the ones described in Sec. 4.1.1 as follows :

$$\int_{\partial\Omega_I} G_S q \,|\mathbf{N}|\, ds = -\int_{\Omega_C} f(\Psi, r)\, G_S \, dX dY , \tag{4.94}$$

where $q = \partial\Psi/\partial n$ and the fundamental solution G_S satisfies

$$\nabla\cdot(\kappa\nabla G_S) + 4\pi\delta(Y-Y_0)\,\delta(Y-Y_0) = 0 , \tag{4.95}$$

which is equivalent to

$$\nabla\cdot(\kappa\nabla G_S) + 4\pi\delta(r-r_0)\,\delta(\zeta-\zeta_0)/r = 0 . \tag{4.96}$$

The explicit form of G_S is given by (3.27).

Here note that numerical evaluation of the surface integral in (4.94) is time-consuming compared to that of line integrals. The BE method, therefore, may not be very suitable to the MHD equilibrium analysis. In addition, when the function f is a nonlinear function of Ψ, equation (4.94) must be solved iteratively. In such cases, the adoption of the Picard iteration may be the simplest way to find a solution to (4.94),

$$\int_{\partial\Omega_I} G_S q^{n+1} \,|\mathbf{N}|\, ds = -\int_{\Omega_C} f(\Psi^n, r)\, G_S \, dX dY , \tag{4.97}$$

where n denotes the number of iterative steps. The value of Ψ^{n+1}, which is necessary for the calculation of q^{n+2}, is obtained from

$$4\pi\Psi^{n+1} = \int_{\partial\Omega_I} G_S q^{n+1} \,|\mathbf{N}|\, ds + \int_{\Omega_C} f(\Psi^n, r)\, G_S \, dX dY . \tag{4.98}$$

A usual BE discretization of (4.97) and (4.98) provides the following recursive equations in matrix form

$$[G_{ij}^{BB}][q^{n+1}] = [B^{BI}([\Psi^n])], \tag{4.99}$$

$$4\pi[\Psi^{n+1}] = [G_{ij}^{IB}][q^{n+1}] + [B^{II}([\Psi^n])]. \tag{4.100}$$

On the other hand, the FE formulation is carried out on the basis of the weighted residual representation of (4.85),

$$\int_{V_C} W[\nabla \cdot (\kappa \nabla \Psi) - f(r, \Psi)]\, dV = 0. \tag{4.101}$$

Integrating (4.101) with respect to Z and applying Gauss' theorem, we find

$$\int_{\Omega_C} [\kappa \nabla W \cdot \nabla \Psi + W f(r, \Psi)]\, dX dY = 0. \tag{4.102}$$

The FE discretization of (4.102) and application of the Picard iteration yield the recursive equation in matrix form

$$[K_{ij}][\Psi^{n+1}] = [F([\Psi^n])]. \tag{4.103}$$

In conclusion, the numerical solutions Ψ to the MHD equilibrium equation (4.85) can be obtained from (4.99), (4.100) and (4.103) if the Picard iteration is stable. The convergence of the Picard iteration will be discussed in the next section.

4.4 Analysis of vector potential problems

In this section, the formulation given in the previous section will be applied to the analysis of two helically symmetric MHD equilibrium models which have a circular and bean-shaped cross-sections, respectively. The numerical solutions for the vacuum field for the first model will be compared with the exact solution. Then, the convergence of iterative methods for the nonlinear G-S equation will be investigated numerically and theoretically. Finally, an effective iterative method will be offered and its performance will be shown using the second model.

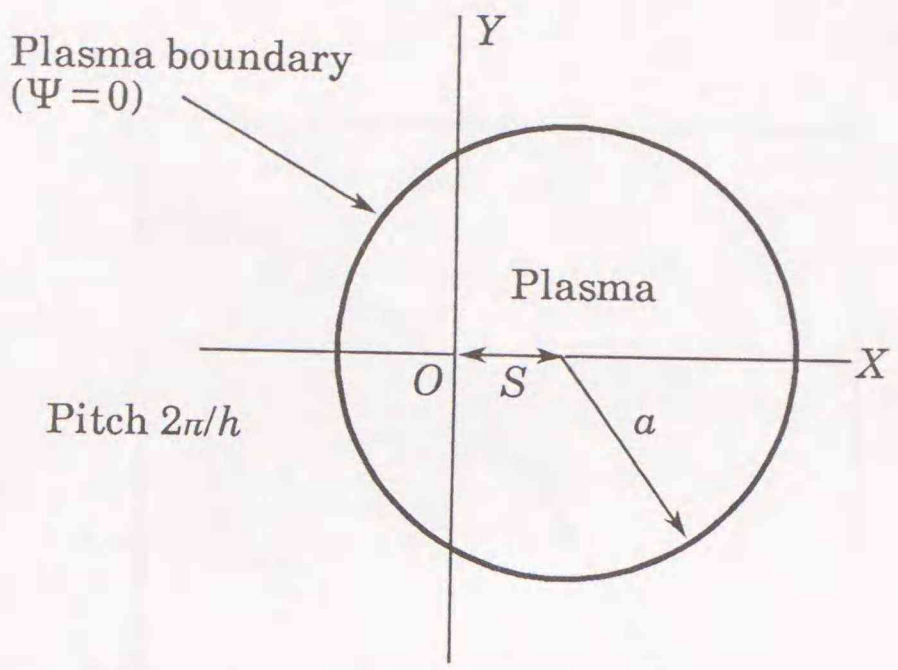

Fig. 4.16 A plasma with circular cross-section

4.4.1 Linear problem

Let us consider the MHD equilibrium with a circular plasma boundary shown in Fig. 4.16. In this model, if $p(\Psi)$ and $g(\Psi)$ take the following special forms,

$$g(\Psi) = g_0 + g_1 \Psi, \quad p'(\Psi) = p_0 \tag{4.104}$$

we can find the exact solution to (4.85) for $S=0$ as follows [4.15] :

$$\Psi = -\frac{g_0}{g_1} - \frac{\mu_0 p_0}{g_1^2}\left(1 + h^2 r^2 + \frac{2h}{g_1}\right) + h\frac{g_0 g_1^2 + \mu_0 p_0 (g_1 + h^2 a^2 g_1 + 2h)}{g_1^3 [\, ah J_1(g_1 a) + J_0(g_1 a)\,]}\left[r J_1(g_1 r) + \frac{1}{h} J_0(g_1 r)\right] \tag{4.105}$$

where J_0 and J_1 are the zeroth- and first-order Bessel functions of the first kind, respectively.

Figures 4.17 and 4.18 show the profiles and convergence of the BE and FE solutions for $g_0 = \mu_0 p_0 = h = a = 1.0$ and $g_1 = -1.0$. As shown in these figures, both numerical methods provide reasonable solutions, which can be obtained after less than 10 iterations [4.16].

The vacuum configurations computed by BE method for $p_0 = g_1 = 0$ (see the last paragraph of Sec. 4.3.1) are shown in Figs. 4.19 (a)~(e) [4.17]. These calculations do not need iteration since the right hand sides of (4.99) and (4.103) do not include Ψ any longer. In the figures, the solid lines denote magnetic surfaces, which are defined as contour lines of Ψ. As mentioned in Sec. 4.3.1, plasma pressure is constant on these surfaces and magnetic lines lie on them. From figures (a)~(c),

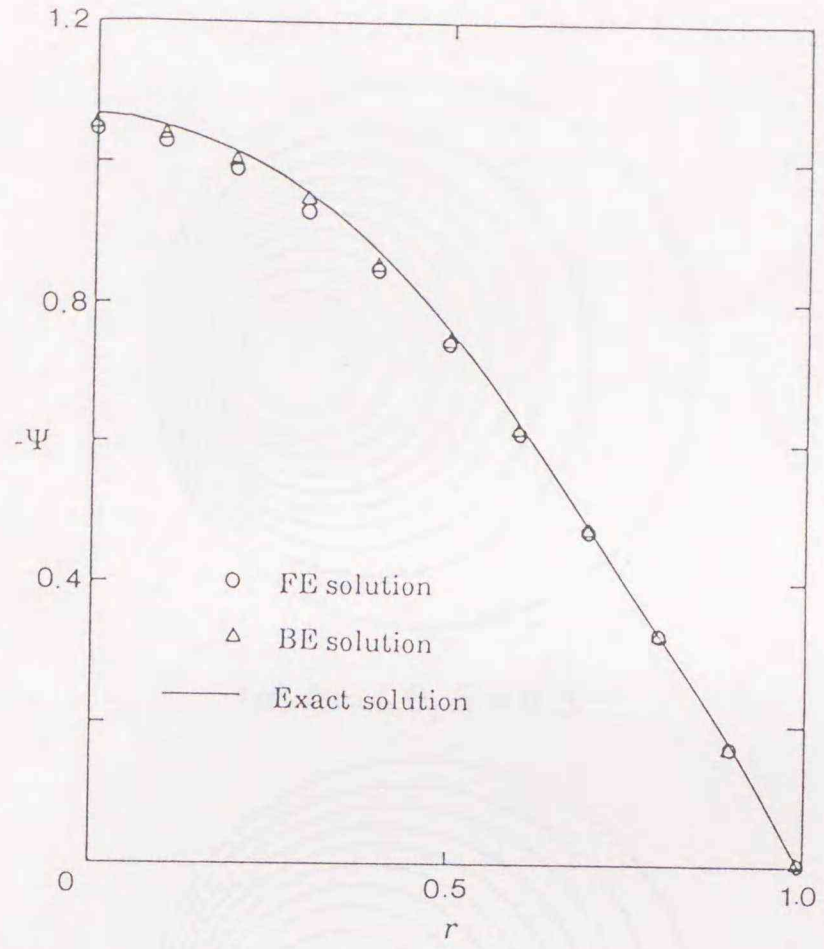

Fig. 4.17 Numerical and exact solutions for the circular boundary plasma model. (p and g are given by (4.104) and $S=0$)

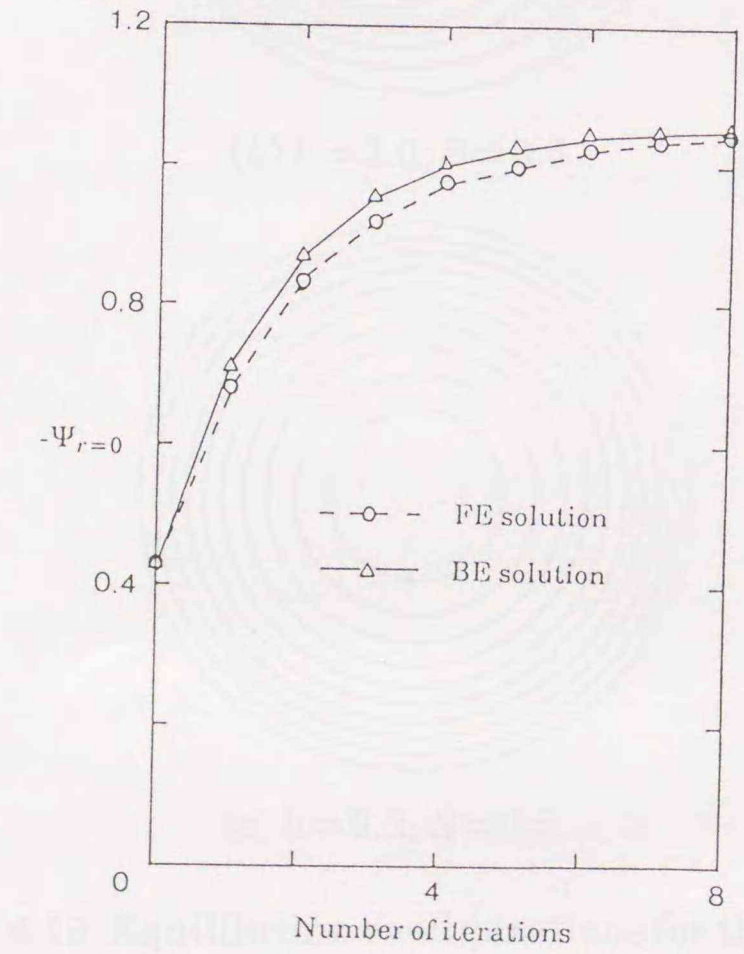

Fig. 4.18 Convergence of the Picard iteration for the solution shown in Fig. 4.17.

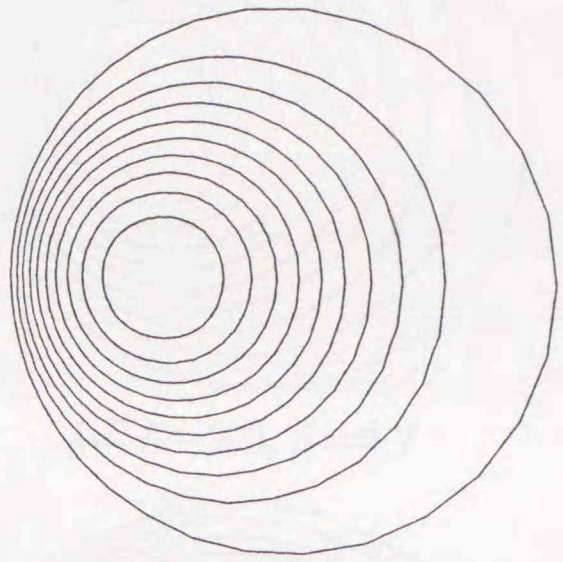

(*a*) $h=4.0, S=0.5$

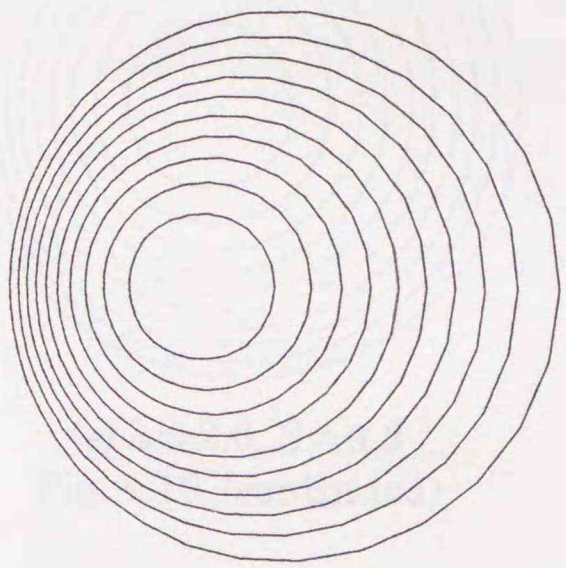

(*b*) $h=2.0, S=0.5$

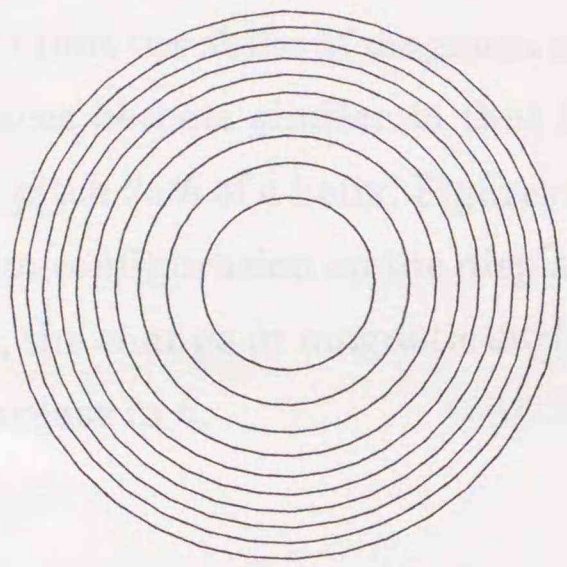

(*c*) $h=0.2, S=0.5$

Fig. 4.19 Equilibrium configurations for the circular boundary plasma model.

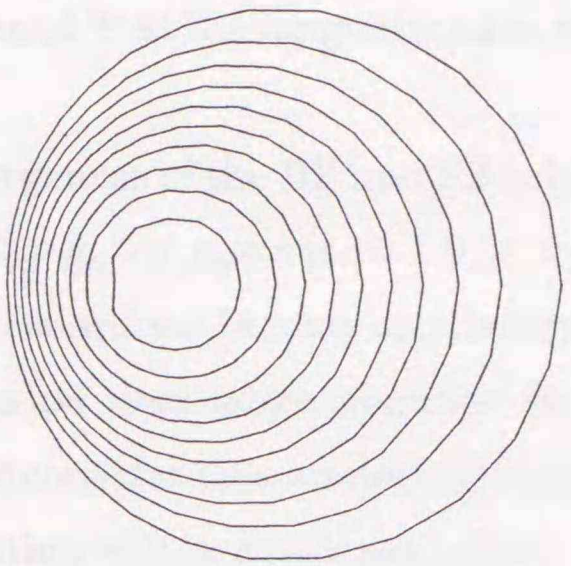

(*d*) $h=2.0, S=0.7$

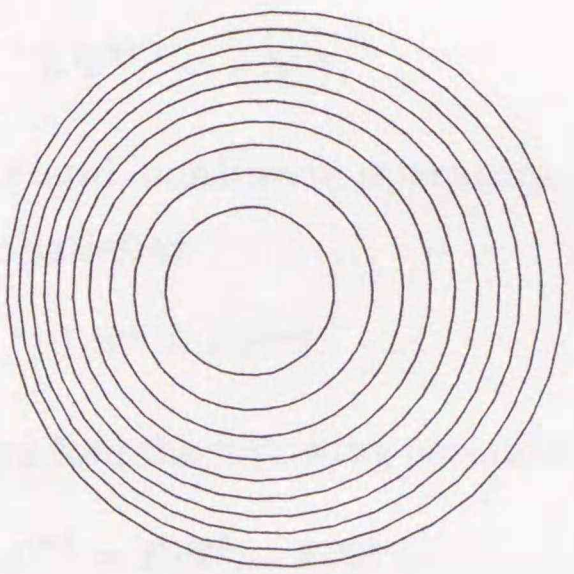

(*e*) $h=2.0, S=0.2$

Fig. 4.19 (continued)

which represent the dependence of the equilibrium configuration on the helical wavenumber h, it can be seen that the shifts of magnetic surfaces decrease with h or, in other words, the surfaces become similar to that in the straight circular cylinder with increase in the pitch $2\pi/h$ of a helix. Figures (*b*), (*d*) and (*e*) show the dependence of the equilibrium configuration on the displacement from the origin S. As shown in these figures, the change in magnetic surfaces with decrease in S is similar to that with the decrease in h.

4.4.2 Non-linear problem

In the plasma models considered below, the functions $p(\Psi)$ and $g(\Psi)$ are taken to be of the form

$$g(\Psi) = g_0 + g_1 \frac{\Psi}{\Psi_m}, \quad p'(\Psi) = p_0 \frac{1}{\Psi_m} + 2p_1 \frac{\Psi}{\Psi_m^2} \tag{4.106}$$

where Ψ_m denotes the value of Ψ at the magnetic axis, which can not be known *a priori*.

Figure 4.20 shows convergences of the BE and FE solution procedures given by (4.99), (4.100) and (4.103) for $g_0=\mu_0 p_0=h=a=1.0$, $g_1=$-1.0 and $p_1=0$. As shown in this figure, the iterative solutions become oscillatory in contrast to the linear case. Moreover, it is revealed that more increase in g_1 makes the iteration divergent [4.18]. In order to consider this numerical instability, the mathematical property of the Picard iteration will be discussed below.

Let us consider the Picard iteration

$$L\,\Psi^{n+1} = F(\Psi^n), \tag{4.107}$$

where L and F are linear and nonlinear operators, respectively. The exact solution Ψ^* to this problem satisfies

$$L\,\Psi^* = F(\Psi^*). \tag{4.108}$$

From (4.107) and (4.108), we find the following equation for the error $e_n=\Psi_n-\Psi^*$

$$\begin{aligned} L\,e^{n+1} &= F(\Psi^n) - F(\Psi^*) \\ &\simeq \frac{\partial F}{\partial \Psi}\, e^n \end{aligned} \tag{4.109}$$

Then,

$$\begin{aligned} e^{n+1} &= L^{-1}\,\frac{\partial F}{\partial \Psi}\, e^n \\ &= \lambda\, e^n, \end{aligned} \tag{4.110}$$

where λ denotes the eigenvalue of the operator $L^{-1}\partial F/\partial\Psi$. Consequently, the necessary condition for the convergence of the Picard iteration is given by $|\lambda|<1$ [ex. 4.19].

For this reason, one can see that the convergence of the Picard iteration for G-S equation (4.85) depends on the functions $g(\Psi)$ and $p(\Psi)$ since they determine the eigenvalue, and there may exist the functions which make the iteration divergent. This explains the numerical instability we have seen in Fig. 4.20.

A simple way to resolve the above problem is to modify the Picard iteration as

$$
\begin{aligned}
L\,\Psi^{n+1/3} &= F(\Psi^n)\,,\\
L\,\Psi^{n+2/3} &= F(\Psi^{n+1/3})\,,\\
\Psi^{n+1} &= (1-\varepsilon)\,\Psi^n + 2\varepsilon\Psi^{n+1/3} - \varepsilon\Psi^{n+2/3}.
\end{aligned}
\tag{4.111}
$$

This iteration having two supplementary steps is called the Marder-Weitzner iteration [4.20], which expands convergent region as will be shown below. The values of $\Psi^{n+1/3}$ and $\Psi^{n+2/3}$ in (4.111) can be written in the form

$$
\begin{aligned}
\Psi^{n+1/3} &\simeq \Psi^* + L^{-1}\frac{\partial F}{\partial \Psi}\,e^n\,,\\
\Psi^{n+2/3} &\simeq \Psi^* + L^{-1}\frac{\partial F}{\partial \Psi}\,e^{n+1/3}\\
&= \Psi^* + \left(L^{-1}\frac{\partial F}{\partial \Psi}\right)^2 e^n\,.
\end{aligned}
\tag{4.112}
$$

Hence we have

$$
\begin{aligned}
e^{n+1} &= \left[(1-\varepsilon) + 2\varepsilon L^{-1}\frac{\partial F}{\partial \Psi} - \varepsilon\left(L^{-1}\frac{\partial F}{\partial \Psi}\right)^2\right] e^n\\
&= [\,(1-\varepsilon) + 2\varepsilon\lambda - \varepsilon\lambda^2\,]\,e^n\,.
\end{aligned}
\tag{4.113}
$$

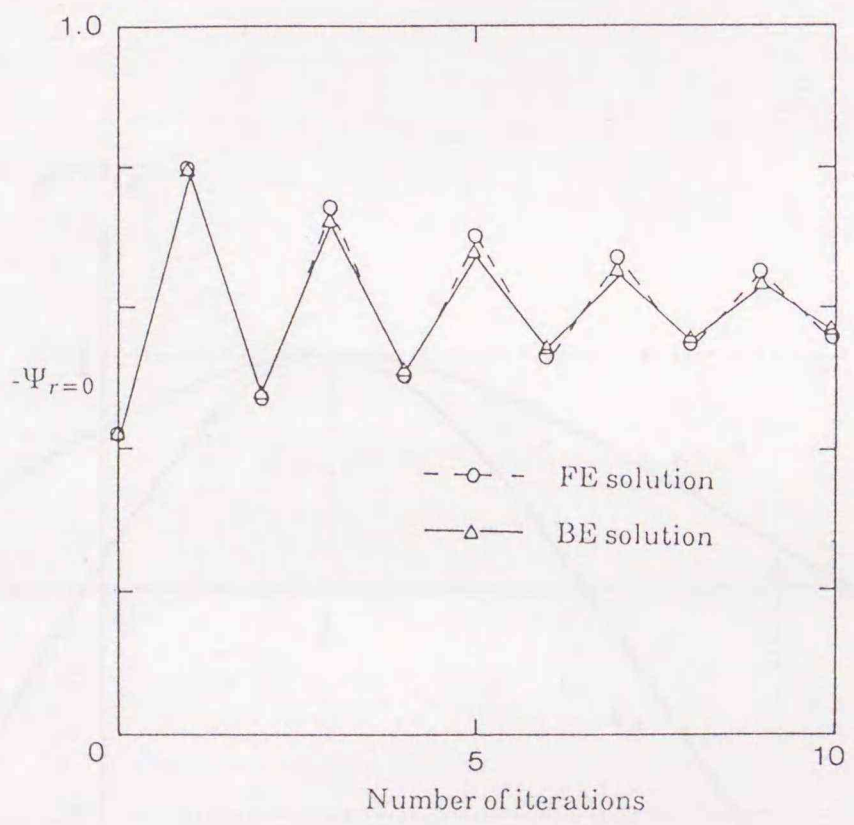

Fig. 4.20 Convergence of the Picard iteration for the circular boundary plasma model. (p and g are given by (4.106) and $S=0$)

Consequently, for arbitrary λ, one can make the ratio $|e^{n+1}/e^n| = |(1-\varepsilon)+2\varepsilon\lambda-\varepsilon\lambda^2|$ smaller than unity by using sufficiently small ε as shown in Fig. 4.21.

Figure 4.22 shows a convergence improved by the Marder-Weitzner iteration for the same condition as Fig. 4.20. Moreover, as shown in Fig. 4.23, there are not significant discrepancies between the final solutions obtained by BE and FE methods. A convergent solution can also be obtained for $h=2.0$ by the Marder-Weitzner iteration as shown in Figs. 4.24 and 4.25.

As we have seen, the BE and FE methods with the Marder-Weitzner iteration can successfully solve the G-S equation. However, in the Marder-Weitzner iteration, the constant ε, which controls the convergence of this iteration, must be determined by error and trial so that the iteration fast converges. This is one of the weak points of this iteration method.

As regards the solver of the G-S equation, the BE method is considerably expensive because of the numerical evaluations of the surface integral in (4.97) and (4.98) at all iterative steps. Moreover, computations of the fundamental solution (3.27) for the surface integrals are also time-consuming in comparison with translational and axial symmetric models. On the other hand, FE method does not need computations of the fundamental solution and can easily evaluate

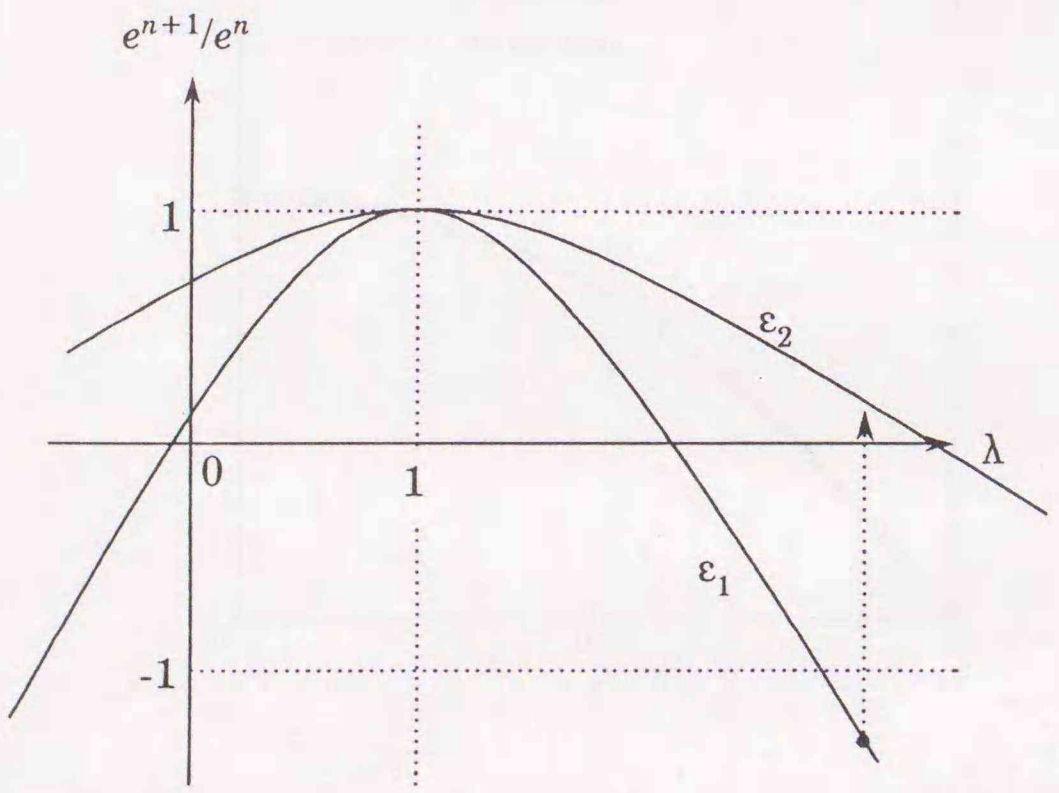

Fig. 4.21 Ratio e^{n+1}/e^n plotted against eigenvalue λ for ε_1 and ε_2 ($\varepsilon_1 > \varepsilon_2$).

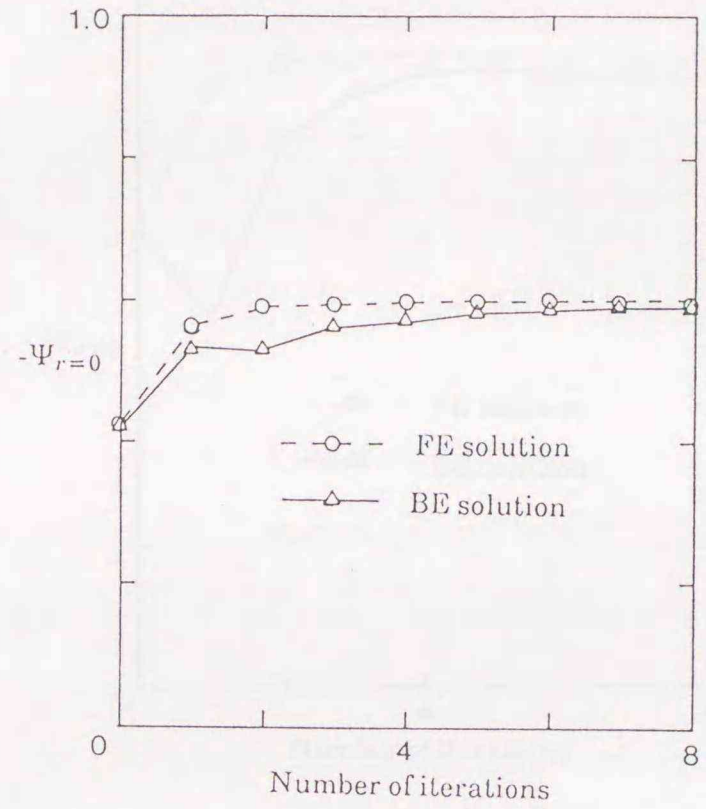

Fig. 4.22 Convergence improved by the Marder-Weitzner iteration for the same condition in Fig. 4.20.

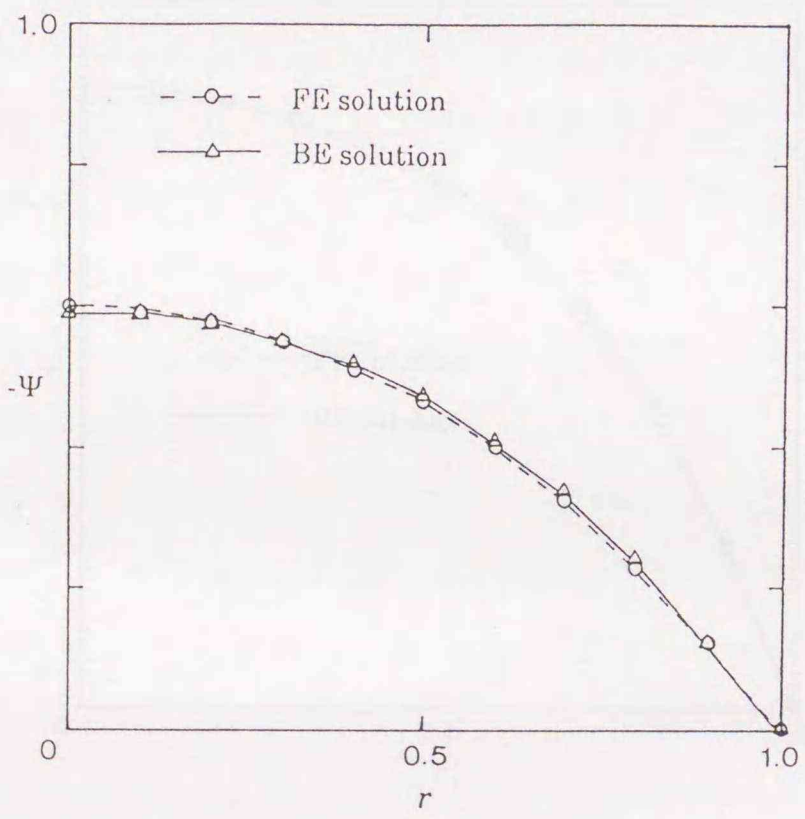

Fig. 4.23 Final solutions by BE and FE methods for Fig. 4.21.

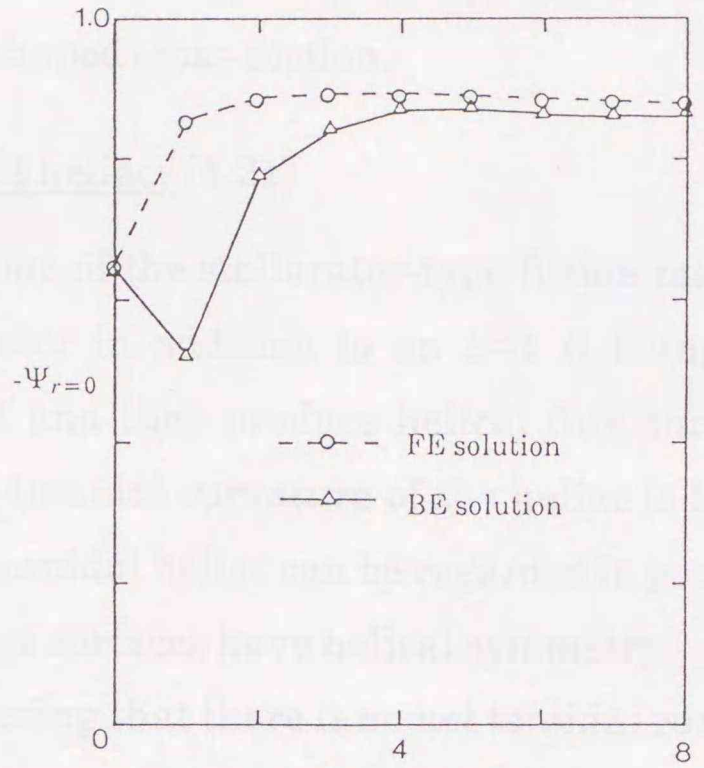

Fig. 4.24 Convergence of the Marder-Weitzner iteration for the same condition in Fig. 4.20 except $h=2.0$.

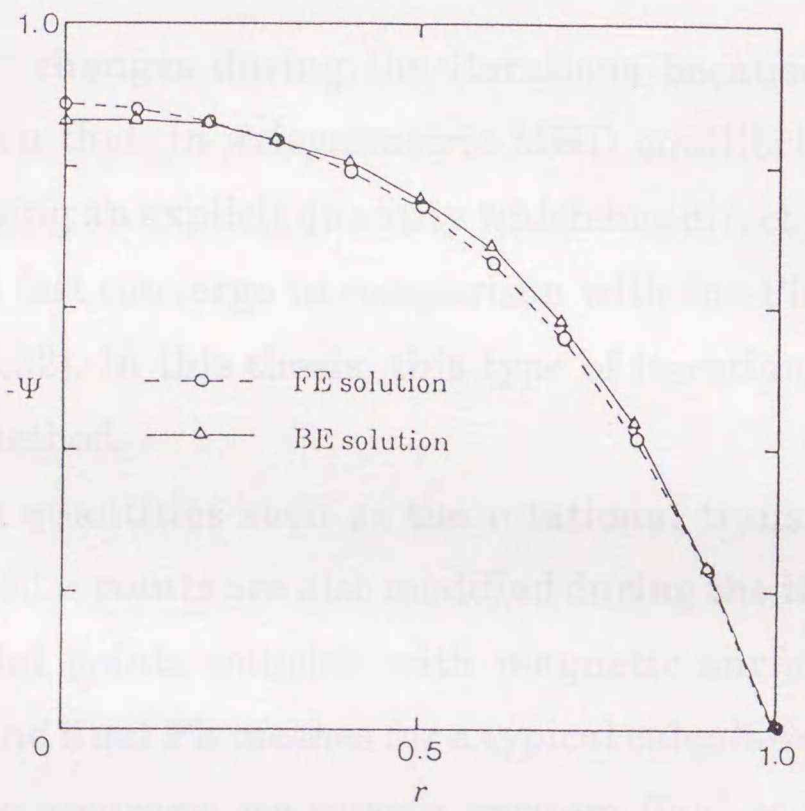

Fig. 4.25 Final solutions by BE and FE methods for Fig. 4.22.

the nonlinear term. For these reasons, it is concluded that FE method is superior to BE method for the solution of the helically symmetric G-S equation.

In the next section, FE method will be applied to the analysis of MHD equilibria with a bean-shaped cross-section.

4.4.3 Analysis of straight heliacs [4.21]

The heliac, which is one of the stellarator-type fusion machine, has a toroidal current-carrying conductor in addition to an $l=1$ (l being the poloidal mode number) stellarator coil and they produce helical flux surfaces of bean-shaped cross-section. When the toroidal curvature of the heliac is large compared to the poloidal curvature, the toroidal heliac can be regarded in good approximation as a straight heliac whose flux surfaces have helical symmetry.

In this section, considering that there is no net toroidal current over the plasma cross-section in the heliac, the MHD equilibrium is analyzed by the FE method. In order to obtain the solution satisfying the above condition, the value of p_1 in (4.106) is successively modified during the iteration. Here, the toroidal current density J^Z is given by (4.89). This iterative process may be expressed in the form

$$[K_{ij}][\Psi^{n+1}]=[F^n([\Psi^n])] \ . \tag{4.114}$$

where the function F^n changes during the iterations because it contains the constant p_1. It is known that, in axisymmetric MHD equilibrium analyses, the iteration schemes keeping an explicit quantity which has direct physical meaning like the above method fast converge in comparison with the Picard and Marder-Weitzner iterations [4.22]. In this thesis, this type of iteration method is called the inverse iteration method.

To calculate surface quantities such as the rotational transform and specific volume, the places of nodal points are also modified during the iteration (4.114) so that the layers of nodal points coincide with magnetic surfaces. Figure 4.26 illustrates the initial and final FE meshes for a typical calculation.

For validation of the accuracy, we solve a vacuum field bounded by a bean-shaped magnetic surface given by,

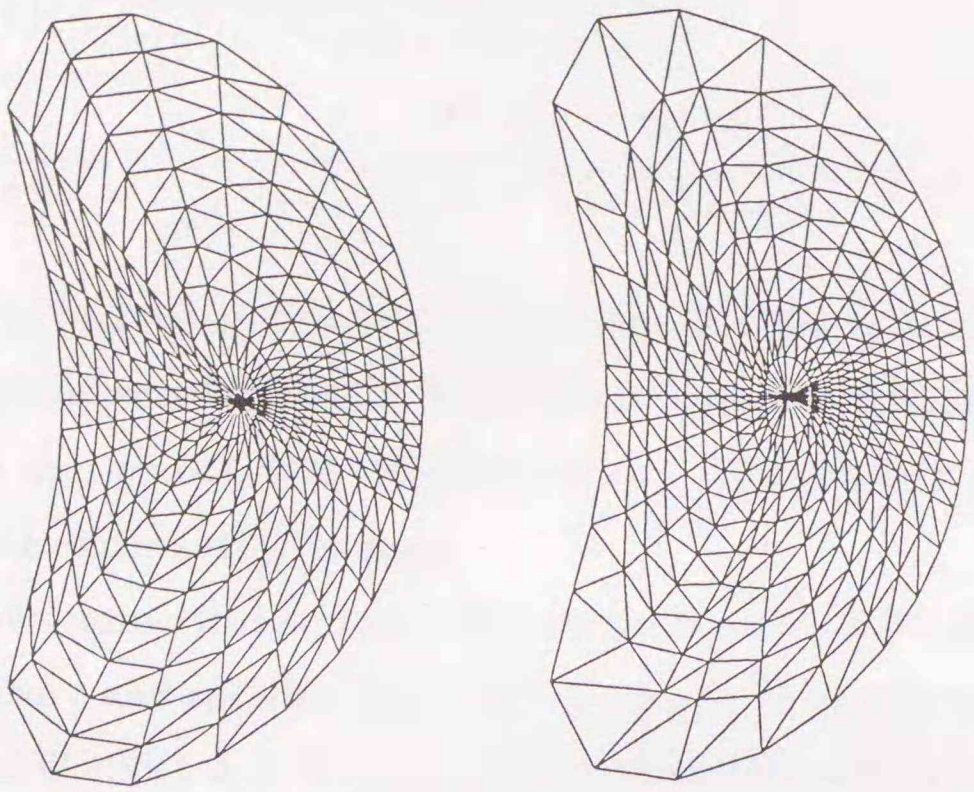

Initial Final

Fig. 4.26 Initial and final finite elements.

$$\Psi = \frac{r^2}{2} + c_1 \log r - c_2 r I_1'(r) \cos\zeta, \tag{4.115}$$

where I_1 is the 1st order modified Bessel function of the 1st kind and coefficients c_1 and c_2 are determined so that the magnetic axis is located at $X=1.0$, $Y=0.0$. (The values of the coefficients are approximately -0.76 and 0.21, respectively.) The second term of (4.115) denotes the magnetic field of a current flowing along the z-axis, which makes magnetic surfaces bean-shaped. The other two terms express a uniform field in the z-direction and the field of a helical winding of $h=1.0$, respectively. The field (4.115) is a solution to the helical equilibrium equation for $p_0=p_1=g_1=0$ and $g_0=1-c_1$. To estimate accuracy of the numerical solution over the whole plasma cross section, we calculate analytically and numerically the rotational transform $\iota=2\pi[1-2\pi(d\Phi/d\Psi)^{-1}]$ and the specific volume $V'=2\pi(dS/d\Psi)\ /\ (d\Phi/d\Psi)$, where S is the area enclosed by a magnetic surface on plane of $Z=$constant and Φ is the toroidal flux. The analytic values of these quantities can be obtained from [4.23]

$$\frac{dS}{d\Psi} = 2\int_{r_0}^{r_1} \frac{r\,dr}{\sqrt{[c_2 r I_1'(r)]^2 - (\Psi - r^2/2 - c_1 \log r)^2}} \quad , \tag{4.116}$$

$$\frac{d\Phi}{d\Psi} = \frac{dS}{d\Psi} + 2\int_{r_0}^{r_1} \frac{I_1(r)\,(\Psi - r^2/2 - c_1 \log r)\,dr}{I_1'(r)\sqrt{[c_2 r I_1'(r)]^2 - (\Psi - r^2/2 - c_1 \log r)^2}} \quad . \tag{4.117}$$

The integrations in (4.116) and (4.117) are performed from r_0 to r_1 at which the contour line of Ψ intersects the X-axis. Since the integrands in (4.116) and (4.117) singular at these end-points, the integrations are numerically performed by means of the double exponential formula.

Figure 4.27 shows numerical and analytical profiles of Ψ ($1.0 \leqq X \leqq 1.2$, $Y = 0$), rotational transform ι and specific volume V', normalized by appropriate values. The contour line of $\Psi = \Psi(1.2, 0)$ is chosen as the boundary of this example. From Fig. 4.27, one can see that the numerical values are in good agreement with the analytical values and the calculation of bean-shaped equilibria can be performed by the present FE method in sufficiently good accuracy.

To systematically investigate the dependence of the convergence of the present method on the boundary shape, the boundary is specified as follows [4.24] :

$$X = \rho \cos\gamma + S_X, \quad Y = \rho \sin\gamma \, , \tag{4.118}$$

where

$$\gamma = B \sin(\pi - \zeta), \quad \rho = a[1 - b\cos(\pi - \zeta)] . \tag{4.119}$$

In the following, the parameters in (4.118) and (4.119) are fixed as $a = 0.5$, $b = 0.5$, $S_X = 0.2$, $h = 1.0$, $g_1 = 2.0$ and $g_2 = 1.0$. Figure 4.28 shows the magnetic surfaces numerically calculated for $B = 0.8$, 1.2 and 1.6. Figure 4.29 (a) and (b) shows the convergence of the net toroidal current over the whole plasma cross section and the value of the stream function at the magnetic axis Ψ_m, respectively [4.21]. As shown in these figures, for all cases, the net toroidal current rapidly approaches zero and Ψ_m sufficiently converges to a finite value after less than 10 iterations [4.21]. The other calculations under various conditions confirmed that this property did not change for wide range of S_X, h, g_1 and g_2.

Figure 4.30 shows the convergence of the Marder-Weitzner iteration for $\varepsilon = 0.4$ and 0.5 when p_0 is taken to be 5.65 which is the resultant value for $B = 1.2$ in Fig. 4.29. The vertical axis denotes the relative error defined as $(\Psi_m{}^T - \Psi_m{}^M)/\Psi_m{}^T$,

where $\Psi_m{}^T$ and $\Psi_m{}^M$ are the values of Ψ_m calculated by the inverse iteration and Marder-Weitzner methods, respectively. As shown in this figure, the value of $\Psi_m{}^M$ slowly approaches $\Psi_m{}^T$ in both cases and the Marder-Weitzner method needs three times iterations at least to get a convergent solution in comparison with the inverse iteration method [4.21]. (When we calculate this equilibrium for the same parameters by the Picard iteration, the solution rapidly diverges.)

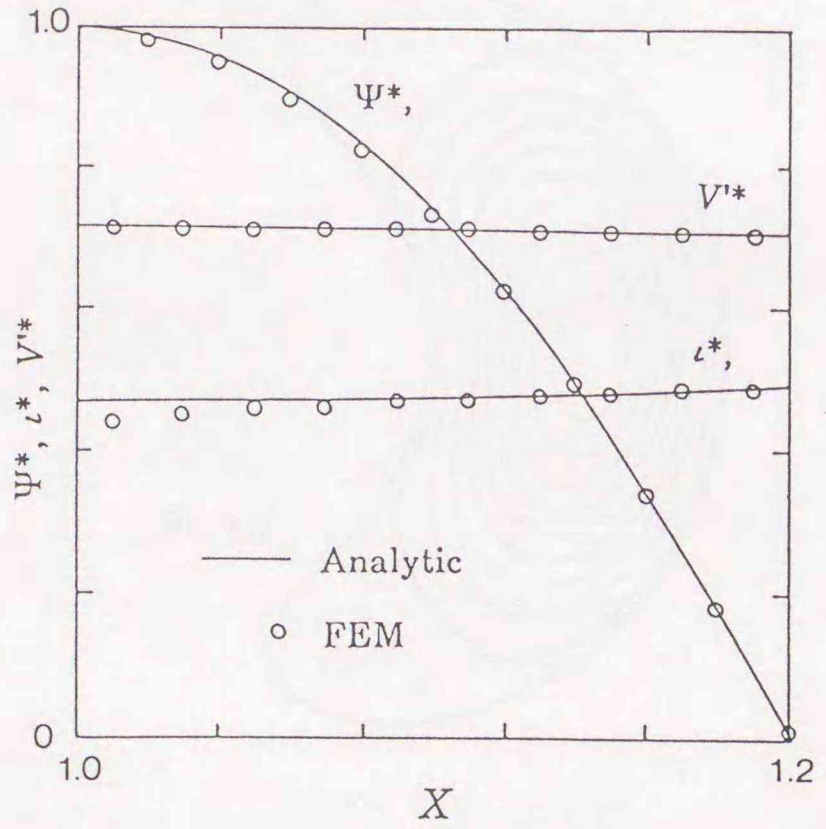

Fig. 4.27 Profiles of stream function Ψ^*, retational transform ι^* and specific volume V'^*, where $\Psi^* = \Psi_{Y=0}/\Psi_m$, $\iota^* = \iota/2\pi$ and $V'^* = 0.1V'$.

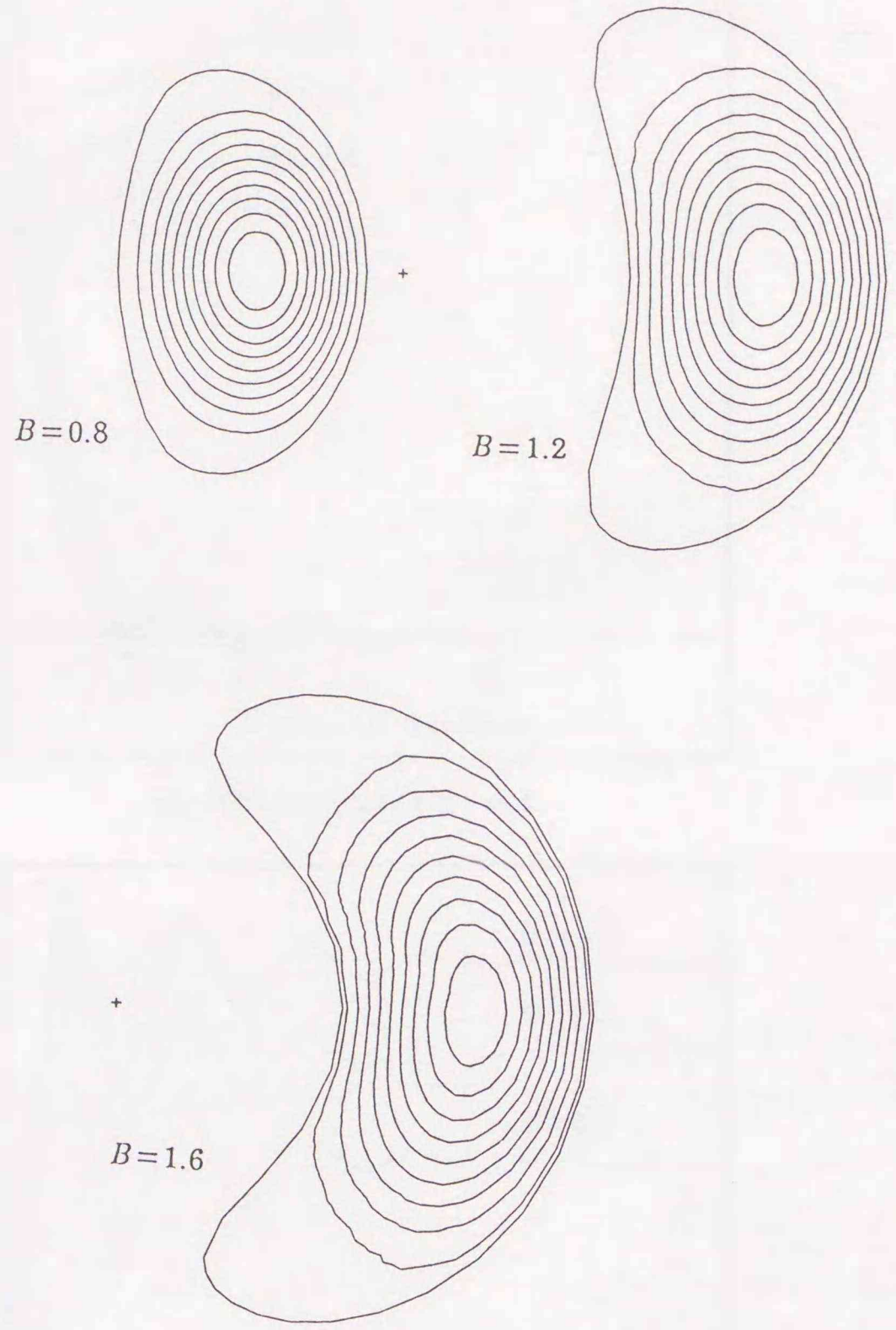

Fig. 4.28 Equilibrium configurations for $a = b = 0.5$, $S_X = 0.2$, $h = 1.0$, $g_1 = 2.0$ and $g_2 = 1.0$.

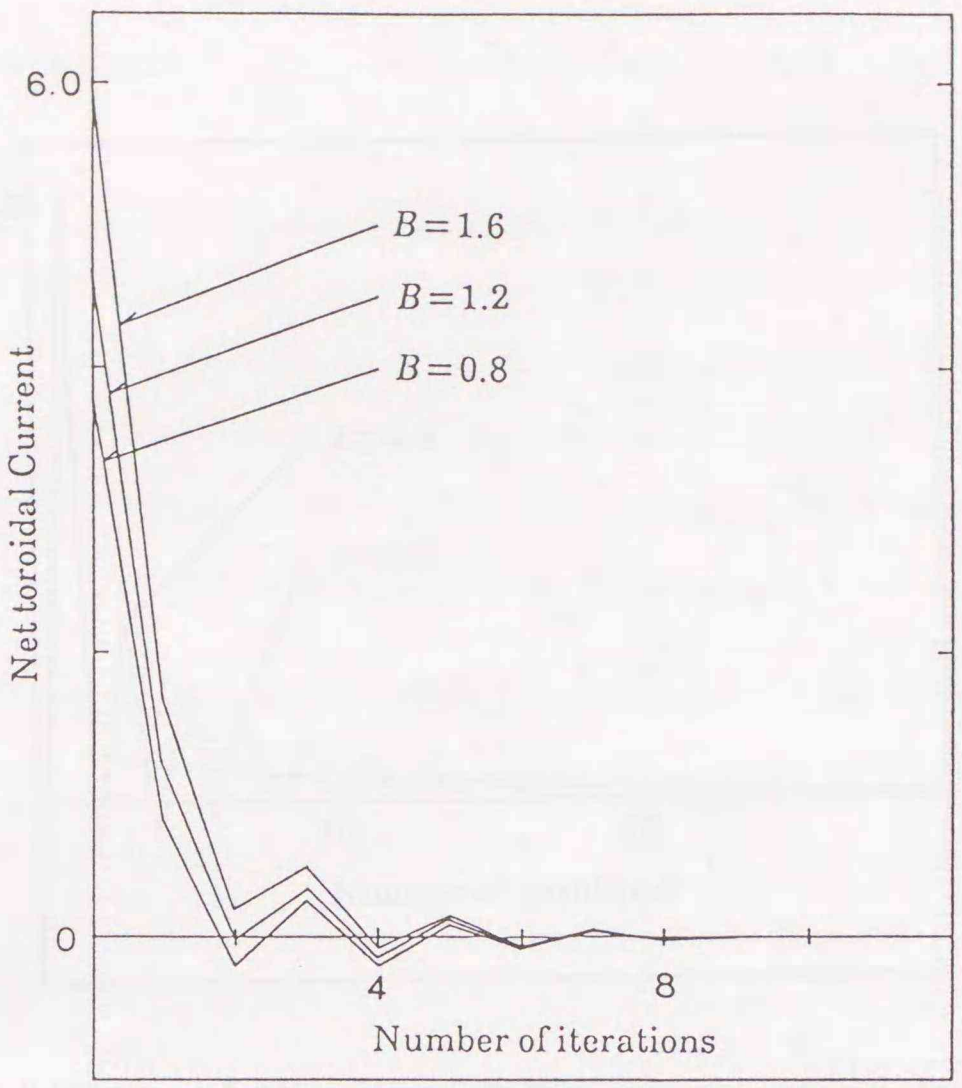

(a) Net toroidal current

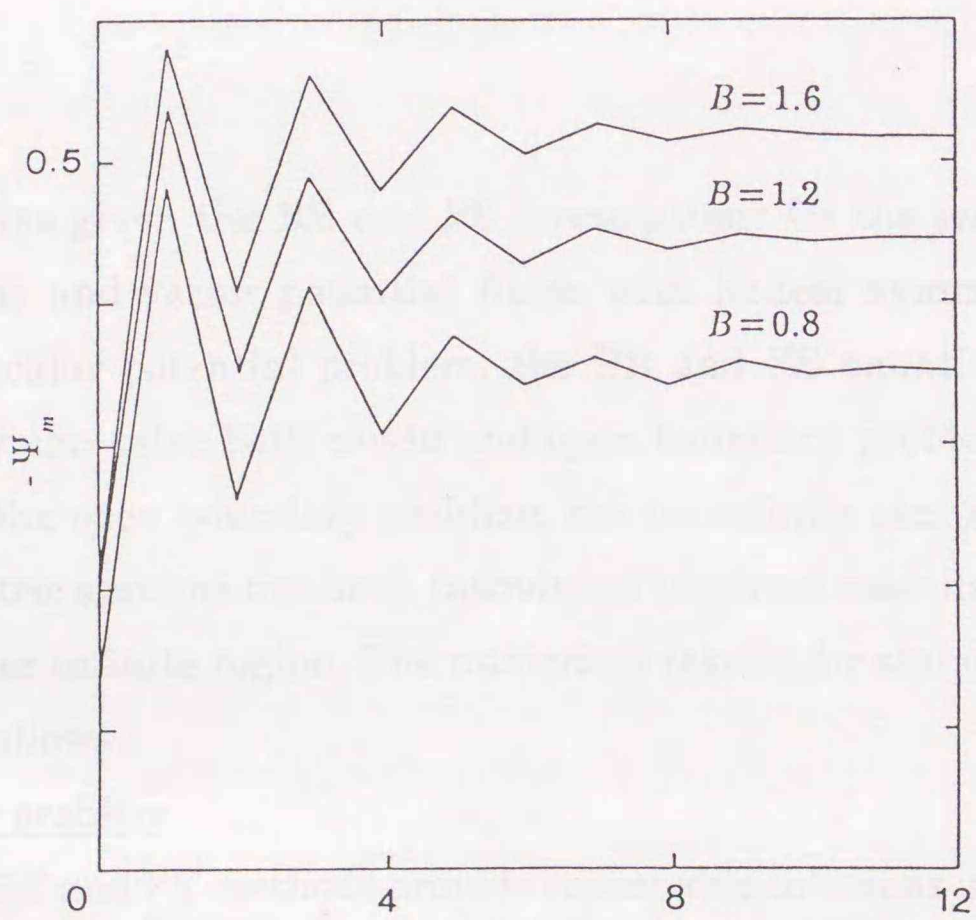

(b) Value of Ψ_m

Fig. 4.29 Convergenve of the inverse iteration method for $a=b=0.5$, $S_X=0.2$, $h=1.0$, $g_1=2.0$ and $g_2=1.0$.

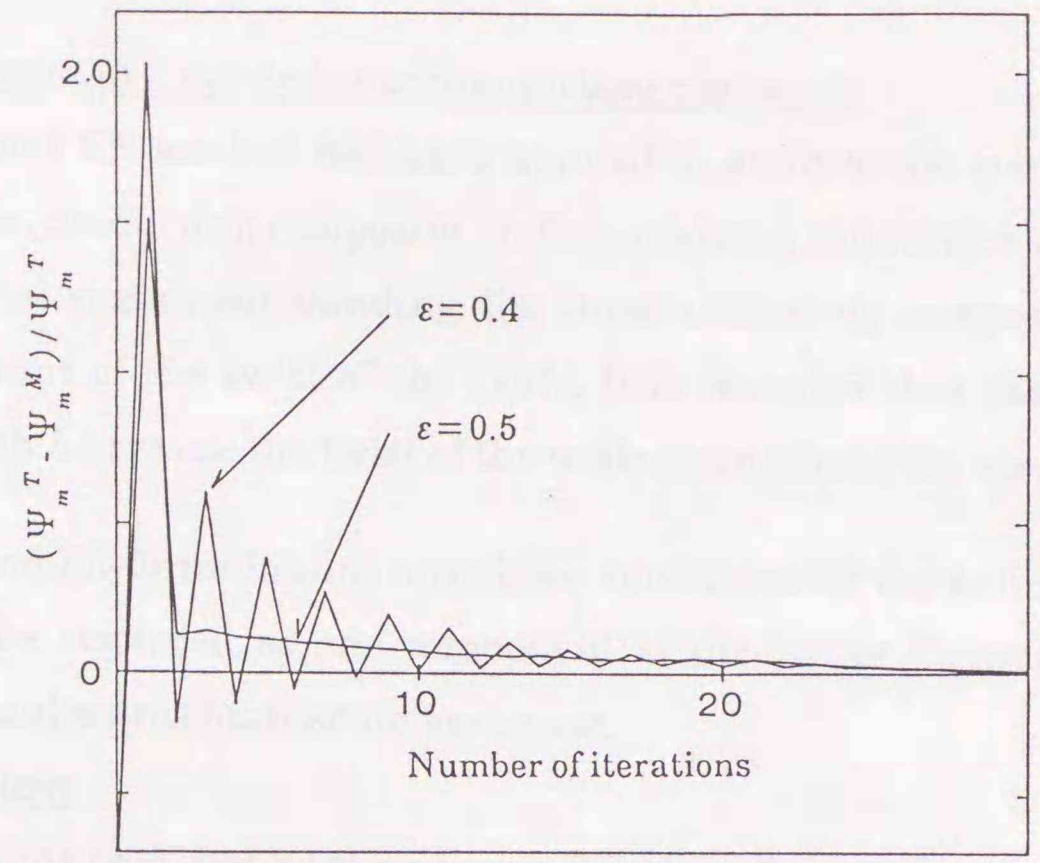

Fig. 4.30 Convergence of the Marder-Weitzner method for $a=b=0.5$, $S_X=0.2$, $h=1.0$, $g_1=2.0$, $g_2=1.0$ and $p_0=5.65$.

4.5 Summary

This chapter has given the BE and FE formulations for the two-dimensional analysis of scalar and vector potential fields with helical symmetry. For the solution of the scalar potential problem, the BE and FE equations have been introduced. They can solve both closed and open boundary problems. In the FE formulation for the open boundary problem, the transfinite element method for helically symmetric systems has been introduced to give a reasonable treatment of an integral over infinite region. The numerical results for scalar problems are summarized as follows :

Closed boundary problem

The proposed BE and FE methods provide reasonable solutions whose accuracy is independent from the value of helical wavenumber h while the second order perturbed solution becomes inaccurate for large h.

Open boundary problem

The potential fields around the helical coil and the twisted-pair line have been effectively solved by the present numerical methods. In particular, the transfinite

element method has given more accurate solutions than the conventional FE method.

Coupling losses in a twisted superconducting composite

The present FE method has been applied to analyze the coupling losses in a twisted superconducting composite. In this analysis, the static electric field in the normal metal region surrounding the superconducting composite is calculated taking account of the twist of the cable. It is revealed that the coupling losses increase with h because the twist of the cable strengthens the electric field.

The BE and FE formulations have been submitted for the helical G-S equation, which can be regarded as one component of the vector Poisson equation. The following results are obtained for each case.

Linear problem

The solutions obtained by the present BE and FE methods agree well with the exact solution.

Non-linear problem

The Marder-Weitzner iterative method can get stable solutions under severe conditions which make the Picard iteration unstable. The BE and FE solutions converge to the same values. The BE method is more expensive than the FE method because the former includes time-consuming surface integration processes.

MHD equilibria in straight stellarators with bean-shaped cross-sections

The present FE method has been applied to the analysis of the MHD equilibria in straight stellarators with bean-shaped cross-sections. The equilibria have been iteratively calculated under the condition of vanishing the net toroidal current over the whole plasma cross section. The profiles of the stream function, rotational transform and specific volume for a helically symmetric vacuum field with bean-shaped cross section are in good agreement with analytical values. The convergence of the present method is little affected by the shape of boundary and it is stable for wide range of parameters of the MHD equilibria. The present iterative method gives the solution faster than the Marder-Weitzner method.

REFERENCES

4.1 J.-F. Lee and Z. Cendes, Transfinite Elements, A highly Efficient Procedure for Modeling Open Field Problems, *J. Appl. Phys.*, **61**, pp. 3913-3915, 1987.

4.2 H. Igarashi and T. Honma, A Boundary Element Analysis of Helically Symmetric Potential Fields, *Eng. Anal. with Boundary Elements*, in press.

4.3 H. Igarashi and T. Honma, BE and FE Solutions to Open Boundary Potential Problems with Helical Symmetry, *IEEE Trans. Mag.*, **28**, pp. 1671-1674, 1992.

4.4 M. V. K. Chari and G. Bedrosian, Hybrid Harmonic / Finite Element Method for Two-Dimensional Open Boundary Problems, *IEEE Trans. Mag.*, **23**, pp. 3572-3574, 1987.

4.5 C. A. Brebbia, *The Boundary Element Method for Engineers*, Pentech Press, London, 1978.

4.6 R. L. Dewar and H. J. Gardner, A Harmonic Expansion for the Magnetic Field of the Helical Solenoid, *J. Comp. Phys.*, **77**, pp. 485-500, 1988.

4.7 H. Igarashi and T. Honma, A Numerical Analysis of Coupling Losses in a Superconducting Composite, Proc. of ISEM-Nagoya (1992. Jan.), in press.

4.8 B. Turck, Coupling Losses in Various Outer Normal Laylers Surrounding the Filament Bundle of a Superconducting Composite, *J. Appl. Phys.*, **50** (1979) pp. 5397-5401.

4.9 F. Sumiyoshi, H. Nagaishi, O. Ichimaru and K. Yamafuji, Increase of Coupling-Current Losses in Superconducting Cables Due to First-Stage Cableing, *Cryogenics*, **26** (1986) pp. 39-44.

4.10 F. Sumiyoshi, H. Kasahara, T. Kawashima and T. Tanaka, Numerical Calculation Method of Inter-Strand Coupling Current Losses in Superconducting Conductors, *Cryogenics*, **29** (1989) pp. 741-747.

4.11 Y. N. Dnestrovskii and D. P. Kostomarov, *Numerical Simulation of Plasmas*, Springer-Verlag, Berlin, pp.98-179, 1986.

4.12 R. Gruber and J. Rappaz, *Finite Element Methods in Linear Ideal Magnetohydrodynamics*, Springer-Verlag, Berlin, pp.42-133, 1985.

4.13 J. W. Edenstrasser, Unified treatment of symmetric MHD equilibria, *J. Plasma Phys.*, **24**, pp. 299-313, 1980.

4.14 I. Hirota and K. Chiyoda, Vector Laplacian in General Curvilinear Coordinates, *J. IEE Japan* (in Japanese), **102**, A3, pp. 119-126, 1982.

4.15 D. Correa and D. Lortz, A Class of Helically Symmetric MHD-Equilibria, *Nucl. Fusion*, **13**, pp. 127-129, 1973.

4.16 H. Igarashi and T. Honma, BE and FE analyses of helically symmetric MHD equilibrium configuration, *Int. J. Appl. Electromagnetics in Materials*, 2, pp. 127-134, 1990.

4.17 H. Igarashi and T. Honma, An Equilibrium Analysis of Helically Symmetric Plasmas Using Boundary Element Method, *IEEE Trans. Mag.*, **26**, pp. 1774-1776, 1990.

4.18 H. Igarashi and T. Honma, An iterative Boundary Element Analysis of Helically Symmetric MHD Equilibria, Proc. IABEM-90, Rome (in press)

4.19 J. Blum, *Numerical Simulation and Optimal Control in Plasma Physics with Application to Tokamaks*, John Wiley & Sons, Ch. 1, pp. 30-40, 1989.

4.20 B. Marder and H. Weitzner, A Bifurcation Problem in *E*-Layer Equilibria, *Plasma Phys.*, **12**, pp. 435-445, 1970.

4.21 H. Igarashi and T. Honma, An analysis of MHD equilibria in Straight Stellarators Using Finite Element Method, *Electromagnetic Forces and Applications, Elsevier Studies in Applied Electromagnetics in Materials 1*, (Eds. J. Tani and T. Takagi), Elsevier, Amsterdam, pp. 275-278, 1992.

4.22 K. Lackner, Computation of ideal MHD equilibria, *Comp. Phys. Comm.*, **12**, pp. 33-44, 1976.

4.23 N. M. Zueva and L. S. Solov'ev, Spiral Magnetic Configurations with Minimum B, *Plasma Phys.*, **8**, pp.765-774, 1966.

4.24 D. A. Monticello, R. L. Dewar, H. P. Furth and A. Reiman, Heliac Parameter Study, *Phys. Fluids*, **27**, pp. 1248-1252, 1984.

CHAPTER 5

EIGENVALUE PROBLEMS

This chapter deals with the analysis of eigenvalue problems in helically symmetric systems. In particular, electromagnetic wave propagation in a twisted waveguide will be analyzed by BE and FE methods under scalar approximation in which electromagnetic fields are assumed to be described by the scalar Helmholtz equation. The numerical solutions will be compared with the perturbed solution which is obtained by Lewin [5.1] provided that the helical pitch of the waveguide is sufficiently large compared with the size of its cross-section. Moreover, for more accurate evaluation of the characteristics of the twisted waveguide, a vectorial FE method for the analysis of electromagnetic wave propagation in helical systems will be introduced, and the FE solution will be compared with the perturbed solution derived by Yabe *et al.* [5.2, 5.3] from the vectorial Helmholtz equation.

5.1 Formulation for scalar eigenvalue problems

5.1.1 Hertz vector and scalar Helmholtz equation

In the following, we consider the guided electromagnetic wave in the closed region Ω_C with helical symmetry shown in Fig. 4.1. For simplicity, it is assumed that Ω_C is of an isotoropic and homogeneous medium within which there are neither conduction currents nor free charges.

The time-harmonic Maxwell equations are given by

$$\nabla \times \mathbf{H} = j\omega\varepsilon\mathbf{E}\,, \tag{5.1}$$

$$\nabla \times \mathbf{E} = -j\omega\mu\mathbf{H}\,, \tag{5.2}$$

where H and E are magnetic and electric fields, ω the angular frequency, ε the permittivity and μ the permeability. The electric and magnetic flux densities D and B are related with E and H as follows :

$$\mathbf{D} = \varepsilon\mathbf{E}\,, \tag{5.3}$$

$$\mathbf{B} = \mu\mathbf{H}\,. \tag{5.4}$$

From (5.2) and (5.4), E and B can be written in the following forms in terms of

the scalar electric potential ϕ and magnetic potential $\mathbf{A}$,

$$\mathbf{E} = -\nabla\phi - j\omega\mathbf{A}\,, \tag{5.5}$$

$$\mathbf{B} = \nabla\times\mathbf{A}\,. \tag{5.6}$$

Moreover, if the potentials ϕ and $\mathbf{A}$ can be expressed in terms of a vector Π,

$$\mathbf{A} = j\omega\varepsilon\mu\,\Pi\,, \tag{5.7}$$

$$\phi = -\nabla\cdot\Pi\,, \tag{5.8}$$

they always satisfy the Lorentz condition

$$\nabla\cdot\mathbf{A} + j\omega\varepsilon\mu\,\phi = 0\,. \tag{5.9}$$

The vector Π is called the Hertzian vector of electric type since it can be regarded as an electric polarization which produces the electromagnetic field (see p. 30 of Ref. 2.1).

The insertion of (5.7) and (5.8) into (5.5) and (5.6) yields

$$\mathbf{E} = \nabla\nabla\cdot\Pi + k^2\Pi\,, \tag{5.10}$$

$$\mathbf{B} = j\omega\varepsilon\mu\,\nabla\times\Pi\,, \tag{5.11}$$

where $k^2=\mu\varepsilon\omega^2$ is the wavenumber of an electromagnetic wave in unbounded region. Substituting (5.10) and (5.11) into (5.1), we have the vector Helmholtz equation for Π,

$$\nabla\nabla\cdot\Pi - \nabla\times\nabla\times\Pi + k^2\Pi\,,$$

$$= \nabla^2\Pi + k^2\Pi = 0\,. \tag{5.12}$$

Consequently, if one can find a non-trivial solution to (5.12) and the electromagnetic field derived from it satisfies the boundary condition under consideration, the electromagnetic field is the desired solution to the Maxwell equation.

On the other hand, $\mathbf{D}$ as well as $\mathbf{B}$ satisfies $\nabla\cdot\mathbf{D}=0$ since there is no free charges. Hence, the introduction of the Hertzian vector of magnetic type Ψ permits the dual representation of electromagnetic field,

$$\mathbf{D} = -\nabla\times\mathbf{A}_e$$

$$= -j\omega\varepsilon\mu\,\nabla\times\Psi\,, \tag{5.13}$$

$$\mathbf{H} = -\nabla\phi_m - j\omega\mathbf{A}_e$$

$$= \nabla\nabla\cdot\Psi + k^2\Psi\,, \tag{5.14}$$

where Ψ satisfies again the vector Helmholtz equation,

$$\nabla\nabla\cdot\Psi - \nabla\times\nabla\times\Psi + k^2\Psi\,,$$
$$= \nabla^2\Psi + k^2\Psi = 0\,, \tag{5.15}$$

and Φ_m and $\mathbf{A}_e$ are called the magnetic scalar potential and the electric vector potential, respectively.

The superposition of Π and Ψ represents more general electromagnetic field

$$\mathbf{E} = \nabla\nabla\cdot\Pi + k^2\Pi - j\omega\mu\,\nabla\times\Psi\,, \tag{5.16}$$
$$\mathbf{H} = j\omega\varepsilon\,\nabla\times\Pi + \nabla\nabla\cdot\Psi + k^2\Psi\,. \tag{5.17}$$

When the vector **a** along which a guided electromagnetic wave propagates has a constant direction, and in addition, Π and Ψ can be expressed by $\Pi=\Pi\mathbf{a}$ and $\Psi=\Psi\mathbf{a}$, (5.16) and (5.17) become

$$\mathbf{E} = \nabla\nabla\cdot(\Pi\mathbf{a}) + k^2\Pi\mathbf{a} - j\omega\mu\,\nabla\times(\Psi\mathbf{a})\,, \tag{5.18}$$
$$\mathbf{H} = j\omega\varepsilon\,\nabla\times(\Pi\mathbf{a}) + \nabla\nabla\cdot(\Psi\mathbf{a}) + k^2\Psi\mathbf{a}\,, \tag{5.19}$$

where both Π and Ψ satisfy the scalar Helmholtz equation

$$\nabla^2\Pi + k^2\Pi = 0\,, \tag{5.20}$$
$$\nabla^2\Psi + k^2\Psi = 0\,. \tag{5.21}$$

Moreover, the field for $\Pi=0$,

$$\mathbf{E} = -j\omega\mu\,\nabla\times(\Psi\mathbf{a})\,, \tag{5.22}$$
$$\mathbf{H} = \nabla\nabla\cdot(\Psi\mathbf{a}) + k^2\Psi\mathbf{a}\,, \tag{5.23}$$

represents the TE mode which has only the electric field components perpendicular to **a**. If one can find, therefore, the solution to (5.21) under appropriate boundary conditions, we readily obtain the electromagnetic field of TE mode from (5.22) and (5.23).

Here notice that though the electromagnetic fields represented by (5.18)-(5.21) do satisfy the Maxwell equations, all solutions to the Maxwell equations may not be written in those forms. However, if we find the solutions to (5.20) and (5.21) under a boundary condition, the electromagnetic fields derived from those is the unique solution to the Maxwell equations under the boundary condition.

The TE mode may also be described by the scalar Helmholtz equation by the use of the longitudinal component of magnetic field $H_a=\mathbf{H}\cdot\mathbf{a}$ as well as Ψ. In that

case, however, the electromagnetic field can not be written in such simple forms as (5.22) and (5.23).

5.1.2 Lewin's perturbation analysis [5.1]

The TE mode of a twisted waveguide shown in Figs. 5.1 and 5.2 has been analyzed by Lewin on the basis of the perturbation method [5.1]. In his analysis, the scalar Helmholtz equation in the twisted coordinates

$$\nabla^2\Psi + k^2\Psi = 0 \ , \tag{5.24}$$

$$\nabla^2\Psi = (1+h^2Y^2)\frac{\partial^2\Psi}{\partial X^2} - 2h^2XY\frac{\partial^2\Psi}{\partial X\partial Y} + (1+h^2X^2)\frac{\partial^2\Psi}{\partial Y^2} + \frac{\partial^2\Psi}{\partial Z^2}$$

$$+2hY\frac{\partial^2\Psi}{\partial X\partial Z} - 2hX\frac{\partial^2\Psi}{\partial Y\partial Z} - h^2X\frac{\partial\Psi}{\partial X} - h^2Y\frac{\partial\Psi}{\partial Y} \ , \tag{5.25}$$

is solved, where Ψ is the Herzian potential defined by $\Psi = \Psi\cdot\mathbf{e}_Z$. From (5.22) and (5.23), electromagnetic field can be written in terms of Ψ as follows :

$$E^X = -j\omega\mu\frac{\partial\Psi}{\partial Y} \ , \quad E^Y = j\omega\mu\frac{\partial\Psi}{\partial X} \ , \quad E^Z = 0 \ , \tag{5.26}$$

$$\mathbf{H} = k^2\Psi\,\mathbf{e}^Z + \nabla\left(\frac{\partial\Psi}{\partial Z}\right) , \tag{5.27}$$

Moreover , the potential Ψ is assumed to take the form

$$\Psi = \phi(X,Y)e^{-j\beta Z} \ , \tag{5.28}$$

where β denotes the phase constant.

For the rectangular guide shown in Fig. 5.2, Lewin gives the following boundary conditions

$$E^X = -j\omega\mu\frac{\partial\Psi}{\partial Y} = 0 \ , \qquad \text{on } C_1 , \tag{5.29}$$

$$E^Y = j\omega\mu\frac{\partial\Psi}{\partial X} = 0 \ , \qquad \text{on } C_2 , \tag{5.30}$$

$$E^Z = 0 \ , \qquad \text{on } C_1 \text{ and } C_2 . \tag{5.31}$$

The condition (5.31) is automatically satisfied by the last identity of (5.27). The conditions (5.29)-(5.31) are derived from $\mathbf{E}\times\mathbf{n}=\mathbf{0}$, where $\mathbf{n}$ denotes the normal vector of the guide wall, providing that $\mathbf{n}$ is parallel or antiparallel to $\mathbf{e}^X$ on C_2 and $\mathbf{e}^Y$ on C_1. However, as has been pointed out by Yabe *et al.* [5.2], $\mathbf{n}$ is parallel or

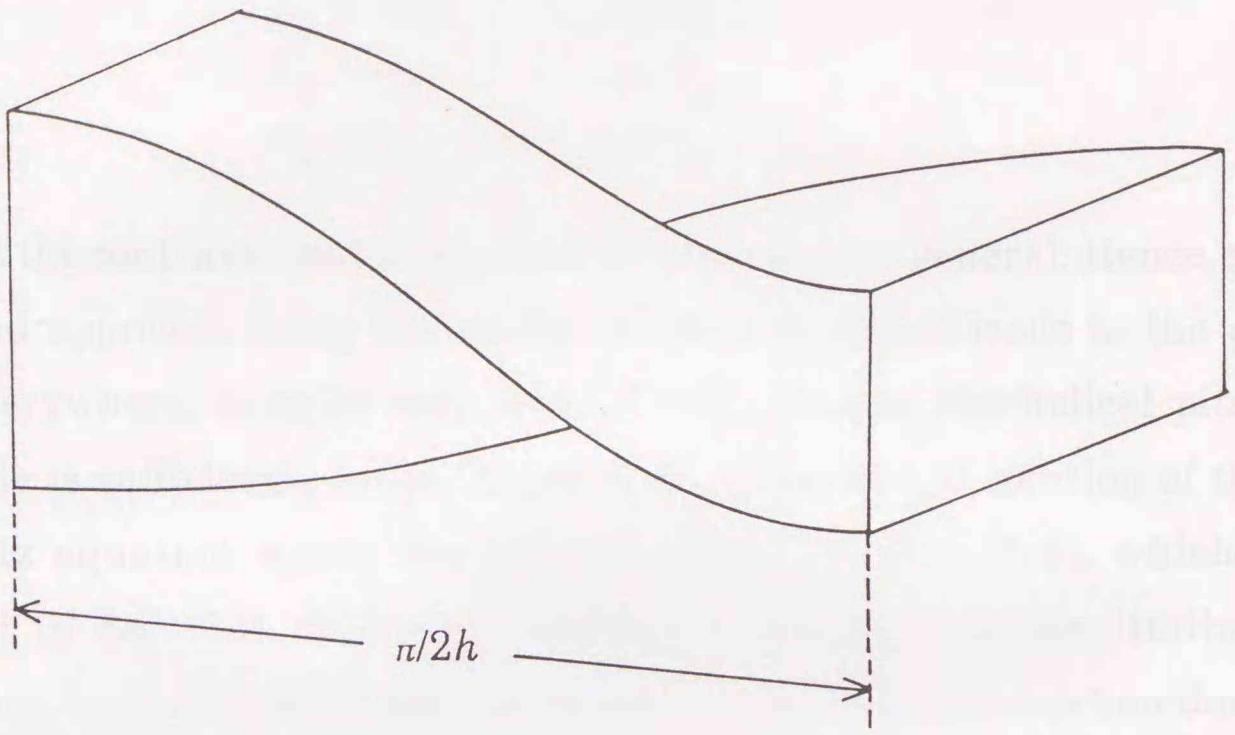

Fig. 5.1 A twisted waveguide

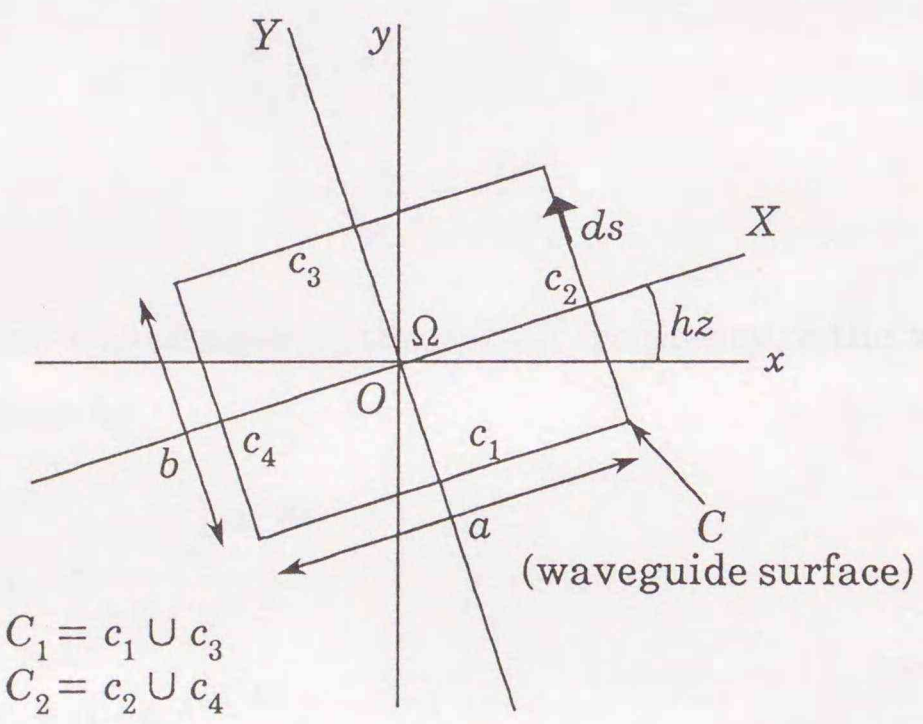

Fig. 5.2 Cross-section of a twisted waveguide and the twisted coordinates (X, Y, Z)

antiparallel to unitary vectors $\mathbf{e}_X$ and $\mathbf{e}_Y$ rather than $\mathbf{e}^X$ and $\mathbf{e}^Y$, and therefore, the exact boundary conditions are given by

$$E_X = 0, \qquad \text{on } C_1, \tag{5.32}$$

$$E_Y = 0, \qquad \text{on } C_2, \tag{5.33}$$

$$E_Z = 0, \qquad \text{on } C_1 \text{ and } C_2. \tag{5.34}$$

Note that the contravariant component E^Z is not zero in general. Hence, the above mentioned approach using the scalar function Ψ, which leads to the condition $E^Z=0$ everywhere, is valid only when $E^i \simeq E_i$, that is, the helical pitch of the waveguide is sufficiently large. Exact analysis needs full solution of the vector Helmholtz equation under the conditions (5.32)-(5.34) [5.2], which will be discussed in Sec. 5.3. Although Lewin's approach has the limitation for application, it is considerably simple in comparison with the exact method.

The dispersion formulas derived by Lewin [5.1, see also 5.3] are summarized as follows :

$$\lambda_g = \frac{\lambda}{p_2\left[1-\left(\frac{\lambda}{2p_1 a}\right)^2\right]^{1/2}}, \tag{5.35}$$

$$\left(\frac{\beta}{p_2}\right)^2 = k^2 - \left(\frac{\pi}{p_1 a}\right)^2, \tag{5.36}$$

$$f_c = \frac{c}{2p_1 a} = \frac{ck}{2\pi p_1} \tag{5.37}$$

where λ_g is the guide wavelength, f_c the cut-off frequency, c the velocity of light and p_1 and p_2 are given by

$$p_1 = \left(\frac{1-q_2 h'^2}{1+q_1 h'^2}\right)^{1/2}, \tag{5.38}$$

$$p_2 = (1-q_2 h'^2)^{1/2}, \tag{5.39}$$

$$q_1 = \frac{8}{3}\eta^2 - 4 - \pi^2 + \frac{128\tan\eta}{\pi^2\eta} + \frac{256}{\pi^2\eta} \times \sum_{m=2,4,\ldots}^{\infty} \frac{(2m^2+1)\tanh[\eta(m^2-1)^{1/2}]}{(m^2-1)^{9/2}}, \tag{5.40}$$

$$q_2 = -\frac{4}{3}\eta^2 + 6 + \pi^2 - \frac{128\tan\eta}{\pi^2\eta} - \frac{256}{\pi^2\eta} \times \sum_{m=2,4,\ldots}^{\infty} \frac{(2m^2+1)\tanh[\eta(m^2-1)^{1/2}]}{(m^2-1)^{9/2}} . \tag{5.41}$$

The constants η and h' in the above equations are defined by $\pi b/2a$ and $ha/2\pi$, respectively.

The next two sections give BE and FE formulations for the scalar Helmholtz equation (5.24).

5.1.3 BE Formulation for scalar Helmholtz equation [5.4]

There are two types of BE formulations for the solution of the scalar Helmholtz equation (5.24). The first one employs the fundamental solution of (5.24) which has k in its argument and, consequently, it seems to be ineffective since the eigenvalue k must be found, for example, by a determinant search method. On the other hand, the second regards $k^2\Psi$ in (5.24) as an inhomogeneous term and uses the fundamental solution to the Laplace equation [5.5]. This method is reduced to a linear proper equation, which can be easily solved by various standard numerical methods. For this reason, the second method, which is sometimes referred to as the hybrid BE method, is here applied to the analysis of the twisted waveguide.

We first give a BE formulation for the scalar Helmholtz equation (5.24) in the helical column V_C shown in Fig. 4.1. Green's identity for Ψ and $G' = Ge^{j\beta Z}$, where G satisfies (4.3), is

$$\int_{V_C} (G'\nabla^2\Psi - \Psi\nabla^2 G')\, dV = \int_{\partial V_I} \left(G'\frac{\partial\Psi}{\partial n} - \Psi\frac{\partial G'}{\partial n} \right) dS . \tag{5.42}$$

The integrands in eq. (5.42) can be written in the form

$$G'\nabla^2\Psi = -k^2 G\phi , \tag{5.43}$$

$$\Psi\nabla^2 G' = \Psi\left(\nabla_T^2 + \frac{\partial^2}{\partial Z^2} + 2hY\frac{\partial^2}{\partial X\partial Z} - 2hX\frac{\partial^2}{\partial Y\partial Z} \right) G'$$

$$= -4\pi\phi\delta(X-X_0)\delta(X-X_0) + \phi\left(\beta^2 + 2j\beta hY\frac{\partial}{\partial X} - 2j\beta hX\frac{\partial}{\partial Y} \right) G , \tag{5.44}$$

$$G'\frac{\partial \Psi}{\partial n} = \frac{G'}{|\mathbf{N}|}\left[L + h\left(X\frac{dX}{ds} + Y\frac{dY}{ds}\right)\frac{\partial}{\partial Z}\right]\Psi$$

$$= G\left[q - \frac{j\beta h}{|\mathbf{N}|}\left(X\frac{dX}{ds} + Y\frac{dY}{ds}\right)\right]\Phi, \tag{5.45}$$

$$\Psi\frac{\partial G'}{\partial n} = \frac{\Psi}{|\mathbf{N}|}\left[L + h\left(X\frac{dX}{ds} + Y\frac{dY}{ds}\right)\frac{\partial}{\partial Z}\right]G'$$

$$= \frac{\Phi}{|\mathbf{N}|}\left[L + j\beta h\left(X\frac{dX}{ds} + Y\frac{dY}{ds}\right)\right]G, \tag{5.46}$$

where the operators $\nabla^2{}_T$ and L are given by (4.2) and (4.11). Then, (5.42) becomes

$$C_0\Phi_0 = \int_{\partial\Omega_I} G\,q\,|\mathbf{N}|\,ds - \int_{\partial\Omega_I}\Phi\left[L(G) + 2j\beta h\left(X\frac{dX}{ds} + Y\frac{dY}{ds}\right)G\right]ds$$

$$+ \int_{\Omega_C}\Phi\left[(k^2 - \beta^2)G + 2j\beta h\left(Y\frac{dG}{dX} - X\frac{dG}{dY}\right)\right]dXdY, \tag{5.47}$$

where $C_0 = 4\pi$ for (X_0, Y_0) in Ω_C, and $C_0 = 2\pi$ for (X_0, Y_0) on $\partial\Omega_I$ if $\partial\Omega_I$ is smooth.

The functions ϕ and q are approximately expressed in the following forms in terms of the nodal values ϕ_j and q_j, and shape functions ξ_j and ξ_j',

$$\Phi = \sum_j \xi_j \Phi_j\,, \tag{5.48}$$

$$q = \sum_j \xi_j' q_j\,. \tag{5.49}$$

A proper equation in matrix form can be derived from (5.47) using (5.48) and (5.49) as follows :

$$\begin{bmatrix} [2\pi\delta_{ij}C_i] + [H^{BB}] + [S^{BB}] & [G^{BB}] & [S^{BI}] \\ [H^{IB}] + [S^{IB}] & [G^{IB}] & 4\pi[I] + [S^{II}] \end{bmatrix}\begin{bmatrix} [\Phi^B] \\ [q] \\ [\Phi^I] \end{bmatrix} = k^2\begin{bmatrix} [T^{BB}] & [0] & [T^{BI}] \\ [T^{IB}] & [0] & [T^{II}] \end{bmatrix}\begin{bmatrix} [\Phi^B] \\ [q] \\ [\Phi^I] \end{bmatrix}, \tag{5.50}$$

where the elements of the matrices $[H]$, $[G]$, $[S]$ and $[T]$ are given by

$$H_{ij} = \int_{(\partial\Omega_I)_j} \left[L(G_{ij}) + 2j\beta h \left(X\frac{dX}{ds} + Y\frac{dY}{ds} \right) G_{ij}\,\xi_j \right] ds\,, \tag{5.51}$$

$$G_{ij} = -\int_{(\partial\Omega_I)_j} G_{ij}\,|\mathbf{N}_j|\,\xi_j'\,ds\,, \tag{5.52}$$

$$S_{ij} = \int_{(\Omega_C)_j} \left[\beta^2 G_{ij} - 2j\beta h \left(Y\frac{dG_{ij}}{dX} - X\frac{dG_{ij}}{dY} \right) \right] \xi_j\,dX dY\,, \tag{5.53}$$

$$T_{ij} = \int_{(\Omega_C)_j} G_{ij}\,\xi_j\,dX dY\,. \tag{5.54}$$

If functions ϕ and q are assumed to be constant in domain and boundary elements, (5.50) is reduced to

$$\begin{bmatrix} [2\pi\delta_{ij}C_i]+[H^{BB}] & [G^{BB}] & [\mathrm{S}^{BI}] \\ [H^{IB}] & [G^{IB}] & 4\pi[I]+[\mathrm{S}^{II}] \end{bmatrix} \begin{bmatrix} [\phi^B] \\ [q] \\ [\phi^I] \end{bmatrix} = k^2 \begin{bmatrix} [0] & [0] & [T^{BI}] \\ [0] & [0] & [T^{II}] \end{bmatrix} \begin{bmatrix} [\phi^B] \\ [q] \\ [\phi^I] \end{bmatrix}. \tag{5.55}$$

Since (5.50) and (5.55) are linear proper equations, they can be numerically solved under appropriate boundary conditions.

We next consider a BE formulation for the TE mode analysis of the twisted waveguide shown in Figs. 5.1 and 5.2 with Lewin's boundary conditions (5.29)-(5.31), which specify the values of $\partial\phi/\partial X$ and $\partial\phi/\partial Y$ instead of q.

Using (4.11), (5.47) can be rewritten for $\beta=0$ as follows :

$$C_0\phi_0 = \int_C G\left(f_X\frac{\partial\Phi}{\partial X} + f_Y\frac{\partial\Phi}{\partial Y} \right) ds - \int_C \phi\,L(G)\,ds + k^2\int_\Omega G\Phi\,dX dY, \tag{5.56}$$

where

$$f_X = h^2XY\frac{dX}{ds} + (1+h^2Y^2)\frac{dY}{ds}\,,$$

$$f_Y = -(1+h^2X^2)\frac{dX}{ds} + h^2XY\frac{dY}{ds}\,. \tag{5.57}$$

From the boundary conditions (5.29) and (5.30), (5.56) becomes

$$C_0\phi_0 = \int_{C_1} G f_X\frac{\partial\Phi}{\partial X}\,ds + \int_{C_2} G f_Y\frac{\partial\Phi}{\partial Y}\,ds - \int_C \phi\,L(G)\,ds + k^2\int_\Omega G\Phi\,dX dY. \tag{5.58}$$

Discretizing (5.59) and writing $\partial\phi/\partial X$ and $\partial\phi/\partial Y$ in terms of Φ_j, we have again a linear proper equation in the following form

$$\begin{bmatrix} [2\pi\delta_{ij}C_i]+[P^{BB}] & [0] \\ [Q^{IB}] & [4\pi I] \end{bmatrix} \begin{bmatrix} [\phi^B] \\ [\phi^I] \end{bmatrix} = k^2 \begin{bmatrix} [0] & [T^{BI}] \\ [0] & [T^{II}] \end{bmatrix} \begin{bmatrix} [\phi^B] \\ [\phi^I] \end{bmatrix} . \tag{5.59}$$

5.1.4 FE formulation for scalar Helmholtz equation [5.6]

In the following, we first give an FE formulation for the scalar Helmholtz equation (5.24) in the helical column V_C shown in Fig. 4.1.

Multiplying (5.24) by the weight function W and integrating over one period $2\pi/h$ (*i.e.*, $-\pi/h \leqq Z \leqq \pi/h$) of the helical region V_C enclosed by the boundary ∂V_I yield

$$\int_{V_C} W(\nabla^2\Psi + k^2\Psi)\, dV = 0 . \tag{5.60}$$

We obtain the weak form of (5.60) through the adoption of Gauss' divergence theorem as follows :

$$\int_{V_C} (\nabla W \cdot \nabla \Psi - k^2 W \Psi)\, dV - \int_{\partial V_I} W \frac{\partial \Psi}{\partial n}\, dS = 0 . \tag{5.61}$$

Note that the surface integral in (5.61) over the end of the cut helical region V_C, *i.e.*, the surface of $Z = \pm\pi/h$, cancel by periodicity. In (5.61), in terms of the phase constant β, the functions Ψ and W are written in the form

$$\Psi = \phi(X,Y)e^{-j\beta Z} , \quad W = w(X,Y)\, e^{j\beta Z} . \tag{5.62}$$

Using (4.6), (4.9) and (5.62), the boundary term in (5.61) can be rewritten on the plane of $Z = 0$ as follows :

$$\begin{aligned} \int_{\partial V_I} W \frac{\partial \Psi}{\partial n}\, dS &= \frac{2\pi}{h} \int_{\partial \Omega_I} w \frac{\partial \phi}{\partial n} |\mathbf{N}|\, ds \\ &= \frac{2\pi}{h} \int_{\partial \Omega_I} w \frac{\partial \Phi}{\partial n} \left[1 + h^2 \left(X \frac{dX}{ds} + Y \frac{dY}{ds} \right)^2 \right]^{1/2} ds \end{aligned} \tag{5.63}$$

On the other hand, $\nabla W \cdot \nabla \Psi$ in the first integral in (5.61) can be written as

$$\nabla W \cdot \nabla \Psi = \sum_{i=1}^{3} \sum_{j=1}^{3} g^{ij} \frac{\partial W}{\partial u^i} \frac{\partial \Psi}{\partial u^j} \ , \tag{5.64}$$

where g^{ij} is given by (2.55). Consequently, using (5.62)-(5.64), (5.61) can be written in the two dimensional form

$$\int_{\Omega_C} \left[(\beta^2 - k^2) w\phi + (1+h^2Y^2) \frac{\partial w}{\partial X} \frac{\partial \phi}{\partial X} - h^2 XY \left(\frac{\partial w}{\partial X} \frac{\partial \phi}{\partial Y} + \frac{\partial w}{\partial Y} \frac{\partial \phi}{\partial X} \right) + (1+h^2X^2) \frac{\partial w}{\partial Y} \frac{\partial \phi}{\partial Y} \right.$$

$$\left. - j\beta hY \left(\phi \frac{\partial w}{\partial X} - w \frac{\partial \phi}{\partial X} \right) + j\beta hX \left(\phi \frac{\partial w}{\partial Y} - w \frac{\partial \phi}{\partial Y} \right) \right] dX\, dY$$

$$- \int_{\partial \Omega_I} w \frac{\partial \phi}{\partial n} \left[1 + h^2 \left(X \frac{dX}{ds} + Y \frac{dY}{ds} \right)^2 \right]^{1/2} ds = 0 \ . \tag{5.65}$$

Interpolating the function ϕ in (5.65) by use of the shape function ξ_j

$$\phi = \sum_j \xi_j \phi_j \ . \tag{5.66}$$

and employing ξ_j as the weight function w, we have a proper equation in matrix form as

$$[K][\phi] = k^2 [M][\phi] \ . \tag{5.67}$$

We next give an FE formulation for the analysis of TE mode of the twisted waveguide shown in Figs. 5.1 and 5.2. In order to consider Lewin's boundary conditions (5.29) and (5.30) on the boundary C, the boundary term in (5.65) is rewritten in terms of $\partial\phi/\partial X$ and $\partial\phi/\partial Y$ as follows :

$$\int_{\partial \Omega_I} W \frac{\partial \Psi}{\partial n} dS = \int_C w \left[- \frac{dX}{ds} \left\{ -h^2 XY \frac{\partial \phi}{\partial X} + (1+h^2X^2) \frac{\partial \phi}{\partial Y} + j\beta hX\phi \right\} \right.$$

$$\left. + \frac{dY}{ds} \left\{ (1+h^2Y^2) \frac{\partial \phi}{\partial X} - h^2 XY \frac{\partial \phi}{\partial Y} - j\beta hY\phi \right\} \right] ds$$

$$= - \int_{C_1} w \left[-h^2 XY \frac{\partial \phi}{\partial X} + (1+h^2X^2) \frac{\partial \phi}{\partial Y} + j\beta hX\phi \right] dX$$

$$+ \int_{C_2} w \left[(1+h^2Y^2) \frac{\partial \phi}{\partial X} - h^2 XY \frac{\partial \phi}{\partial Y} - j\beta hY\phi \right] dY \ . \tag{5.68}$$

Moreover, we introduce the following quantities so that the solutions satisfy the boundary condition (5.29) and (5.30),

$$\int_{C_1} w \frac{\partial \Phi}{\partial Y}\, dX = 0\,, \tag{5.69}$$

$$-\int_{C_2} w \frac{\partial \Phi}{\partial X}\, dY = 0\,. \tag{5.70}$$

Adding these conditions to (5.65) and using (5.68), we obtain

$$\begin{aligned}\int_\Omega \Bigg[&(\beta^2 - k^2)\, w\Phi + (1+h^2Y^2)\frac{\partial w}{\partial X}\frac{\partial \Phi}{\partial X} - h^2XY\left(\frac{\partial w}{\partial X}\frac{\partial \Phi}{\partial Y} + \frac{\partial w}{\partial Y}\frac{\partial \Phi}{\partial X}\right) + (1+h^2X^2)\frac{\partial w}{\partial Y}\frac{\partial \Phi}{\partial Y} \\ &- j\beta hY\left(\Phi\frac{\partial w}{\partial X} - w\frac{\partial \Phi}{\partial X}\right) + j\beta hX\left(\Phi\frac{\partial w}{\partial Y} - w\frac{\partial \Phi}{\partial Y}\right)\Bigg]\, dX\, dY \\ &= \int_{C_1} w\left(h^2XY\frac{\partial \Phi}{\partial X} - h^2X^2\frac{\partial \Phi}{\partial Y} - j\beta hX\Phi\right) dX \\ &+ \int_{C_2} w\left(h^2Y^2\frac{\partial \Phi}{\partial X} - h^2XY\frac{\partial \Phi}{\partial Y} - j\beta hY\Phi\right) dY\,, \end{aligned} \tag{5.71}$$

where the region Ω_C in (5.65) is replaced by Ω. A linear proper equation of the same form as (5.67), which can be solved by standard numerical methods, is derived from (5.71).

5.2 Analysis of a scalar eigenvalue problem

The BE and FE methods provided in the previous section are here applied to a TE mode analysis of the twisted waveguide shown in Fig. 5.2. The cut-off frequencies calculated by BE and FE methods and Lewin's formula [5.1] (see (5.37)) are summarized in Table 5.1, in which the numerical solutions agree well with Lewin's solutions for both $b=0.8$ and $b=0.3$ [5.4, 5.6]. This result shows the validity of the BE and FE formulations hitherto described.

On the other hand, the computing time of the BE method for this case was more than 10 times compared with that of the FE method. In order to consider this result, a brief estimation of the computing times is given in the following.

Let us consider a square solution region with $4n$ boundary elements and $2n^2$ triangle domain elements shown in Fig. 5.3. In a BE analysis with linear elements, the times for the formation of matrices consisting of line integrals such as G and H matrices may increase like $at_G n^2$, while those for matrices including surface integrals such as S and T in (5.50) grows like $a't_G n^4$, where a and a' are constants and t_G is the computing time of the fundamental solution (4.4). (It should be here noted that the number of source points are $(n+1)^2$ in the formation of S and T matrices.) Hence the formation of S and T is the most time-consuming in the hybrid BEM. On the other hand, the formation of FE matrices K and M in (5.67) with linear elements may take $a''t_F n^2$, where a'' and t_F are a constant and the computing time of one component of 3×3 element matrices. The matrix

Table 5.1 Cut-off wavenumbers k for $a=1.0$

h	0.1	0.3	0.5	0.7	0.9
BEM ($b=0.8$)	3.146	3.160	3.186	3.224	3.274
FEM ($b=0.8$)	3.146	3.159	3.184	3.220	3.268
Lewin ($b=0.8$)	3.143	3.156	3.178	3.206	3.235
BEM ($b=0.3$)	3.146	3.153	3.167	3.188	3.217
FEM ($b=0.3$)	3.146	3.154	3.168	3.190	3.219
Lewin ($b=0.3$)	3.143	3.150	3.164	3.186	3.214

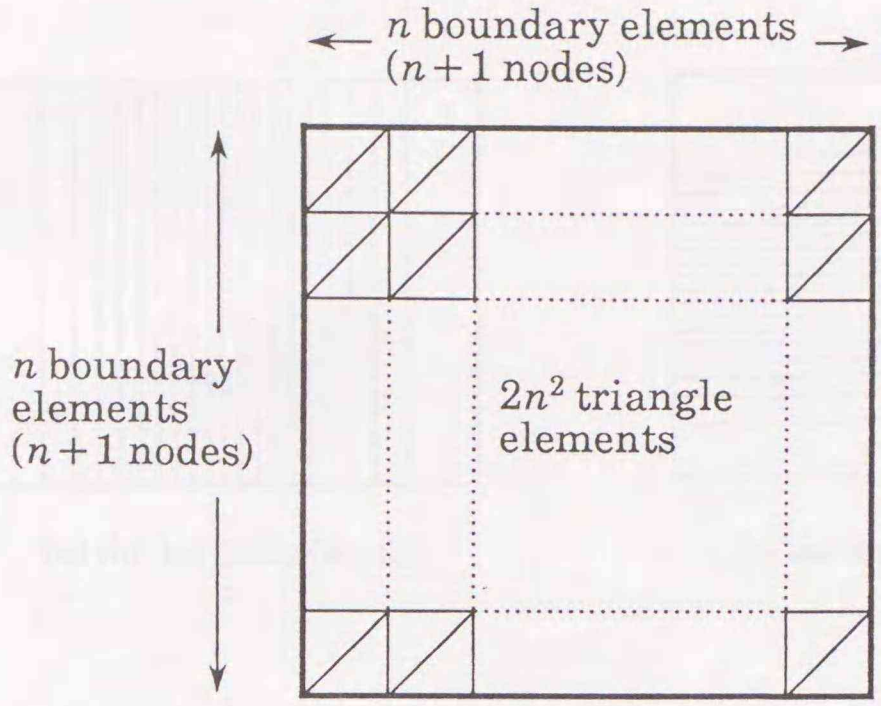

Fig. 5.3 Discretization of a square solution region

formation for hybrid BE method becomes therefore considerably expensive in comparison with FE method especially for large-scale computation. Moreover, it is obvious that $t_F \ll t_G$ because the element matrix for the FE method consists of only algebraic equations of low order. For the above mentioned reasons, the FE method is concluded to be more suitable than BE method for the solution of scalar eigenvalue problems.

Figure 5.4 illustrates the field distributions of the first and second TE modes calculated by the FE method. From this figure, it can be seen that when h increases, the higher modes come to appear in addition to the dominant modes. Figure 5.5 shows the dependence of field distributions on S, the shift of waveguide from the origin. In the calculation, S is taken to be $a/5$ and the boundary conditions are chosen as

$$E^X = \frac{\partial \Psi}{\partial Y} = 0, \qquad \text{at } Y = \pm b/2,$$
$$E^Y = -\frac{\partial \Psi}{\partial X} = 0, \qquad \text{at } X = \pm a/2 + a/5. \tag{5.72}$$

The field distribution of the second mode strongly depends on h in comparison with that of the first mode.

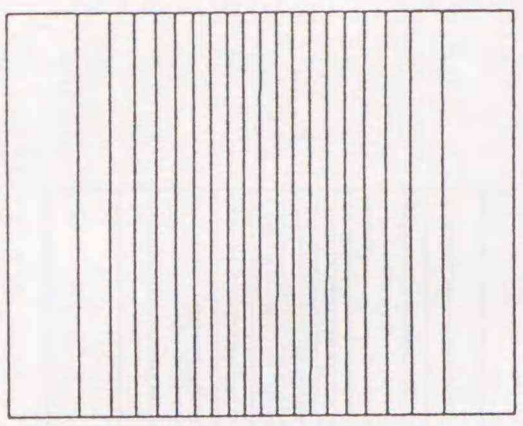

(a) the 1st mode ($h=0$)

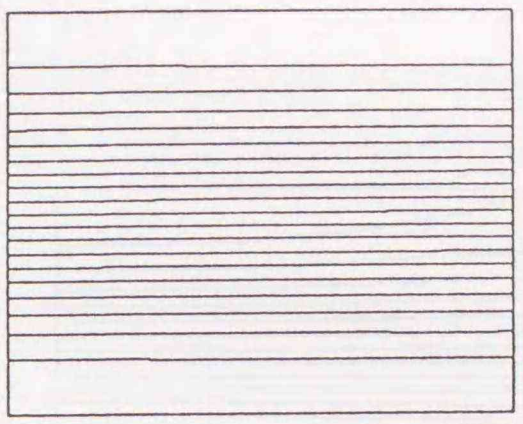

(b) the 2nd mode ($h=0$)

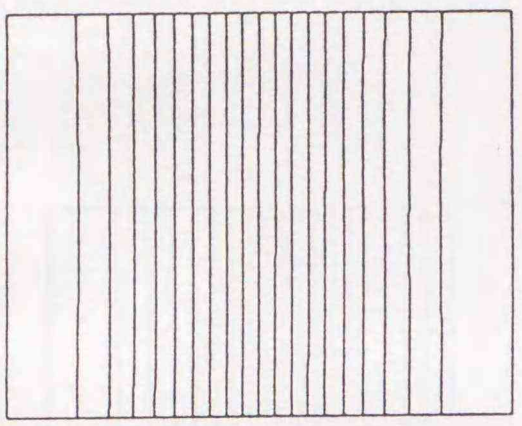

(c) the 1st mode ($h=0.5$)

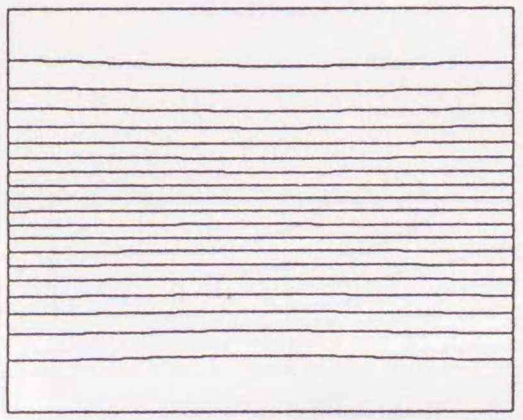

(d) the 2nd mode ($h=0.5$)

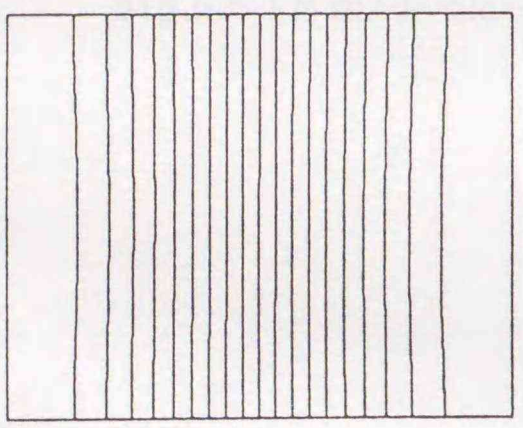

(e) the 1st mode ($h=0.9$)

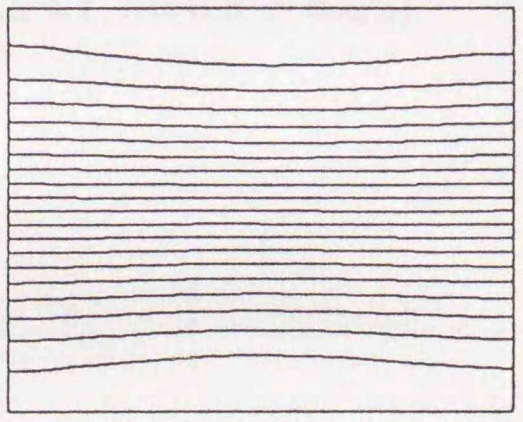

(f) the 2nd mode ($h=0.9$)

Fig.5.4 TE mode distributions ($a=1.0$, $b=0.8$, $S=0.0$).

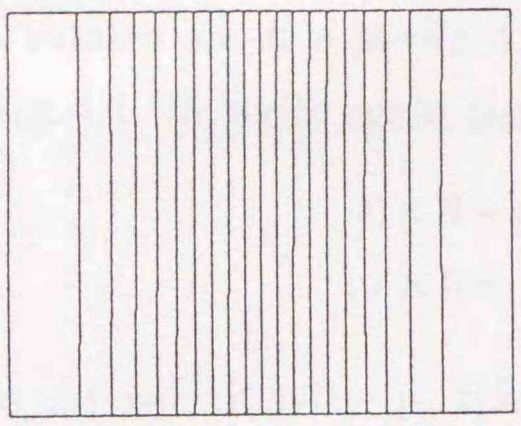

(a) the 1st mode ($h=0.5$)

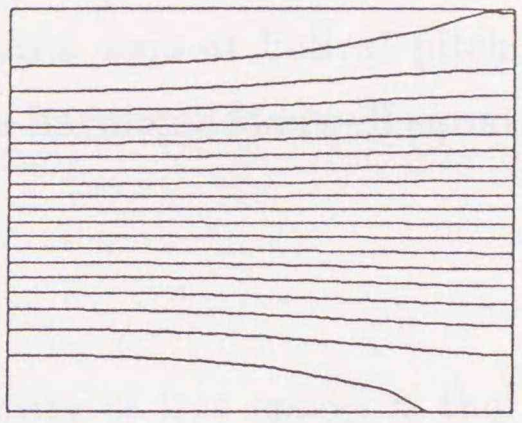

(b) the 2nd mode ($h=0.5$)

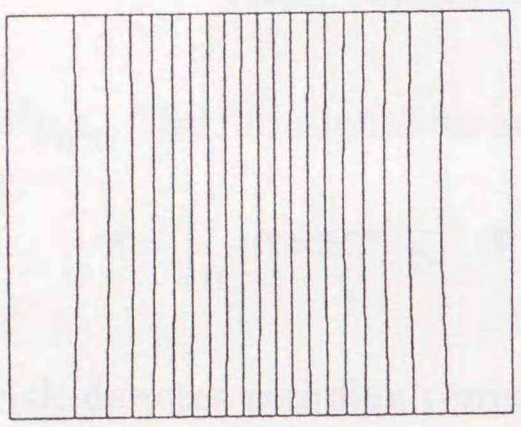

(c) the 1st mode ($h=0.9$)

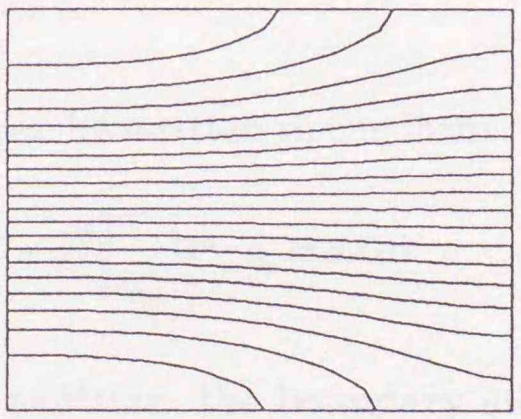

(d) the 2nd mode ($h=0.9$)

Fig.5.5 TE mode distributions ($a=1$, $b=0.8$, $S=a/5$).

5.3 Formulation for vectorial eigenvalue problems [5.7]

This section gives a vectorial FE formulation for wave propagation in helical systems. Let us consider a helical, arbitrarily shaped waveguide whose cross section Ω_C rotates about a straight, longitudinal axis at helical pitch $2\pi/h$ as shown in Fig. 4.1. We write again here the time-harmonic Maxwell equations

$$\nabla \times \mathbf{H} = j\omega\varepsilon_r\varepsilon_0 \mathbf{E}\,, \tag{5.73}$$

$$\nabla \times \mathbf{E} = -j\omega\mu_r\mu_0 \mathbf{H}\,, \tag{5.74}$$

where ε_0 is the permittivity, μ_0 the permeability of free space, ε_r the relative permittivity and μ_r the relative permeability. The vector Helmholtz equation for H, which is chosen as an unknown variable in this section, can be derived from (5.73) and (5.74) as follows :

$$\nabla\times(\varepsilon_r^{-1}\nabla\times\mathbf{H}) - k^2\mu_r\mathbf{H} = 0\,, \tag{5.75}$$

where $k^2=\omega^2\mu_0\varepsilon_0$. The functional for eq. (5.75) can be written in the form

$$F = \int_{\Omega_C} (\nabla\times\mathbf{H})^* \cdot \varepsilon_r^{-1} (\nabla\times\mathbf{H})\, dXdY - k^2 \int_{\Omega_C} \mathbf{H}^* \cdot \mu_r \mathbf{H}\, dXdY\,, \tag{5.76}$$

where asterisk denotes complex conjugate. In addition, the boundary $\partial\Omega$ of the domain Ω is assumed to consist of electric or magnetic walls. Since minimization of the functional (5.76) yields the spectrum pollution, we modify it using the penalty method to remove spurious solutions [5.8, 5.9] as follows :

$$F' = F + p\int_{\Omega_C} (\nabla\cdot\mathbf{H})^* (\nabla\cdot\mathbf{H})\, dXdY\,, \tag{5.77}$$

The functional (5.77) can be expressed in terms of the covariant or contravariant components of magnetic fields when it is described in the twisted coordinates. When using the covariant components H_i, magnetic fields are interpolated in finite elements Ω_m as

$$[H_i] = [\Phi]^T [h_m]\,, \tag{5.78}$$

where

$$[\Phi] = \begin{bmatrix} [\phi] & [0] & [0] \\ [0] & [\phi] & [0] \\ [0] & [0] & j[\phi] \end{bmatrix}, \quad [h_m] = \begin{bmatrix} [h_X] \\ [h_Y] \\ [h_Z] \end{bmatrix}, \tag{5.79}$$

$[\phi]$ and $[h_i]$ are the column vectors which consist of interpolation functions ϕ and the i-th covariant components of magnetic fields at nodal points in Ω_m, respectively. Providing that the electromagnetic field in the helical system varies as $e^{-j\beta Z}$ in Z direction, where β is the phase constant, we can derive the discretized functional for the covariant components from the formulae given in Sec. 2.2 and (5.77)-(5.79) as follows :

$$F' = \sum_m [h_m^*]^T \int_{\Omega_m} \Big[[B_{ij}^*] \varepsilon_r^{-1} [g_{ij}] [B_{ij}]^T - k^2 [\Phi^*] [g^{ij}] \mu_r [\Phi]^T + p [C_i^*] [C_i]^T \Big] dX dY [h_m], \tag{5.80}$$

where

$$[B_{ij}] = \begin{bmatrix} 0 & -j\beta[\phi] & -[\partial\phi/\partial Y] \\ j\beta[\phi] & 0 & [\partial\phi/\partial X] \\ j[\partial\phi/\partial Y] & -j[\partial\phi/\partial X] & 0 \end{bmatrix} \tag{5.81}$$

$$[C_i] = \begin{bmatrix} (1+h^2Y^2)[\partial\phi/\partial X] - h^2XY[\partial\phi/\partial Y] - (h^2X + j\beta hY)[\phi] \\ -h^2XY[\partial\phi/\partial X] + (1+h^2X^2)[\partial\phi/\partial Y] - (h^2Y - j\beta hX)[\phi] \\ \beta[\phi] + j(hY[\partial\phi/\partial X] - hX[\partial\phi/\partial Y]) \end{bmatrix} \tag{5.82}$$

On the other hand, interpolating magnetic fields with the nodal values h^i of the contravariant component H^i as

$$[H^i] = [\Phi]^T [h^m], \tag{5.83}$$

where

$$[h^m] = \begin{bmatrix} [h^X] \\ [h^Y] \\ [h^Z] \end{bmatrix}, \tag{5.84}$$

we can obtain the discretized functional for H^i as follows :

$$F' = \sum_m [h^{m*}]^T \int_{\Omega_m} \Big[[B^{ij*}] \varepsilon_r^{-1} [g_{ij}] [B^{ij}]^T - k^2 [\Phi^*] [g_{ij}] \mu_r [\Phi]^T + p [C^{i*}] [C^i]^T \Big] dX dY [h^m] , \tag{5.85}$$

where

$$[B^{ij}] = \begin{bmatrix} -h[\phi] - hY[\partial\phi/\partial Y] & -j\beta[\phi] + hY[\partial\phi/\partial X] & -[\partial\phi/\partial Y] \\ j\beta[\phi] + hX[\partial\phi/\partial Y] & -h[\phi] - hX[\partial\phi/\partial X] & [\partial\phi/\partial X] \\ -\beta hX[\phi] + 2jh^2 Y[\phi] + & -\beta hY[\phi] - 2jh^2 X[\phi] - & 2jh[\phi] + \\ j(1+h^2r^2)[\partial\phi/\partial Y] & j(1+h^2r^2)[\partial\phi/\partial X] & jh(Y[\partial\phi/\partial Y] + X[\partial\phi/\partial X]) \end{bmatrix} \tag{5.86}$$

$$[C^i] = \begin{bmatrix} [\partial\phi/\partial X] \\ [\partial\phi/\partial Y] \\ \beta[\phi] \end{bmatrix} \tag{5.87}$$

and $r^2 = X^2 + Y^2$. Although the terms which contain the matrices $[C_i]$ and $[B^{ij}]$ in (5.82) and (5.86) are complicated, those integrations can be effectively and easily performed by a numerical integration technique [5.10] without expanding those terms by hand.

It can be seen that when $h \to 0$, (5.80) and (5.85) approach the well-known discretized functional for electromagnetic waves in translational systems described in the Cartesian coordinates.

Next we establish the boundary conditions on the magnetic and electric walls, Γ_m and Γ_e. Using the position vector $\mathbf{r} = \mathbf{r}(X(s), Y(s), Z)$ and the length s measured along $\partial\Omega_I$, the normal vector $\mathbf{n}$ of the boundary $\partial\Omega_I$ can be defined by $\mathbf{n} = \partial\mathbf{r}/\partial s \times \partial\mathbf{r}/\partial Z$. Using the relations $\partial\mathbf{r}/\partial u^i = \mathbf{e}_i$, $\mathbf{e}^X = \mathbf{e}_Y \times \mathbf{e}_Z$ and its permutations, the normal vector $\mathbf{n}$ is rewritten in the form

$$\mathbf{n} = dY/ds\, \mathbf{e}^X - dX/ds\, \mathbf{e}^Y . \tag{5.88}$$

For the covariant components, the boundary conditions are derived from (5.88) and the condition $\mathbf{H} \times \mathbf{n} = \mathbf{0}$ on the magnetic wall Γ_m and $\mathbf{H} \cdot \mathbf{n} = 0$ on the electric wall Γ_e as follows :

$$H_X dX/ds + H_Y dY/ds = 0,\ H_Z = 0\,, \qquad \text{on } \Gamma_m \qquad (5.89)$$

$$[h^2XYH_X - (1+h^2X^2)H_Y + hXH_Z]dX/ds +$$

$$[(1+h^2Y^2)H_X - h^2XYH_Y + hYH_Z]dY/ds = 0\,. \qquad \text{on } \Gamma_e \qquad (5.90)$$

The boundary conditions for contravariant components can be obtained in the same manner as follows :

$$[H^X + h^2X(XH^X + YH^Y)]dX/ds +$$

$$[H^Y + h^2Y(XH^X + YH^Y)]dY/ds = 0\,,$$

$$H^Z = h(YH^X - XH^Y)/(1+h^2r^2)\,, \qquad \text{on } \Gamma_m \qquad (5.91)$$

$$H^X dY/ds - H^Y dX/ds = 0\,. \qquad \text{on } \Gamma_e \qquad (5.92)$$

Imposing the above boundary conditions on the functional (5.80) and (5.85), and differentiating them with respect to h_i and h^i yield the proper equations which can be numerically solved.

5.4 Analysis of a vectorial eigenvalue problem [5.7]

The FE formulation given in the previous section is here applied to the analysis of wave propagation in a rectangular twisted waveguide of width 1.0 and height 0.5 with $\varepsilon_r = \mu_r = 1.0$. Since the guide wall can be regarded as an electric boundary in this case, boundary conditions (5.90) and (5.92) are used for this calculation. Figure 5.6 shows the convergence of cut-off wavenumbers k for the covariant and contravariant formulations with second order interpolation functions. The abscissa denotes the number of nodal points in the solution region Ω_C. Both wavenumbers clearly converge to the same value, and this shows equivalence of the present covariant and contravariant formulations. In addition, from this result, the number of nodes is taken to be 171 in the remain of this thesis.

Figure 5.7 shows the dependence of the cut-off wavenumbers on the helical wavenumber h, which are obtained by the present covariant formulation and the perturbation methods based on the scalar [5.1] and vector [5.3] Helmholtz equations. The ordinate denotes the relative increment $\triangle k$ defined by $(k\text{-}k_0)/k_0$, where k_0 is the cut-off wavenumber for $h=0$. As shown in this figure, the three solutions are in good agreement for relatively large pitch. This is a reasonable result because small changes of proper modes can be well estimated by the perturbation method. On the other hand, the scalar perturbed solution becomes inaccurate as the pitch is decreased because, as pointed out in Ref. [5.2], the boundary condition in that analysis is inappropriate for small pitch. In addition, a further increase in the wavenumber h also expands the discrepancy between the vector perturbed solution and the FE solution. This discrepancy may not be reduced by increasing the order of the expansion without incurring a severe computational penalty.

The dependence of cut-off wavenumbers for several low modes on the wavenumber is shown in Fig. 5.8. As shown in this figure, the degenerate modes gradually separate as the pitch is increased.

In the above mentioned calculations, the times for computing the matrix components are considerably shorter than those for the solution of the proper

equations. (For example, the ratio is one twelfth for 171 nodes for the covariant formulation.)

The present method may be easily applied to the analyses of guided wave propagation in helical devices with arbitrarily shaped cross section and with dielectric loads.

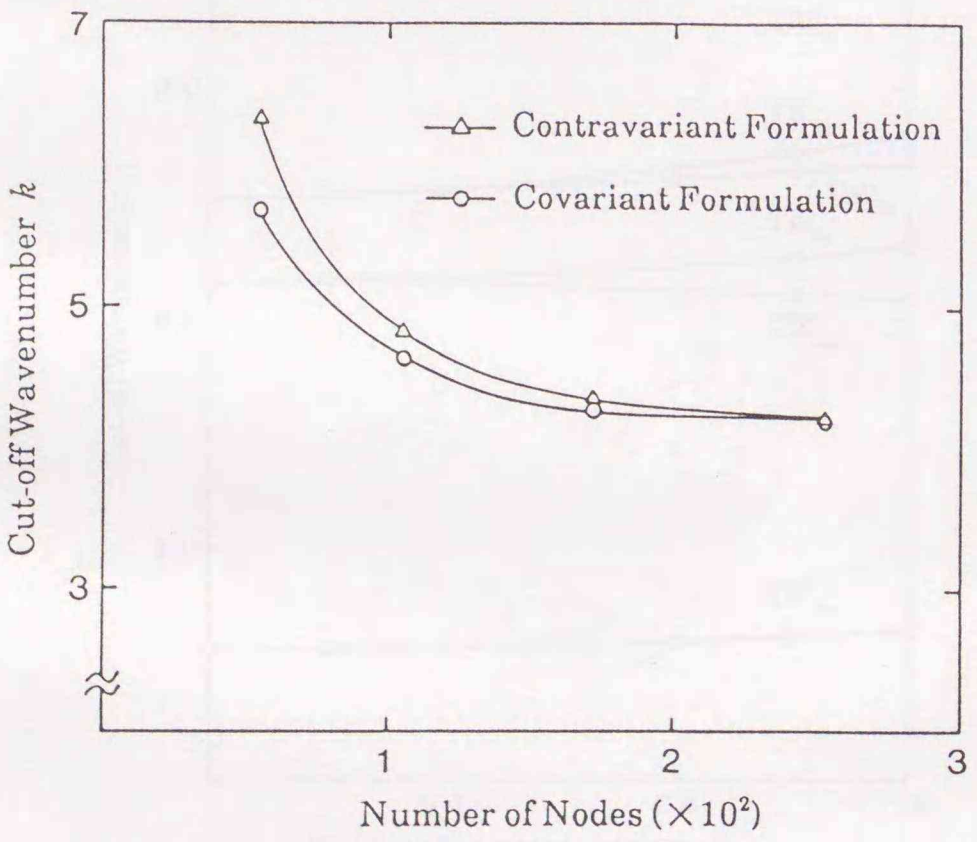

Fig. 5.6 Convergence of cut-off wavenumbers k by the present FE formulations for $h = 1.0$.

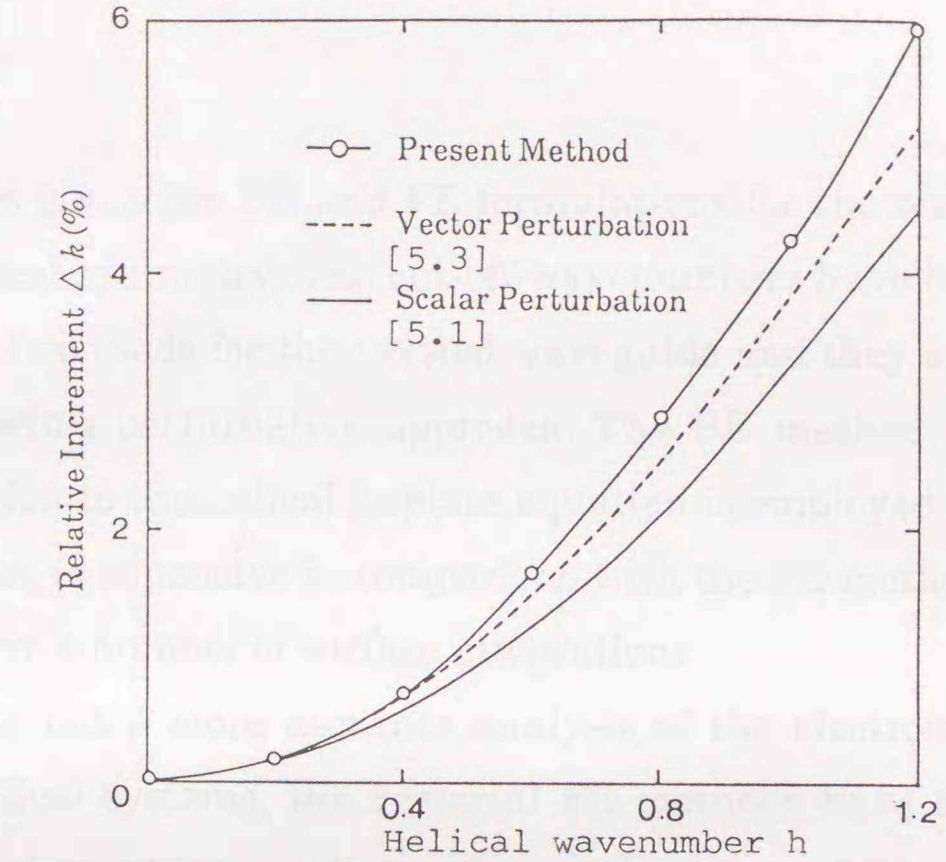

Fig. 5.8 Dependence of cut-off wavenumbers k on h by the present and perturbation methods. $\triangle k$ denotes the relative increment defined by $(k\text{-}k_0)/k_0$, where k_0 is the cut-off wavenumber for $h=0$.

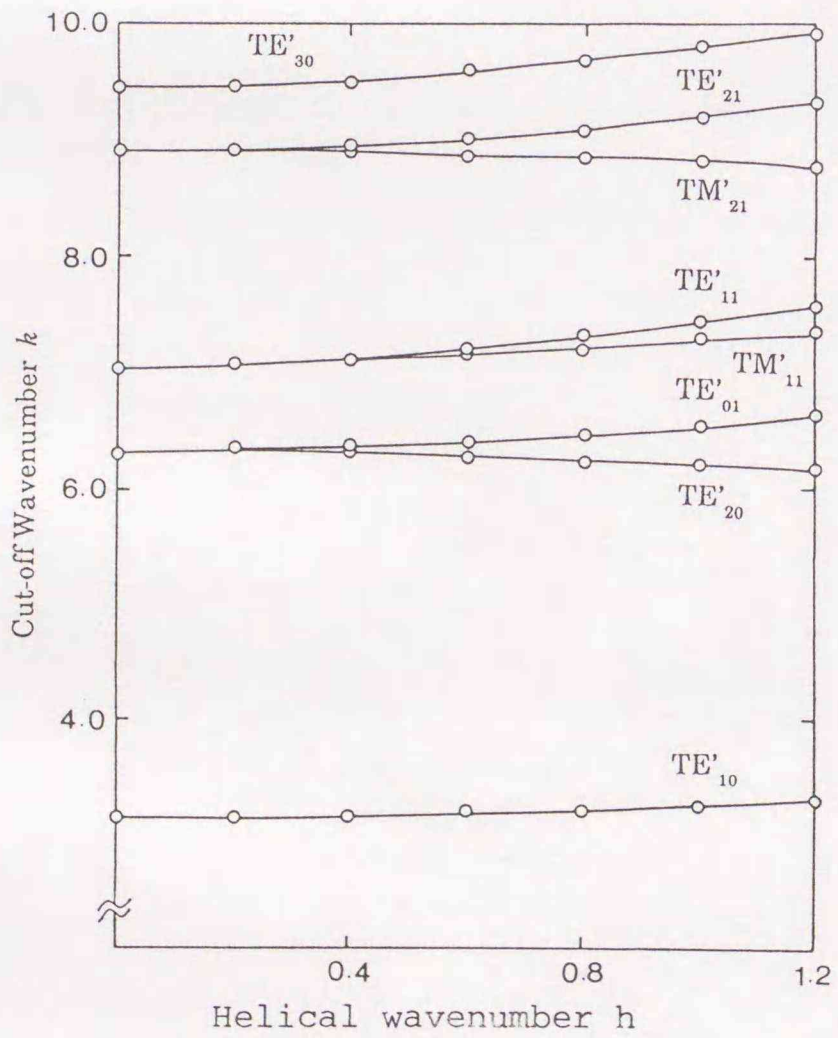

Fig. 5.9 Cut-off wavenumbers k plotted against h for low modes. Primes denote quasi-modes of usual TE and TM modes in a straight waveguide.

5.5 Summary

This chapter has given the BE and FE formulations for the scalar Helmholtz equation with helical symmetry. The cut-off wavenumbers have been calculated by those numerical methods for the twisted waveguide and they agree well with the results by Lewin's perturbative approach. The BE method, in which the fundamental solution to the helical Laplace equation is employed to get a linear eigenvalue problem, is expensive in comparison with the FE method because the former must perform a number of surface integrations.

In order to carry out a more accurate analysis of the electromagnetic wave propagation in helical systems, the vectorial FE methods have been provided. They involve two different formulations whose unknown variables are covariant and contravariant components of magnetic fields, respectively. The spurious solutions have been removed by the penalty method. The two formulations have been shown equivalent.

REFERENCES

5.1 L. Lewin, *Theory of Waveguides*, Newnes-Butherworths, London, pp.96-101, 1975.

5.2 H. Yabe and Y. Mushiake, "An Analysis of a Hybrid-Mode in a Twisted Rectangular Waveguide", *IEEE Trans. Microwave Theory Tech.*, **32**, pp.65-71, 1984.

5.3 H. Yabe, K. Nishio and Y. Mushiake, "Dispersion Characteristics of Twisted Rectangular Waveguides", *ibid*, **32**, pp.91-96, 1984.

5.4 H. Igarashi and T. Honma, Boundary Element Analysis of Electromagnetic Fields in Helically Symmetric Systems, *Boundary Element Technology VI*, (Eds. C. A. Brebbia), Computational Mechanics Publications & Elsevier, Southampton, pp. 65-76, 1991.

5.5 N. Tosaka and K. Kakuda, New Integral Equation Method for Approximate Solution of Eigenvalue Problems, *Trans. Architectural Inst. Japan,* **328**, pp. 36-43, 1983, (in Japanese).

5.6 H. Igarashi and T. Honma, A Finite Element Analysis of TE Modes in Twisted Waveguides, *IEEE Trans. Mag.*, **27**, pp. 4052-4055, 1991.

5.7 H. Igarashi and T. Honma, A Vectorial Finite Element Formulation for Electromagnetic Wave Propagation in Helical Systems, *J. Appl. Phys.*, **71**, 11, pp. 5689-5693, 1992.

5.8 M. Koshiba, K. Hayata and M. Suzuki, *Trans. Inst. Electron. Comm. Eng. Japan*, **E67**, pp. 191-196, 1894.

5.9 B. M. Rahman and J. B. Davies, *IEEE Trans. Microwave Theory Tech.*, **32**, pp. 922-928, 1984.

5.10 See e. g., G. Strang and G. J. Fix, *An Analysis of the Finite Element Method*, Prentice-Hall, New Jersey, p. 156, 1973.

CHAPTER 6

SUMMARY AND CONCLUSIONS

The BE and FE methods for the two-dimensional analysis of helically symmetric electromagnetic fields have been presented. These formulations have been given in the helical coordinates system.

Chapter 1 surveys the helical systems in electric engineering and conventional analyses of them. Chapter 2 describes some foundations of the general curvilinear coordinates system and introduces the twisted and helical polar coordinates systems which belong to the helical coordinates system. The results obtained in this work are following.

Chapter 3

The fundamental solutions to helically symmetric Helmholtz-type equations, which play an important role in the BE analysis, can be derived in a unified form by integrating the three-dimensional fundamental solutions along a source helix. This chapter also estimates the computing times and singularity of the fundamental solutions. The results are

(a) The convergence of the fundamental solution can be improved by analytically evaluating the singular part of it.

(b) The infinite-series representation of the fundamental solution can be calculated in good accuracy much faster than the integral representation.

(c) The singularity in the fundamental solution is evaluated simply as $-4\beta \log l$, where β is a constant and l is the length measured along a boundary element.

Chapter 4

The BE and FE formulations for the two-dimensional analysis of scalar and vector potential fields with helical symmetry are provided.

For the scalar potential problem, the BE and FE formulations that can be applied to both closed and open boundary problems are presented. In the FE formulation for the open boundary problem, in order to give a reasonable treatment of an integral over infinite region, the transfinite element method for helically symmetric systems has been introduced. The numerical results for scalar problems are summarized as follows :

(a) For a closed boundary problem, the proposed BE and FE methods provide reasonable solutions whose accuracy is independent from the value of helical wavenumber h while the second order perturbed solution becomes inaccurate for large h.

(b) The open potential fields around the helical coil and the twisted-pair line can be effectively solved by the present numerical methods. In particular, the transfinite element method has given more accurate solutions than the conventional FE method.

(c) The present FE method is successfully applied to analyze the coupling losses in a twisted superconducting composite. In this analysis, the static electric field in the normal metal region surrounding the superconducting composite is calculated taking account of the twist of the cable. It is revealed that the coupling losses increase with h because the twist of the cable strengthens the electric field.

In order to analyze helically symmetric MHD equilibria, the BE and FE formulations are derived for the helical G-S equation, which can be regarded as one component of the vector Poisson equation. The following results are obtained for each case.

(d) The solutions obtained by the present BE and FE methods agree well with the exact solution to the linear G-S equation.

(e) The Marder-Weitzner iterative method can get stable solutions to the non-linear G-S equation under severe conditions which make the Picard iteration unstable. The BE and FE solutions converge to the same values. The BE method is more expensive than the FE method because the former includes time-consuming surface integration processes.

(f) The present FE method is applied to the analysis of the MHD equilibria in straight stellarators with bean-shaped cross-sections. The equilibria have been iteratively calculated under the condition of vanishing the net toroidal current over the whole plasma cross section. The profiles of the stream function, rotational transform and specific volume for a helically symmetric

vacuum field with bean-shaped cross section are in good agreement with analytical values. The convergence of the present method is little affected by the shape of boundary and it is stable for wide range of parameters of the MHD equilibria. The present iterative method gives the solution faster than the Marder-Weitzner method.

Chapter 5

The BE and FE formulations for the scalar Helmholtz equation with helical symmetry are presented. The cut-off wavenumbers are calculated by those numerical methods for the twisted waveguide. We find the following results.

(a) The BE and FE solutions agree well with the results by Lewin's perturbative approach.

(b) The BE method, in which the fundamental solution to the helical Laplace equation is employed to get a linear eigenvalue problem, is expensive in comparison with the FE method because the former must perform a number of surface integrations.

In order to carry out a more accurate analysis of the electromagnetic wave propagation in helical systems, the vectorial FE methods are provided. They involve two different formulations whose unknown variables are covariant and contravariant components of magnetic fields, respectively. The numerical results are following.

(c) The spurious solutions are successfully removed by the penalty method.

(d) The two formulations, which need approximately same amount of computation to get solutions, give equivalent solutions.

Appendices

A-1 Three classes of symmetry in $\mathbb{R}^3$

The theorem which states that there are only the three classes of symmetry in the three dimensional Euclidean space $\mathbb{R}^3$ is proved as follows.

Let us consider a system having an ignorable coordinate u^3 in (u^1, u^2, u^3). Since this system is symmetric in u^3-direction (or it can be described in terms of only the two space variables u^1, u^2), the metric tensor g_{ij} must be independent of u^3

$$\frac{\partial g_{ij}}{\partial u^3} = 0 . \tag{A1.1}$$

It is known that this condition is equivalent to Killing's differential equation [e.g. A1] for the basis vector $\mathbf{e}_3$

$$\xi_{i;j} + \xi_{j;i} = 0 , \tag{A1.2}$$

where ξ_j are the covariant components of $\mathbf{e}_3$, *i.e.*, $\xi_j = g_{j3}$ and suffixes denote the covariant differentiation defined as

$$\xi_{i;j} = \frac{\partial \xi_i}{\partial u^j} - \Gamma^h_{ij}\xi_h , \tag{A1.3}$$

$$\Gamma^h_{ij} = \frac{1}{2} g^{hk}\left(\frac{\partial g_{jk}}{\partial u^i} + \frac{\partial g_{ki}}{\partial u^j} - \frac{\partial g_{ij}}{\partial u^k} \right). \tag{A1.4}$$

Equation (A1.2) is the necessary and sufficient condition in order that the fundamental form

$$\Phi = g_{ij}\, du^i\, du^j , \tag{A1.5}$$

is invariant with respect to an infinitesimal transformation

$$u^{i\,\prime} = u^i + \varepsilon \xi^i , \tag{A1.6}$$

where ε is an infinitesimal constant. In $\mathbb{R}^3$, it can be shown that the condition (A1.2) is reduced to the following simple equations in the Cartesian coordinates (x^1, x^2, x^3),

---

A.1 L. P. Eisenhart, *Continuous Groups of Transformations*, Dover, New York, pp. 208-217, 1961.

$$\frac{\partial \xi^i}{\partial x^j} + \frac{\partial \xi^j}{\partial x^i} = 0\,,\ (i,j=1,2,3)\,. \tag{A1.7}$$

Moreover, since the transformation (A1.6) is an infinitesimal affine transform, the components ξ^i must satisfy the condition

$$\frac{\partial^2 \xi^i}{\partial x^j \partial x^k} = 0\,,\ (i,j,k=1,2,3)\,. \tag{A1.8}$$

Consequently, from (A1.7) and (A1.8), we can see that the vector $\mathbf{e}_3$ takes the form

$$\mathbf{e}_3 = \mathbf{a}\times\mathbf{r} + \mathbf{b}\,, \tag{A1.9}$$

where **a** and **b** are constant vectors, and **r** is the position vector. (Here note that ξ^i coincides with ξ_i in the Cartesian coordinates.) Hence, as mentioned above, the symmetry in $\mathbb{R}^3$ can be grouped into translational symmetry ($\mathbf{a}=0$), axial symmetry ($\mathbf{b}=0$) and helical symmetry ($\mathbf{a}\neq 0$, $\mathbf{b}\neq 0$).

A-2 Derivation of (3.9) and (3.10)

Equation (3.9) can be obtained from the following integral formulae

$$\int_{-\infty}^{\infty} e^{-Z(\xi^2+k^2)^{1/2}} \cos(\theta-\theta_0)\,dz_0 = \frac{2(\xi^2+k^2)^{1/2}}{\xi^2+k^2+h^2}\cos(\zeta-\zeta_0)\,, \tag{A2.1}$$

$$\begin{aligned}
&\int_{-\infty}^{\infty} e^{-Z(\xi^2+k^2)^{1/2}} \cos(\theta-\theta_0)\cos[m(\theta-\theta_0)]\,dz_0 \\
&= 2\cos(\zeta-\zeta_0)\cos[m(\zeta-\zeta_0)]\int_0^{\infty} e^{-Z(\xi^2+k^2)^{1/2}}\cos(hZ)\cos(mhZ)\,dZ \\
&\quad + 2\sin(\zeta-\zeta_0)\sin[m(\zeta-\zeta_0)]\int_0^{\infty} e^{-Z(\xi^2+k^2)^{1/2}}\sin(hZ)\sin(mhZ)\,dZ \\
&= (\xi^2+k^2)^{1/2}\left[\frac{\cos\{(m+1)(\zeta-\zeta_0)\}}{\xi^2+k^2+(m+1)^2h^2} + \frac{\cos\{(m-1)(\zeta-\zeta_0)\}}{\xi^2+k^2+(m-1)^2h^2}\right]\,.
\end{aligned} \tag{A2.2}$$

Similarly, one can derive (3.10) using the integral formulae

$$\int_{-\infty}^{\infty} e^{-Z(\xi^2+k^2)^{1/2}}\, dz_0 = 2(\xi^2+k^2)^{-1/2}\,, \tag{A2.3}$$

$$\int_{-\infty}^{\infty} e^{-Z(\xi^2+k^2)^{1/2}} \cos[m(\theta-\theta_0)]\, dz_0 = 2\cos[m(\zeta-\zeta_0)] \int_0^{\infty} e^{-Z(\xi^2+k^2)^{1/2}} \cos(mhZ)\, dZ$$

$$= 2\cos[m(\zeta-\zeta_0)] \frac{(\xi^2+k^2)^{1/2}}{\xi^2+k^2+m^2h^2}\,. \tag{A2.4}$$

A-3 Derivation of (3.26)

Using the well known formulae of the Bessel function

$$I_m'(z) = I_{m-1}(z) - \frac{m}{z} I_m(z)\,, \tag{A3.1}$$

$$K_m'(z) = -K_{m-1}(z) - \frac{m}{z} K_m(z)\,, \tag{A3.2}$$

the left hand side of (3.26) can be rewritten as

$$-4xy\, I_m'(mx) K_m'(my) = 4[\, xy\, I_{m-1}(mx) K_{m-1}(my) + x\, I_{m-1}(mx) K_m(my)$$
$$- y\, I_m(mx) K_{m-1}(my) - I_m(mx) K_m(my)\,]\,. \tag{A3.3}$$

Similarly, applying the formulae

$$I_{m+1}(z) = I_{m-1}(z) - \frac{2m}{z} I_m(z)\,, \tag{A3.4}$$

$$K_{m+1}(z) = K_{m-1}(z) + \frac{2m}{z} K_m(z)\,, \tag{A3.5}$$

to the second and third terms in the right hand side of (A3.3), we have

$$4x\, I_{m-1}(mx) K_m(my) - 4y\, I_m(mx) K_{m-1}(my) =$$
$$2x\, y\, I_{m+1}(mx) K_{m+1}(my) - 2xy\, I_{m-1}(mx) K_{m-1}(my) + 8\, I_m(mx) K_m(my)\,. \tag{A3.6}$$

The substitution of (A3.6) in (A3.3) yields (3.26).

A-4 Derivation of (3.27) by the variable separation technique

In the following, the fundamental solution (3.27) which satisfies (3.21) will be derived by means of a variable separation technique.

We here write (3.21) again,

$$\frac{h^2}{r}\left\{\frac{\partial}{\partial r}\left(\frac{r}{1+h^2r^2}\frac{\partial G_S}{\partial r}\right)+\frac{1}{r}\frac{\partial^2 G_S}{\partial \zeta^2}\right\}=-\frac{4\pi}{r}\delta(r-r_0)\delta(\zeta-\zeta_0). \tag{A4.1}$$

For a function $u(x)$, the delta function $\delta(x - x_0)$ satisfies

$$u(x)=\int_{-\infty}^{\infty}\delta(x-x_0)\,u(x_0)\,dx_0\,. \tag{A4.2}$$

On the other hand, the Fourier-series expansion of the function $u(x)$ can be written as

$$u(x)=\frac{1}{2\pi}\int_{-\infty}^{\infty}u(x_0)\sum_{m=-\infty}^{\infty}e^{jm(x-x_0)}dx_0 \tag{A4.3}$$

Hence $\delta(\zeta - \zeta_0)$ in (A4.1) can be written in the form

$$\delta(\zeta-\zeta_0)=\frac{1}{2\pi}\sum_{m=-\infty}^{\infty}e^{jm(\zeta-\zeta_0)} \tag{A4.4}$$

Substituting (A4.4) into (A4.1) and expanding also the function G_S in the Fourier-series as

$$G_S(r,\zeta;r_0,\zeta_0)=\frac{1}{2\pi}\sum_{m=-\infty}^{\infty}g_m(r,r_0)\,e^{jm(\zeta-\zeta_0)} \tag{A4.5}$$

we have an ordinary differential equation for g_m

$$\frac{d}{dr}\left(\frac{r}{1+h^2r^2}\frac{dg_m}{dr}\right)-\frac{m^2}{r}g_m=-\frac{4\pi}{h^2}\delta(r-r_0)\,. \tag{A4.6}$$

In order to solve (A4.6), we consider the homogeneous differential equation

$$\frac{d}{ds}\left(\frac{s}{1+s^2}\frac{dg_m}{ds}\right)-\frac{m^2}{s}g_m=0\,, \tag{A4.7}$$

where $s=hr$. We rewrite (A4.7) as

$$s^2(1+s^2)g_m''+s(1-s^2)g_m'-m^2(1+s^2)^2g_m=0\,, \tag{A4.8}$$

and assume that the solution to this equation takes the form

$$g_m = s^{\lambda} \sum_{n=0}^{\infty} a_n s^n \ , \tag{A4.9}$$

where $a_0 \neq 0$. The insertion of (A4.9) in (A4.8) yields

$$\sum_{n=0}^{\infty} a_n [\,(n+\lambda)(n+\lambda-1)(s^{n+\lambda}+s^{n+\lambda+2})+(n+\lambda)(s^{n+\lambda}-s^{n+\lambda+2})$$

$$-m^2(s^{n+\lambda}+2s^{n+\lambda+2}+s^{n+\lambda+4})\,] = 0 \ . \tag{A4.10}$$

Recursive equations for a_n are obtained from (A4.10) as follows :

$$\text{for } s^{\lambda} \ ; \ (\lambda^2-m^2)\,a_0 = 0 \quad \therefore \ \lambda = \pm m \tag{A4.11}$$

$$\text{for } s^{\lambda+1} \ ; \ (\lambda^2+2\lambda+1-m^2)\,a_1 = 0 \quad \therefore \ a_1 = 0 \tag{A4.12}$$

$$\text{for } s^{\lambda+2} \ ; \ (\lambda^2+4\lambda+4-m^2)\,a_2+(\lambda^2-2\lambda-2m^2)\,a_0 = 0$$

$$\therefore \begin{cases} \text{for } \lambda = m \ ; \ a_2 = \dfrac{m(m+2)}{4(m+1)}\,a_0 \ , (m \neq 0) \\ \text{for } \lambda = -m \ ; \ a_2 = \dfrac{m(m-2)}{4(1-m)}\,a_0 \ , (m \neq 0, 1) \end{cases} \tag{A4.13}$$

$$\text{for } s^{\lambda+3} \ ; \ (3+\lambda)(2+\lambda)a_3+(1+\lambda)\lambda a_1+(3+\lambda)a_3-(1+\lambda)a_1-m^2(a_3+a_1) = 0$$

$$\therefore \ a_3 = 0 \tag{A4.14}$$

$$\text{for } s^{n+\lambda+4} \ ; \ (n^2+8n+2n\lambda+8\lambda+16)\,a_{n+4}$$

$$+[n^2+2n(1+m)+2m-m^2]\,a_{n+2}-m^2a_n = 0$$

$$\therefore \begin{cases} \text{for } \lambda = m \ ; \ a_{n+4} = -\dfrac{[n^2+2n(1+m)+2m-m^2]a_{n+2}-m^2a_n}{[n+2(m+2)]\,(n+4)} \ , \\ \text{for } \lambda = -m \ ; \ a_{n+4} = -\dfrac{[n^2+2n(1-m)-2m-m^2]a_{n+2}-m^2a_n}{[n-2(m-2)]\,(n+4)} \ . \end{cases} \tag{A4.15}$$

From these results, a_n may be written as

$$a_1 = a_3 = a_5 = \ldots = a_{2n+1} = 0 \ , \tag{A4.16}$$

$$a_2 = \frac{m(m+2)}{2^2(m+1)} a_0 \ , \tag{A4.17}$$

$$a_4 = \frac{m^3(m+4)}{2^5(m+1)(m+2)} a_0 \ , \tag{A4.18}$$

$$a_6 = \frac{m^5(m+6)}{2^7 \cdot 3(m+1)(m+2)(m+3)} a_0 \ , \ldots \tag{A4.19}$$

Consequently, we have

$$\text{for } \lambda = m \ ; b_n = \frac{m^{2n-1}(m+2n)}{2^{2n} n! \, \Gamma(m+n+1)} \Gamma(m+1) a_0 \ , \ (m \neq 0) \ , \tag{A4.20}$$

$$\text{for } \lambda = -m \ ; b_n = \frac{m^{2n-1}(m-2n)}{2^{2n} n! \, \Gamma(n-m+1)} \Gamma(1-m) a_0 \ , \ (m \neq 0) \ , \tag{A4.21}$$

where $b_n = a_{2n}$.

Here it is known that the function $sI_m'(sm)$ is expanded as

$$\begin{aligned} s \frac{d}{ds} I_m(sm) &= s \frac{d}{ds} \sum_{n=0}^{\infty} \frac{(sm)^{2n+m}}{2^{2n+m} n! \, \Gamma(m+n+1)} \\ &= \sum_{n=0}^{\infty} \frac{m^{2n-1}(m+2n)}{2^{2n} n! \, \Gamma(n-m+1)} \frac{m^{m+1}}{2^m} s^{2n+m} . \end{aligned} \tag{A4.22}$$

Hence the solutions to (A4.7) can be simply written in the form

$$g_m = \begin{cases} sI_m'(sm) \\ sI_{-m}'(-sm) \end{cases} \quad (m \neq 0) , \tag{A4.23}$$

or

$$g_m = \begin{cases} sI_m'(sm) \\ sK_m'(sm) \end{cases} \quad (m \neq 0) . \tag{A4.24}$$

On the other hand, the solution for $m = 0$ is readily obtained as

$$g_0 = \log r + \frac{h^2 r^2}{2} . \tag{A4.25}$$

From (A4.24) and (A4.25), we find a solution to (A4.6)

$$g_m = \begin{cases} Ah^2 r r_0 I_m'(mhr_<) K_m'(mhr_>), & (m \neq 0), \\ B\left(\log r_> + \dfrac{h^2 r_>^2}{2}\right), & (m=0), \end{cases} \tag{A4.26}$$

which is regular for $r=0$ and $r \longrightarrow \infty$ and has the symmetry in r and r_0. In order to determine the constant A in (A4.26), we integrate (A4.6) from r_0-ε to $r_0+\varepsilon$ and take the limit $\varepsilon \longrightarrow 0$ as follows :

$$\lim_{\varepsilon \to 0} \left[\frac{r}{1+h^2 r^2} \frac{dg_m}{dr} \right]_{r_0-\varepsilon}^{r_0+\varepsilon} - \lim_{\varepsilon \to 0} \int_{r_0-\varepsilon}^{r_0+\varepsilon} \frac{m}{r} g_m \, dr = -\frac{4\pi}{h^2}, \quad (m \neq 0). \tag{A4.27}$$

While the second term in the left hand side of (A4.27) vanishes, the first is reduced to A as

$$\begin{aligned} \lim_{\varepsilon \to 0} \left[\frac{r}{1+h^2 r^2} \frac{dg_m}{dr} \right]_{r_0-\varepsilon}^{r_0+\varepsilon} &= \frac{A r_0^3 h^3 m}{1+h^2 r_0^2} [I_m'(mhr_0) K_m''(mhr_0) - I_m''(mhr_0) K_m'(mhr_0)] \\ &= A \quad , \end{aligned} \tag{A4.28}$$

where the identity

$$I_m'(z) K_m''(z) - I_m''(z) K_m'(z) = \frac{1}{z}\left(1+\frac{m^2}{z^2}\right). \tag{A4.29}$$

is adopted. Hence, for $m \neq 0$, we have

$$A = -\frac{4\pi}{h^2}. \tag{A4.30}$$

Similarly, integration of g_0 yields

$$B = -\frac{4\pi}{h^2}. \tag{A4.31}$$

Consequently, the fundamental solution (A4.5) becomes

$$\begin{aligned} G_S(r, \zeta; r_0, \zeta_0) &= \frac{1}{2\pi}\left[g_0 + 2 \sum_{m=1}^{\infty} g_m(r, r_0) \cos\{m(\zeta - \zeta_0)\} \right] \\ &= -r_>^2 + \frac{2}{h^2} \log\left(\frac{1}{r_>}\right) - 4 r r_0 \sum_{m=1}^{\infty} I_m'(mhr_<) K_m'(mhr_>) \cos[m(\zeta - \zeta_0)]. \end{aligned} \tag{A4.32}$$

This coincides with the solution (3.27) within a constant.

A-5 Derivation of the perturbed solution (4.43) - (4.46)

Here the Laplace equation with helical symmetry (4.1) is solved by the perturbation. Assuming that the helical wavenumber h is sufficiently small, the solution to (4.1) is expanded with respect to h,

$$\Phi = \Phi_0 + h^2\Phi_1 + h^4\Phi_2 + \ldots, \tag{A5.1}$$

The boundary conditions for Φ_k $(k=0, 1, 2 \ldots)$ is

$$\Phi_0 = 300, \qquad X=-a/2, \tag{A5.2a}$$

$$\Phi_k = 0 \ (k=1, 2, 3 \ldots), \qquad X=-a/2, \tag{A5.2b}$$

$$\Phi_k = 0 \ (k=0, 1, 2 \ldots), \qquad X= \ a/2, \tag{A5.2c}$$

$$\frac{\partial \Phi_k}{\partial n} = 0 \ (k=0, 1, 2 \ldots), \qquad Y=\pm b/2. \tag{A5.2d}$$

The insertion of (A5.1) into (4.1) yields

$$\sum_{k=0}^{\infty} h^{2k} \left\{ (1+h^2Y^2)\frac{\partial^2\Phi_k}{\partial X^2} - 2XYh^2 \frac{\partial^2\Phi_k}{\partial X \partial Y} + (1+h^2X^2)\frac{\partial^2\Phi_k}{\partial Y^2} \right.$$

$$\left. -h^2X\frac{\partial\Phi_k}{\partial X} - h^2Y\frac{\partial\Phi_k}{\partial Y} \right\} = 0 . \tag{A5.3}$$

Hence the zero-th order solution Φ_0 satisfies

$$\frac{\partial^2\Phi_0}{\partial X^2} + \frac{\partial^2\Phi_0}{\partial Y^2} = 0 . \tag{A5.4}$$

From (A5.4) and the boundary conditions (A5.2a) and (A5.2c)-(A5.2d), one can readily obtain the solution Φ_0 as follows :

$$\Phi_0 = -300\,\frac{X}{a} + 150 . \tag{A5.5}$$

Moreover the first order solution Φ_1, which satisfies

$$\frac{\partial^2\Phi_1}{\partial X^2} + \frac{\partial^2\Phi_1}{\partial Y^2} = -Y^2\frac{\partial^2\Phi_0}{\partial X^2} + 2XY\,\frac{\partial^2\Phi_0}{\partial X \partial Y} - X^2\frac{\partial^2\Phi_0}{\partial Y^2} + X\frac{\partial\Phi_0}{\partial X} + Y\frac{\partial\Phi_0}{\partial Y}$$

$$= -300\,X/a\,, \tag{A5.6}$$

is found to be

$$\Phi_1 = -50\,\frac{X}{a}\left(X+\frac{a}{2}\right)\left(X-\frac{a}{2}\right). \tag{A5.7}$$

Further the second order solution ϕ_2 satisfies

$$\frac{\partial^2\Phi_2}{\partial X^2}+\frac{\partial^2\Phi_2}{\partial Y^2} = -Y^2\frac{\partial^2\Phi_1}{\partial X^2}+2XY\,\frac{\partial^2\Phi_1}{\partial X\partial Y}-X^2\frac{\partial^2\Phi_1}{\partial Y^2}+X\frac{\partial\Phi_1}{\partial X}+Y\frac{\partial\Phi_1}{\partial Y}$$

$$= \frac{300}{a}XY^2-\frac{150}{a}X^3+\frac{25}{2}aX\ . \tag{A5.8}$$

Here ϕ_2 can be divided into three parts,

$$\Phi_2 = \Phi_{21}+\Phi_{22}+\Phi_{23}\,, \tag{A5.9}$$

which satisfy

$$\frac{\partial^2\Phi_{21}}{\partial X^2}+\frac{\partial^2\Phi_{21}}{\partial Y^2} = \frac{300}{a}XY^2, \tag{A5.10}$$

$$\frac{\partial^2\Phi_{22}}{\partial X^2}+\frac{\partial^2\Phi_{22}}{\partial Y^2} = -\frac{150}{a}X^3, \tag{A5.11}$$

$$\frac{\partial^2\Phi_{23}}{\partial X^2}+\frac{\partial^2\Phi_{23}}{\partial Y^2} = \frac{25}{2}aX\,. \tag{A5.12}$$

By considering the boundary conditions (A5.2a) and (A5.2c)-(A5.2d), we easily find the solutions to (A5.11) and (A5.12) as

$$\Phi_{22} = -\frac{15X}{2a}\left(X^2+\frac{a^2}{4}\right)\left(X+\frac{a}{2}\right)\left(X-\frac{a}{2}\right), \tag{A5.13}$$

$$\Phi_{23} = \frac{25aX}{12}\left(X+\frac{a}{2}\right)\left(X-\frac{a}{2}\right). \tag{A5.14}$$

On the other hand, the solution ϕ_{21} can be expressed in the form

$$\Phi_{21} = -\frac{300}{a}\int_{-a/2}^{a/2}X_0\,dX\int_{-b/2}^{b/2}Y_0^2\,G(X,Y;X_0,Y_0)\,dY_0\,, \tag{A5.15}$$

where $G(X, Y; X_0, Y_0)$ satisfies

$$\left(\frac{\partial^2}{\partial X^2}+\frac{\partial^2}{\partial Y^2}\right)G(X,Y;X_0,Y_0)+\delta(X-X_0)\delta(Y-Y_0) = 0\ . \tag{A5.16}$$

In order to find the the function $G(X, Y; X_0, Y_0)$ which satisfies the boundary condition (A5.2b)-(A5.2d), it is expressed as

$$G(X,Y;X_0,Y_0)=\sum_{n=0}^{\infty}\sum_{m=1}^{\infty}g_{mn}\sin[mu(X)]\cos[nv(Y)]\,, \tag{A5.17}$$

where

$$u(\xi)=\frac{\pi}{a}\left(\xi+\frac{a}{2}\right), \tag{A5.18}$$

$$v(\eta)=\frac{\pi}{b}\left(\eta+\frac{b}{2}\right). \tag{A5.19}$$

Considering the boundary conditions (A5.2b)-(A5.2d), the delta functions in (A5.16) are also expanded as

$$\delta(X-X_0)=\frac{2}{a}\sum_{m=1}^{\infty}\sin[mu(X)]\sin[mu(X_0)]\,, \tag{A5.20}$$

$$\delta(Y-Y_0)=\frac{1}{b}\sum_{n=0}^{\infty}\varepsilon_n\cos[nv(Y)]\cos[nv(Y_0)]\,, \tag{A5.21}$$

where

$$\varepsilon_0=1$$
$$\varepsilon_n=2\,,\ (n\neq 0)\,. \tag{A5.22}$$

By substituting (A5.17), (A5.20) and (A5.21) into (A5.16), we have

$$g_{mn}=\frac{2\varepsilon_n}{\pi^2 ab}\frac{\sin[mu(X_0)]\cos[nv(Y_0)]}{(m/a)^2+(n/b)^2}\,. \tag{A5.23}$$

Then,

$$G(X,Y;X_0,Y_0)=\frac{2}{\pi^2 ab}\sum_{n=0}^{\infty}\sum_{m=1}^{\infty}\varepsilon_n\frac{\sin[mu(X)]\cos[nv(Y)]}{(m/a)^2+(n/b)^2}\sin[mu(X_0)]\cos[nv(Y_0)]\,. \tag{A5.24}$$

Hence (A5.15) becomes

$$\Phi_{21}=-\frac{600}{\pi^2 a^2 b}\sum_{n=0}^{\infty}\sum_{m=1}^{\infty}\varepsilon_n\frac{\sin[mu(X)]\cos[nv(Y)]}{(m/a)^2+(n/b)^2}\times$$
$$\int_{-a/2}^{a/2}X_0\sin[mu(X_0)]\,dX_0\int_{-b/2}^{b/2}Y_0^2\cos[nv(Y_0)]\,dY_0\,, \tag{A5.25}$$

The integrals with respect to X_0 and Y_0 can be performed as follows

$$\int_{-a/2}^{a/2} X_0 \sin[mu(X_0)]\, dX_0 = -\frac{a^2}{2m\pi}(\cos m\pi + 1)\,, \quad (m \neq 0)\,, \tag{A5.26}$$

$$\int_{-b/2}^{b/2} Y_0^2 \cos[nv(Y_0)]\, dY_0 = \begin{cases} \dfrac{b^3}{n^2\pi^2}(\cos n\pi + 1)\,, & (n \neq 0)\,, \\ \dfrac{b^3}{12}\,, & (n=0)\,. \end{cases} \tag{A5.27}$$

The insertion of (A5.26) and (A5.27) into (A5.25) yields

$$\Phi_{21} = \frac{600a^2b^2}{\pi^5}\sum_{m=1}^{\infty}\frac{1}{m^3}\sin[mu(X)](\cos m\pi + 1)\sum_{n=1}^{\infty}\left\{\frac{1}{n^2} - \frac{1}{n^2+(mb/a)^2}\right\}\times$$

$$\cos[nv(Y)](\cos n\pi + 1) + \frac{25a^2b^2}{\pi^3}\sum_{m=1}^{\infty}\frac{1}{m^3}\sin[mu(X)](\cos m\pi + 1)\,. \tag{A5.28}$$

The infinite series in (A5.28) are evaluated as [3.3]

$$\sum_{n=1}^{\infty}\left\{\frac{1}{n^2} - \frac{1}{n^2+(mb/a)^2}\right\}\cos[nv(Y)] =$$

$$\frac{1}{4}v(Y)^2 - \frac{\pi}{2}v(Y) + \frac{\pi^2}{6} + \frac{1}{2}\left(\frac{a}{mb}\right)^2 - \frac{\pi a}{2mb}\frac{\cosh\left\{\dfrac{b}{a}mv(Y)\right\}}{\sinh\left(\dfrac{b}{a}m\pi\right)}\,, \tag{A5.29}$$

$$\sum_{n=1}^{\infty}\left\{\frac{1}{n^2} - \frac{1}{n^2+(mb/a)^2}\right\}\cos[nv(Y)]\cos n\pi =$$

$$\frac{1}{4}v(Y)^2 - \frac{\pi^2}{12} + \frac{1}{2}\left(\frac{a}{mb}\right)^2 - \frac{\pi a}{2mb}\frac{\cosh\left\{\dfrac{b}{a}mv(Y)\right\}}{\sinh\left(\dfrac{b}{a}m\pi\right)}\,, \tag{A5.30}$$

$$\sum_{m=1}^{\infty} \frac{\sin[mu(X)]}{m^3} = \frac{\pi^2}{6} u(X) - \frac{\pi}{4} u(X)^2 + \frac{1}{12} u(X)^3 , \tag{A5.31}$$

$$\sum_{m=1}^{\infty} \frac{\sin[mu(X)]}{m^3} \cos m\pi = \frac{\pi^2}{6}\{u(X)+\pi\} - \frac{\pi}{4}\{u(X)+\pi\}^2 + \frac{1}{12}\{u(X)+\pi\}^3$$

$$= \frac{u(X)}{12}\{u(X)^2 - \pi^2\}, \tag{A5.32}$$

$$\sum_{m=1}^{\infty} \frac{\sin[mu(X)]}{m^5} = \frac{\pi^4}{90} u(X) - \frac{\pi^2}{36} u(X)^3 + \frac{\pi}{48} u(X)^4 - \frac{1}{240} u(X)^5 , \tag{A5.33}$$

$$\sum_{m=1}^{\infty} \frac{\sin[mu(X)]}{m^5} \cos m\pi = \frac{\pi^4}{90}\{u(X)+\pi\} - \frac{\pi^2}{36}\{u(X)+\pi\}^3 + \frac{\pi}{48}\{u(X)+\pi\}^4 - \frac{1}{240}\{u(X)+\pi\}^5$$

$$= -\frac{7\pi^4}{720} u(X) + \frac{\pi^2}{72} u(X)^3 - \frac{1}{240} u(X)^5 . \tag{A5.34}$$

Substituting (A5.29)-(A5.34) into (A5.28), we obtain

$$\Phi_{21} = \frac{X}{a}\left(X+\frac{a}{2}\right)\left(X-\frac{a}{2}\right)\left(50Y^2 - 5X^2 + \frac{35}{12}a^2\right)$$

$$- \frac{600a^3 b}{\pi^4} \sum_{m=1}^{\infty} \frac{(-1)^m + 1}{m^4} \cosh\left(\frac{Y}{a}\pi m\right) \cosh\left(\frac{b}{2a}\pi m\right) \frac{\sin\left\{m\pi\left(\frac{X}{a}+\frac{1}{2}\right)\right\}}{\sinh\left(\frac{b}{a}m\pi\right)} . \tag{A5.35}$$

Consequently, from (A5.13), (A5.14) and (A5.35), we obtain the second order solution,

$$\Phi_2 = \frac{25X}{8a}\left(X+\frac{a}{2}\right)\left(X-\frac{a}{2}\right)\left(16Y^2 - 4X^2 + a^2\right)$$

$$- \frac{600a^3 b}{\pi^4} \sum_{m=1}^{\infty} \frac{(-1)^m + 1}{m^4} \cosh\left(\frac{Y}{a}\pi m\right) \cosh\left(\frac{b}{2a}\pi m\right) \frac{\sin\left\{m\pi\left(\frac{X}{a}+\frac{1}{2}\right)\right\}}{\sinh\left(\frac{b}{a}m\pi\right)} . \tag{A5.36}$$

inches 1 2 3 4 5 6 7 8

cm 1 2 3 4 5 6 7 8 9 10 11 12 13 14 15 16 17 18 19

Kodak Color Control Patches

© Kodak, 2007 TM: Kodak

Blue Cyan Green Yellow Red Magenta White 3/Color Black

Kodak Gray Scale

C Y M

© Kodak, 2007 TM: Kodak

A 1 2 3 4 5 6 **M** 8 9 10 11 12 13 14 15 **B** 17 18 19